Statistical Mechanics of Polymer Stretching

Thesis submitted for the degree of

Doctor Philosophiæ

Candidate:
Angelo Rosa

Supervisor:
Prof. Amos Maritan

October, 9th 2003

Contents

Introduction

This book is not of today or of the future.
It tells of no place.
It serves no cause, party or class.
It has a moral which grows on the pillar of understanding:
"The mediator between brain and muscle must be the Heart."

Thea von Harbou, *Metropolis*

The interplay between Physics and Biology is certainly one of the most exciting field in modern Science. In particular, the discovery that proteins, DNA and RNA have rather peculiar spatial arrangements [1, 2, 3] has convinced biological physicists that these simple forms may be deduced from an underlying principle. Besides, new experimental techniques have supplied high-quality data, which can be investigated and compared to theoretical models.

In particular, in this Thesis, we have focused our attention on the theoretical study of some elastic and thermodynamic properties of polymers and, in particular, biopolymers such as proteins, DNA and RNA [4].

This research work is organized as follows:

- In Chap. 1, we introduce some basic concept on polymers and biopolymers.

  In particular, biopolymers has attracted the attention of many research groups. Probably, their most appealing property is that they are organized in simple hierarchical structures [5]. In fact, the primary amino acid sequence of proteins is disposed in some fascinating forms as α-helices and β-strands, which at an outer level form compact structures called domains. Moreover, 50 years ago, Watson and Crick [2] discovered the marvelous double helix of DNA.

  Furthemore, polymers seem to display many intriguing features, since they can not be described in terms of ordinary solids. This is due to the *covalent* nature of

the bonds between consecutive monomers. Due to temperature fluctuations of these bonds, a polymer can not be viewed as a rigid macromolecule. Since these fluctuations favor many different spatial conformation, a Statistical Mechanics approach has revealed very useful [3]. Then, we focus on the important problem of polymer elasticity and introduce some preliminary concepts as the Kuhn length and the persistence length [4].

- In Chap. 2, we focus our attention about some recent experiments on polymer stretching.

  Firstly, we begin with a brief introduction to some recent experimental techniques. Mainly, we focus on optical tweezers [6], atomic force microscopes [7] and soft microneedles [8]. We also give a short explanation about their technical features, including practical limitations and available force ranges.

  Besides, we describe in great details many force driven phase transition which occur in real polymers. Then, Statistical Mechanics allows for a rigorous approach to these phenomena. As explained above, we also address the important problem of elasticity in polymers, introducing the freely jointed chain (FJC) model and the worm like chain (WLC) model [3].

- In Chap. 3, we describe the stretching behaviour of polymers, with the introduction of some chosen $2d$ *on-lattice* models and $3d$ *off-lattice* models.

  In the framework of a simplified approach on a self-interacting directed self-avoiding walk (DSAW) [9], we have discussed the importance of some scaling laws that we think to be of more general validity. Then, we introduce a more realistic model for a self-interacting SAW [9]. In particular we are able to describe its phase diagram.

  Through the introduction of an off-lattice self-avoiding polymer, we also give a simple explanation of some recent *puzzling* experimental results described in Chap. 2.

- In Chap. 4, we shall focus our attention on the stretching behaviour of polymer in a *good* solvent [10].

  Generalizing the WLC approach of Marko and Siggia [11], we obtain a *new* interpolation formula, which perfectly describes some numerical data, obtained with Monte Carlo simulations. Furthermore, this formula seems to be more powerful than Marko and Siggia's one. In fact, it fits well some experimental

data taken from literature, that the previous approach was not able to describe correctly.

Finally, we outline final conclusions and perspectives.

Chapter 1

Polymers and biopolymers

I believe... that it's aerodynamically impossible for a bumblefee to fly, that light is a wave and a particle, that there's a cat in a box somewhere who's alive and dead at the same time (although if they don't ever open the box to feed it it'll eventually just be two different kinds of dead),...

Neil Gaiman, *American Gods*

In this Chapter we give some definitions taken from some standard literature on polymers. We do not pretend to be exhaustive and a precise chemical approach is beyond the scopes of this Thesis. In Sec. 1.1 we introduce some simple concepts about polymer chemistry. In Sec. 1.2 we focus on biopolymers such as proteins or DNA. Then, in Sec. 1.3 we discuss the physical origin of polymer flexibility.

1.1 Polymers: basic definitions

The usual description of a polymer is given in terms of its *structural subunits* [12, 10]. These are minimal chemical structures whose valence can be two or more. A *linear* polymer is the most simple example and is illustrated in Fig. 1.1. It is made by a sequential repetition of subunits (indicated with the symbol A) whose valence is strictly two, apart from the endings (A' and A'') which have valence one. x is the degree of polymerization and corresponds to the number of structural units in the chain[1]. Let us remark that the subunits may be equal or different. In this latter

[1]For artificial polymers $x \sim 10^2 - 10^4$. Natural polymers such as DNA may reach $x \sim 10^9 - 10^{10}$ [4].

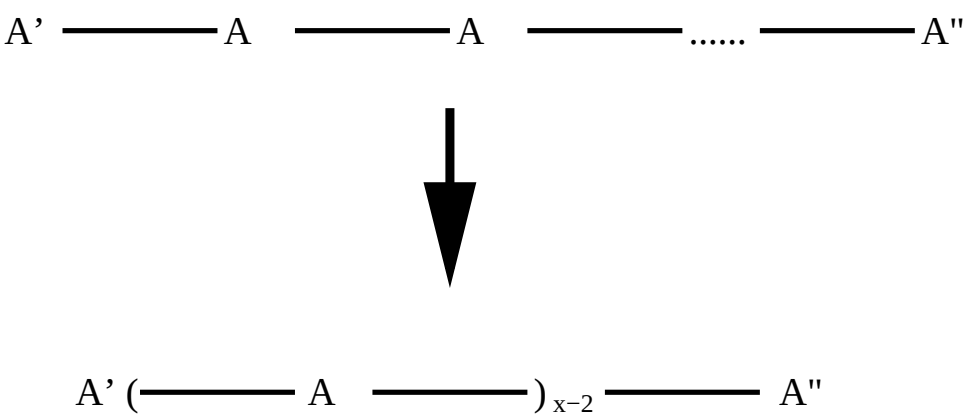

Figure 1.1: Scheme of a linear polymer.

case, more precisely, we call it a (random) *copolymer* or a *heteropolymer*. Typically, covalent bonds (whose energy is about $1 - 10$ eV) link the monomers in the chain.

A more complex polymeric structure emerges when some subunits have a three or higher valence (they are indicated with the capital letter Y in Fig. 1.2). In this case we call it a *branched* polymer. The intriguing feature of these molecules is that they can not usually be described in terms of a regular lattice, as the ordinary solids: they, in fact, form a *network* structure whose arrangement in space may be disordered.

The structural units represent residues from the monomeric compounds employed in the preparation of the polymer. Usually, there is a direct correspondence between the monomer(s) and the structural unit(s): in this case they possess identical atoms occupying similar relative positions. Nevertheless, there are some polymers which may have two or more structural units (they derive from two or more monomers), which form the *repeating* unit of the chain. In accordance with the *functionality* concept given by Carothers [13, 14], all monomers which when polymerized may join with two, and only two, other monomers are termed *bifunctional*. Of course, in branched polymers, we have some *polyfunctional* units, i.e. their functionality exceeds two.

The topic of this Thesis is the theoretical analysis of linear polymers. So in the following we always refer to them simply as polymers, having in mind the simple characterization we have given above.

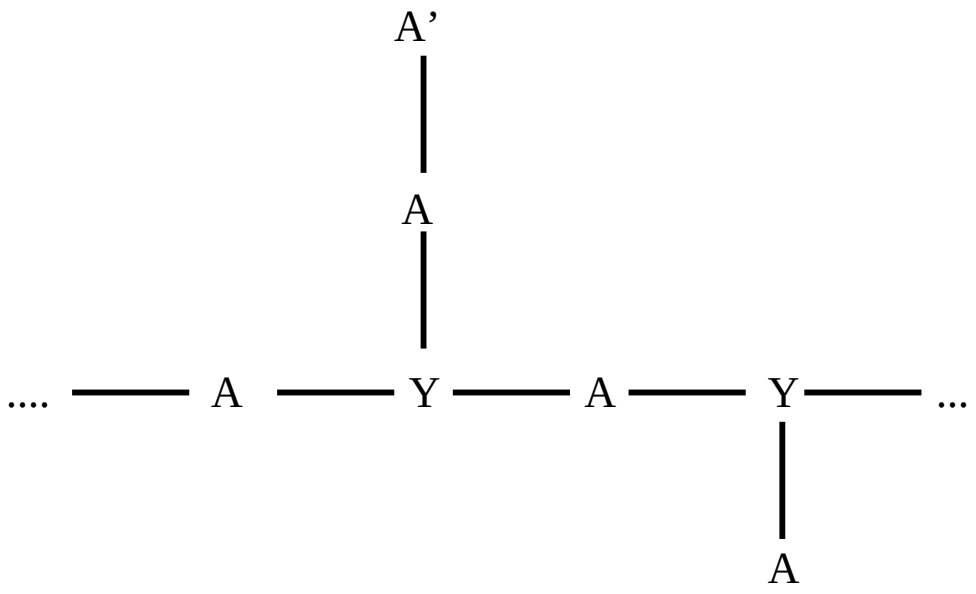

Figure 1.2: Scheme of a branched polymer.

1.2 Biopolymers

In this Section we shall introduce some simple concepts about biopolymers such as proteins, DNA and RNA. Monomer units of a protein chains are residues of the so called amino acids [1] and have structure of the sort $-C'O-C_\alpha HR-NH-$, where R stands for a radical or side chain (see Fig. 1.3 for a schematic picture of alanine). We have 20 different types of radicals [1]. The most simple is just a hydrogen atom (glycine). The sequence of amino acid residues in the chain is different for different proteins and the number of monomer units N in each protein molecule usually varies from a few tens up to a few hundreds.

The chemical structure of a protein chain primary sequence is sketched in Fig. 1.4. The $-C'O-NH-$ bond links together $-C_\alpha HR-$ groups that are specific to each unit. It is called a peptide bond (see Fig 1.5); that is why the whole protein molecule is often referred to as a peptide chain.

The peptide units are effectively rigid groups that are linked into a chain by covalent bonds at the C_α atoms. Then, the only degrees of freedom they have are rotations around these bonds. The Ramachandran's ϕ and ψ angles describe, respectively, the angle of rotation around the $N-C_\alpha$ bond and that around the $C_\alpha - C'$ bond (see Fig. 1.6) [5]. Moreover, the conformation of the whole main chain is completely determined when the ϕ and ψ angles for each amino acid are defined with high accuracy.

Figure 1.3: Schematic diagram of the amino acid alanine. A central carbon atom (C_α) is attached to an amino group (NH_2), a carboxyl group ($C'OOH$), a hydrogen atom (H) and a radical or side chain (R), that in this case is CH_3.

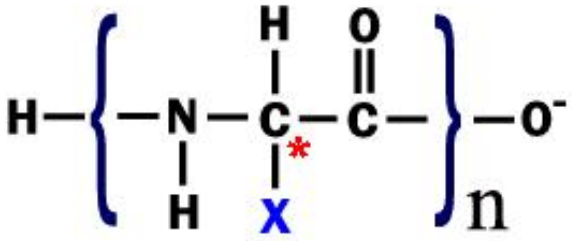

Figure 1.4: The chemical structure of a protein chain primary sequence. The $-N-C_\alpha-$ peptide bonds form the main chain backbone. X symbolizes side groups of various amino acid residues.

Figure 1.5: Scheme of the formation of a peptide bond. The carboxyl group of an amino acid has formed a peptide bond, $C_\alpha - N$, to the amino group of another amino acid. One water molecule is eliminated in this process.

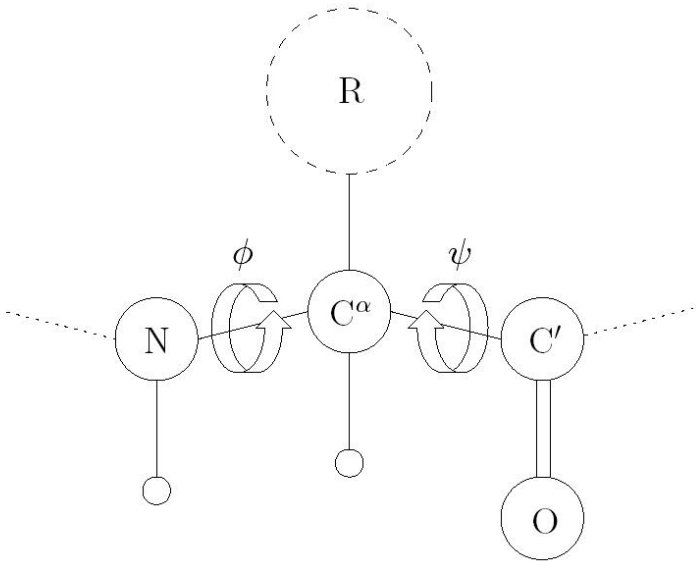

Figure 1.6: The ϕ, ψ angles of an amino acid residue. Protein molecules flexibility results from the rotational freedom of these bonds (see also Sec. 1.3).

Let us remark that most combinations of ϕ and ψ angles for an amino acid are not allowed, due to steric collisions between the side chains and the main chain. The plot of all allowed (ϕ, ψ) pairs is called a Ramachandran plot [5] and is shown in Fig. 1.7.

The chemical structure of DNA is made up of alternating sugar (deoxyribose) and phosphate groups; due to the latter, the whole strand has a negative charge. A nitric base is attached to each sugar group. There are four possible bases: adenine (A), cytosine (C), guanine (G), and thymine (T). RNA strands have a similar structure, with a different type of sugar in the main chain and the base uracil (U) replacing thymine. In Fig. 1.8 a scheme of the chemical structure of *double* stranded DNA (dsDNA) is shown.

1.2.1 Hierarchical structures of biopolymers

Biopolymers are characterized by a hierarchy of structures: there is a primary, secondary, tertiary and sometimes quaternary structure.

The *primary* structure is given by the simple sequence of repeat units in the chain (see Fig. 1.4).

Secondary and tertiary structure are the short-scale and long-scale order in the

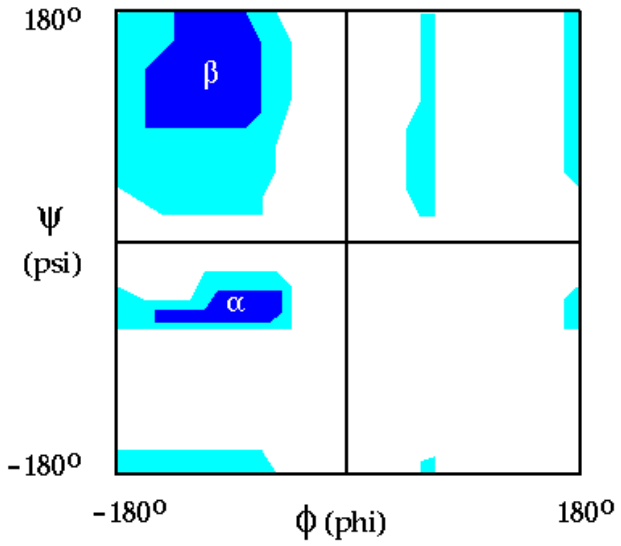

Figure 1.7: Ramachandran plot. Colored areas show sterically allowed regions.

monomers' positions, respectively. The main *secondary* structures of proteins, the α-helices (see Fig. 1.9) and β-sheets (see Fig. 1.10), were discovered in the 1940's and 1950's by the American chemist Linus Pauling [15]. Both these regular structures are characterized by hydrogen-bonding between the main-chain $N-H$ and $C'=O$ groups, and they are formed when a number of consecutive residues have the same ϕ, ψ angles (see Fig. 1.6).

- α-helices are found when a stretch of consecutive residues all have the ϕ, ψ angle pair approximately $-60°$ and $-50°$ (see Fig. 1.7). The α-helix has 3.6 residues per turn with hydrogen bonds between $C'=O$ of residue n and $N-H$ of residue $n+4$, which corresponds to 5.4 Å (1.5 Å per turn) [5] (see Fig. 1.11).

- β-sheets are built up from a combination of several regions (β-strands) of the polypeptide chain, in contrast to α-helices, which are built up from one continuous region [5] (see Fig. 1.12). These β-strands are usually from 5 to 10 residues long and are in an almost fully extended conformation with ϕ, ψ angles within the broad structurally allowed region in the upper left quadrant of the Ramachandran plot (see Fig. 1.7). β-strands are aligned adjacent to each other such that hydrogen bonds can form between $C'=O$ groups of one β-strand and $N-H$ groups on an adjacent β-strand and viceversa. Two configurations are possible: *parallel* and *antiparallel* β-sheets. In the former case,

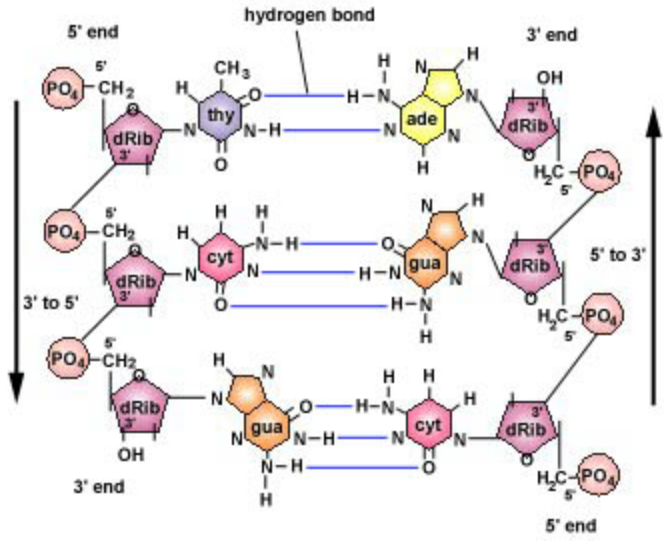

Figure 1.8: Scheme of the chemical structure of double stranded DNA (dsDNA). The phosphate of one deoxyribonucleotide binding to the $3'$ carbon of the deoxyribose of another forms the sugar-phosphate backbone of the DNA (the sides of the "ladder"). The hydrogen bonds between the complementary nucleotide bases (adenine-thymine; guanine-cytosine) form the rungs. Note the antiparallel nature of the DNA. One strand ends in a $5'$ phosphate and the other ends in a $3'$ hydroxyl.

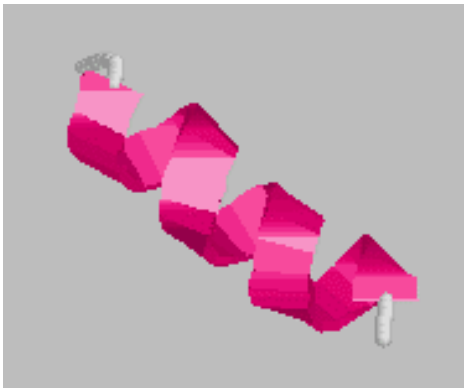

Figure 1.9: Idealized scheme of the path of the main chain in an α-helix.

Figure 1.10: Illustration of the twist of a β-sheet.

the amino acids in the aligned β-strands can all run in the same biochemical direction, amino terminal to carboxy terminal. In the latter one, amino acids in successive strands have alternating directions, amino terminal to carboxy terminal followed by carboxy terminal to amino terminal, followed by amino terminal to carboxy terminal, and so on. Sometimes β-strands can also combine into mixed β-sheets. As they occur in known protein structures, almost all β-sheets (parallel, antiparallel and mixed) have twisted strands (see Fig. 1.10).

As for the three-dimensional structure, it is known that in a living cell, DNA molecules consist of two strands (see Fig. 1.13) that form a double helix. It is essential that these two strands are mutually complementary. This means that, say, adenine in one of the strands always corresponds to thymine in the other, whereas guanine always corresponds to cytosine (see Fig. 1.8). Physically, the reason for this is that the nitric bases are located in the very core of the double helix, where only the pairs A-T and G-C can fit perfectly without distorting the shape of the double helix. Hence, the second strand of the double helix contains no extra information, but merely helps to reproduce the information and to make multiple copies of it. The normal secondary structure of DNA was discovered in 1953 by Francis Crick and James Watson at the University of Cambridge in England [2].

They are made stable by the hydrogen bonds. In fact, the reason why the loops of the helix and the β-folds are formed is simply that this is the arrangement that achieves the maximum saturation of the hydrogen bonds.

The *tertiary* stucture is formed by packing such structural elements (α-helices and β-sheets) into one or several compact globular units called *domain*. A beautiful example is given by β-secretase and plotted in Fig. 1.14.

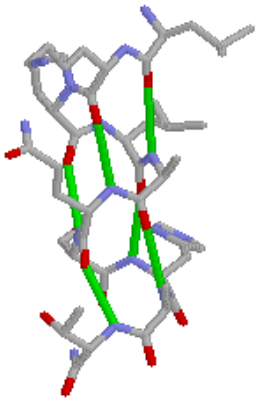

Figure 1.11: Scheme of an α-helix. The hydrogen bonds are shown in green. The hydrogen bonds connect the amido-hydrogens to carbonyl oxygens one loop of the helix above or below them.

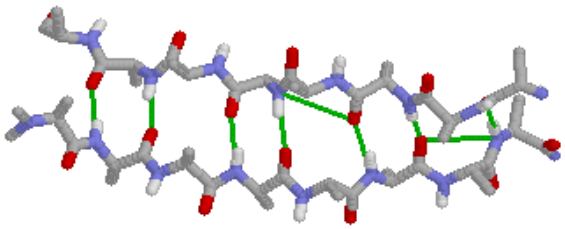

Figure 1.12: Scheme of a *parallel* β-sheet. Two strands run side-by-side, linked by hydrogen bonds (shown in green). This time the hydrogen bonds connect two strands running *parallel* to one another.

Figure 1.13: Picture of a DNA double helix segment (Courtesy of K. Spiegel, Sissa-Isas, Trieste, Italy).

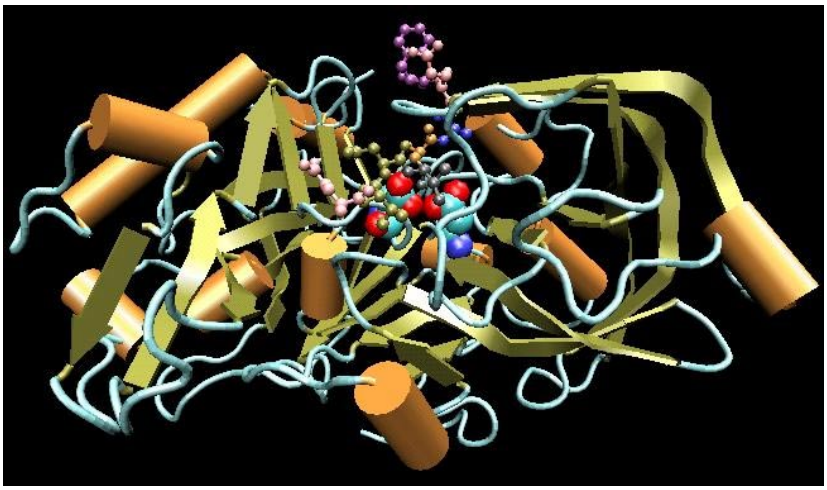

Figure 1.14: Picture of β-secretase (Courtesy of M. Cascella, Sissa-Isas, Trieste, Italy).

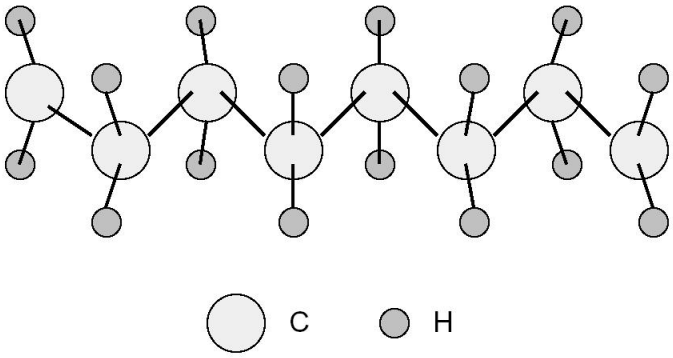

Figure 1.15: Spatial structure of a polyethylene chain segment, whose structure is composed of atoms of carbon and hydrogen.

1.3 Flexibility mechanisms

In spite of their chemical composition, linear polymers cannot be described in terms of a one-dimensional lattice. This is mainly due to their flexibility, which is one of the central issues of this Thesis (see Chap. 4).

To understand this mechanism, let us consider one simple example of linear polymer, polyethylene, whose spatial structure is sketched in Fig. 1.15. The covalent bonds between consecutive carbon atoms fix the spatial arrangement of a short chain segment, which has a one-dimensional character. Nevertheless, due to temperature, fluctuations in bond angles become important on longer length scales. At room temperature (~ 300 K) typical fluctuations are of the order of $1-10$ degrees. In addition, parts of the molecule may rotate with respect to each other, around the axes of single covalent bonds (but not around double ones). In this case, it is said that a molecule may have different *rotational-isomeric forms* [4, 12]. So, for polyethylene, flexibility mechanisms are due to different reasons.

If only temperature fluctuations are possible (due to geometrical constraints, as in double stranded DNA [4]) the polymer is usually less flexible. The flexibility properties of a protein are mainly determined by temperature fluctuations of the Ramachandran angles ϕ and ψ (Sec. 1.2).

Now, let us introduce two length scales, the Kuhn length and the persistence length that will play a central role in this Thesis. As already said, polymer flexibility is not noticeable at short scale, but becomes important at larger scales. Then, a critical length L_K must exist for each polymer. Any polymer segment shorter than L_K can

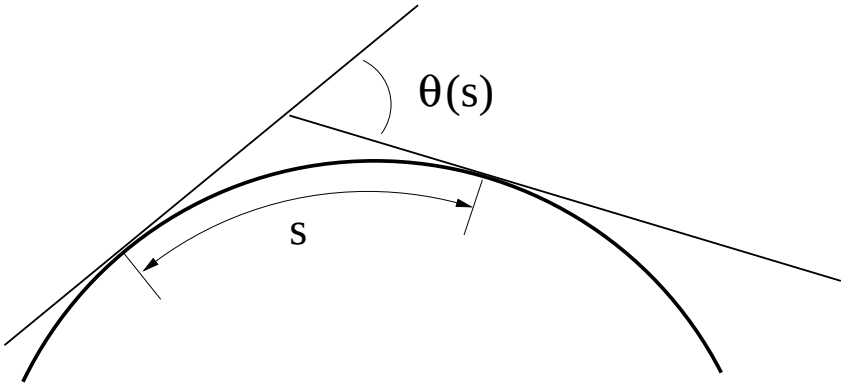

Figure 1.16: Diagram explaining the concept of persistence length.

be regarded as rigid; that is, its end-to-end distance is roughly the same as its contour length. At the same time, different segments of length L_K are virtually independent. For a polymer whose contour length is L_c, there are $N = L_c/L_K$ independent segments. In literature L_K is known as the Kuhn length[2].

There is quite a large range of Kuhn lengths for real polymers: from 1 nm for simple synthetic chain to 100 nm for dsDNA [4, 16].

This is mainly due to the flexibility of the chain. Let us suppose to fix the direction of a segment of the chain. At first, the change in direction is not noticeable. We can say that the chain has a sort of *memory* of the initial direction. Farther on, this memory starts fading, and then completely disappears. So, let us choose two points on the chain, separated by a segment of contour length s (Fig. 1.16). Since the chain flexes, its direction at the two points are different: we call $\theta(s)$ the angle between them. Since this angle fluctuates due to thermal motion a meaningful value is the average $\langle \cos\theta(s) \rangle$. It turns out that for large s,

$$\langle \cos\theta(s) \rangle \simeq \exp\left(-\frac{s}{L_p}\right). \tag{1.1}$$

Eq. (1.1) defines the *persistence* length L_p [4, 16], which, as we shall see, plays a central role in polymer physics. Its physical meaning is the following: memory of chain direction is retained on length scales shorter than L_p, but lost once L_p is exceeded.

In particular, in Appendix B, it is shown that, for a *worm like* chain (WLC), $L_K = 2L_p$.

[2] A more rigorous definition of Kuhn length will be given in Appendix A.

In principle, L_p should vary with the temperature. The higher the temperature of a chain, the more it bends, and hence, the shorter its persistence length and Kuhn length.

1.4 Conclusions

In this Chapter, we have introduced some simple concepts about polymer physics.

- After a brief introduction to polymer chemistry (and, in particular, to linear polymers), we have focused on some important aspects about biopolymers, which will play a central role in this Thesis. A great emphasis was given to their hierarchical organization.

- Then, we have discussed the important problem of polymer flexibility, introducing the Kuhn length L_K and the persistence length L_p. As said above, the first defines the length scale above which different polymer segments may be regarded as independent. The latter measures the length scale over which the memory of the chain direction is retained.

The important issue of excluded volume effects in polymer chains will be discussed in Appendix D.

Chapter 2

Polymer stretching: experimental techniques

You are clever man, friend John; you reason well, and your wit is bold; but you are too prejudiced. You do not let your eyes see nor your ears hear, and that which is outside your daily life is not of account to you. Do you not think that there are things which you cannot understand, and yet which are; that some people see things that others cannot?

Bram Stoker, *Dracula*

In this Chapter we focus on some recent techniques used to monitor the stretching behaviour of some kind of polymers. In particular, in Sec. 2.1 we give a brief description of these techniques. Then, in Sec. 2.2 we emphasize the importance of some recent results whose analysis is the starting point of this research work.

2.1 Experimental apparatus

In this Section we introduce some experimental techniques, used to probe polymer stretching. In particular, we focus on three different apparatus: optical tweezers (Subsec. 2.1.1), atomic force microscopes (AFM, Subsec. 2.1.2) and soft microneedles (Subsec. 2.1.3). Other technique (such as, e.g., *flow fields*) are described in Ref. [8]. Some remarks about the main differences between different tools are also given.

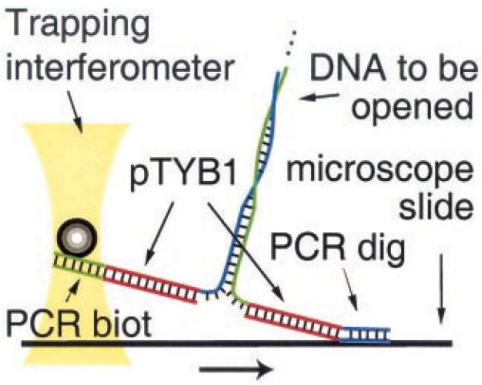

Figure 2.1: Schematic unzipping of a double stranded DNA (dsDNA) with optical tweezers (from Ref. [6]).

2.1.1 Optical tweezers

For the sake of convenience, here we shall refer to Ref. [6], where the authors describe the unzipping of a double stranded DNA (dsDNA). Nevertheless, the pulling behaviour of a generic polymer proceeds, *mutatis mutandis*, in the same fashion. Usually, an optical trapping interferometer is chosen because it combines high measurements stiffness (the trap compliance is almost negligible compared to the molecular compliance) with a sub-pN[1] resolution.

The experimental configuration is schematically presented in Fig. 2.1 (from Ref. [6]). The force measurements are performed in vitro on a molecular construction that is anchored between a glass microscope slide and a silica bead. The bead is held in an optical trap and the surface is laterally displaced which leads to a progressive opening of the double helix. The force is obtained from a measurement of the bead position within the trap. A scheme for the optical trapping interferometer is shown in Fig. 2.2. It allows for measurements of force up to 100 pN with, as already said, a sub-pN resolution.

In brief, a gradient beam optical trap is created by tightly focusing an infrared laser beam with a high-numerical-aperture microscope objective. The force acting on the bead is derived from an interferometric measurement of the position difference between the bead and the trap center. The beam of a diode-pumped Nd-Yag cw laser first passes a Faraday isolator to avoid back-reflection into the laser cavity that otherwise causes important intensity fluctuations. Then, the polarization of the linearly

[1] pN $\equiv$ piconewton.

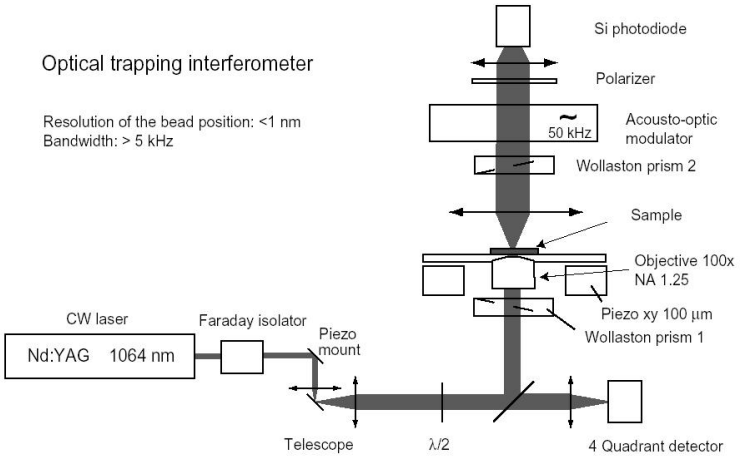

Figure 2.2: Scheme of an optical tweezers apparatus (from Ref. [6]).

polarized laser light is rotated with a $\lambda/2$ plate to illuminate a first Wollastron prism with the electric field tilted by 45° with respect to the prism axis. This leads to an angular splitting of the beam and, in the focal plane of the objective, to two partially overlapping, diffraction-limited spots of equal intensity. The two spots exhibit orthogonal linear polarization and a center-to-center distance of ~ 200 nm: silica beads (mean diameter ~ 1 μm) are then trapped in aqueous solution, close to the center of the twin spot. Since the center-to-center distance is significantly smaller than the bead diameter, the net effect of the trap along the axis of interest (the line connecting the two spots in the sample plane) can be described by an effective Hooke constant, k_{trap}. The two polarization are then recombined by a second Wollastron prism. Finally, the light is modulated and the signal is detected by a silicon photodiode.

2.1.2 Atomic Force Microscopes (AFM)

In the force-measuring mode of the AFM [7], a single molecule is stretched between the microscopic silicon nitride tip of a flexible cantilever and a flat substrate that is mounted on a highly accurate piezoelectric positioner, Fig. 2.3. A layer of protein, or other biological polymer, is either adsorbed to the substrate or linked to it through the formation of covalent bonds. When the tip and substrate are brought together and then withdrawn, one or more molecules can attach to the tip by adsorption. As the distance between the tip and substrate increases, extension of the molecule generates a restoring force that causes the cantilever to bend. This causes deflection of a laser

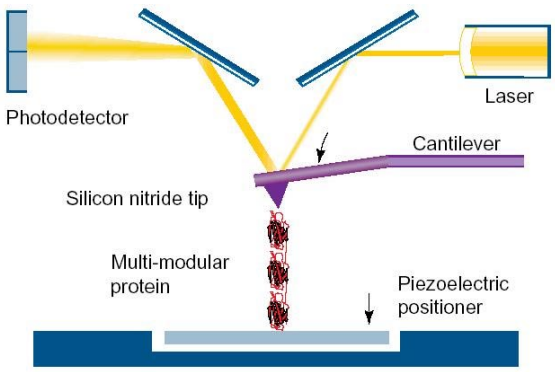

Figure 2.3: Scheme of an Atomic Force Microscope (AFM) (from Ref. [7]).

beam directed toward the upper surface of the cantilever, which is measured using a photodetector. The output of the photodetector can be related to the angle of the cantilever and therefore to the applied force, if the elastic properties of the cantilever are known.

2.1.3 Soft microneedles

In the example shown in Fig. 2.4, a bendable microneedle coated in myosin heads (not shown) catches an actin filament. This filament is brought into contact with a glass coverslip coated in myosin molecules. In the presence of ATP, the myosin drags the actin filament across the coverslip and generates a force on the microneedle, which is observable by videofluorescence spectroscopy.

2.1.4 Some remarks

As pointed out in [8], the three experimental tools described above have different technical features whose knowledge is of extreme importance in designing the right procedure. In Table 2.1 (from Ref. [8]) we have indicated with k and $F_{min-max}$ the achievable stiffness and force ranges, respectively, and with Δx_{min} the minimum displacement. Of course these values are only empirical and do not represent absolute limits. The stiffness parameter k describes the elastic properties of the probe, which is usually assumed to follow the Hooke's law. A softer probe have more sensitivity, although a stiffer one may achieve larger force values.

Strictly speaking, a spring-like device experiences a mean-square displacement noise, $\langle \Delta x^2 \rangle = k_B T/k$, where T is the temperature, and k_B is the Boltzmann con-

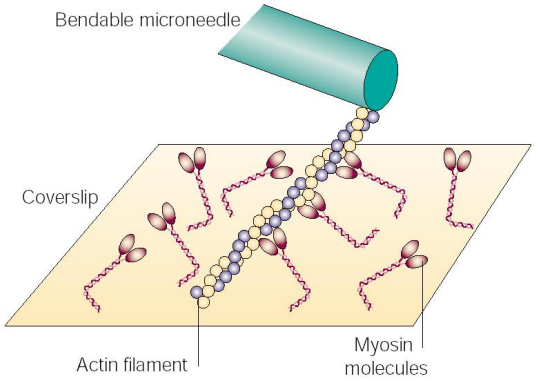

Figure 2.4: Scheme of a soft microneedle used to measure the force of myosin acting on actin (from Ref. [8]).

Methods	k (N·m^{-1})	$F_{min-max}$ (N)	Δx_{min} (m)
opt. tweezers	$10^{-10} - 10^{-3}$	$10^{-13} - 10^{-10}$	10^{-9}
AFM	$0.001 - 100$	$10^{-11} - 10^{-7}$	10^{-10}
microneedles	$10^{-6} - 1$	$10^{-12} - 10^{-10}$	10^{-9}

Table 2.1: Technical features of the experimental methods described in the text (from Ref. [8]).

stant. For a *linear* device, the corresponding mean-square force noise is $\langle \Delta F^2 \rangle = k_B T k$. The signal-to-noise ratio (SNR) $S/N = F/\sqrt{2\gamma k_B T B}$, where F is the force generated by a molecule attached to a transducer, γ is the friction coefficient of the device and B is the sampling bandwidth. So, the SNR is *independent* of the stiffness and can be increased, decreasing γ or B (the latter, being limited by the frequency of the biological event of interest) [17].

2.2 Experimental results

Due to the recent development of the experimental techniques described above and the high quality of data avalaible, there is a growing interest among physicists that have devoted their attention to the topic of polymer stretching. In this paragraph we are going to illustrate some important results recently appeared in literature. Many biologically relevant polymers have been extensively studied and the following large amount of data requires a careful examination. But, why do experimentalists decide to use force probes to study polymers?

In many cases these methods have been applied to the important problem of protein folding [1, 7]. As known, a protein must *fold* to perform its biological function. Proteins are responsible for a wide variety of mechanical functions, such as muscle contraction or vesicular secretion and a common feature is that they contain many individually folded *domains*. Known examples as immunoglobulin (Ig)-type fold and fibronectin-type fold show that unfolding and folding of domains occur when a protein executes its mechanical function.

At a very elementary level, the protein folding can be roughly described as a two-state process between an unfolded state and the folded one (states U and F, respectively, in Fig. 2.5) separated by a potential barrier (transition state, Fig. 2.5). According to the Arrhenius law of thermodynamics the rate of unfolding is $\alpha_0 \sim \exp(-\beta \Delta G_{F-T})$, where $\beta = 1/k_B T$ and ΔG_{F-T} is the free energy difference between the transition state and the folded one. When axial stress is applied to a folded protein (or, simply, to a folded domain) the protein will unravel. If the applied force is F and Δx is the distance over which the unfolding event occurs, the unfolding rate is $\alpha = \alpha_0 \exp(\beta F \Delta x)$. Of course, by releasing the protein, one can observe the *possible* refolding.

As pointed out in [7], the force required to unfold a domain is highly dependent on the topology of the bonds in the fold whose location and strength determine mechanical stability and the dependence of the rates of unfolding and refolding on the applied

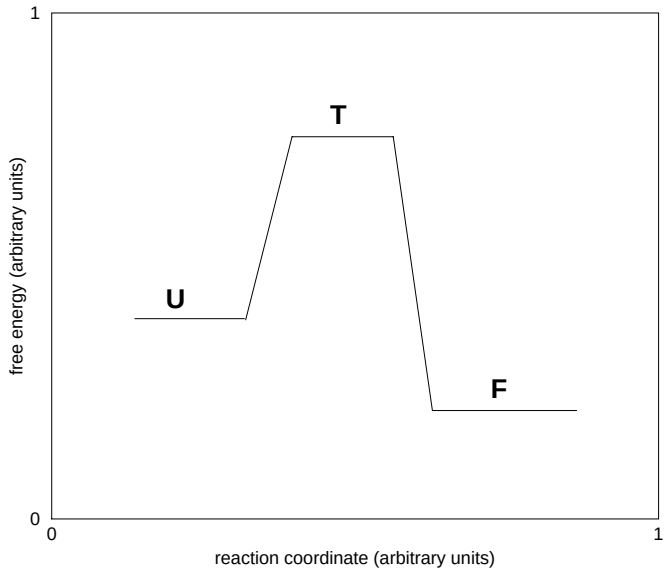

Figure 2.5: Scheme of the free energy barrier describing the protein folding as a two-state process.

force. These properties could be crucial to the physiological function of mechanical proteins.

When a polymer is relaxed in a good solvent, it forms a coiled structure, maximizing its entropy [10]. When it is stretched, its entropy decreases, so an opposing force is generated. This phenomenon is called *entropic elasticity* and usually, in this case, the behaviour of the polymers under stretching is well described by the so called worm-like chain (WLC) model (see, e.g., [11] and Appendix B for more details). This model describes the polymer as a continuous elastic string of a given total contour length. The bending properties are influenced by the persistence length (the distance beyond which two tangent vectors to the string decorrelate).

Nevertheless the stretching behaviour may be more complicated than that described above. Consecutive unfolding of different domains may give rise to a complicated *sawtooth* pattern behaviour, as pointed out for the first time with titin [18] (see Fig. 2.6) and confirmed by Fisher et al. in [7]. The characteristic sawtooth pattern of unfolding can be explained as stepwise increases in the contour length of a polymer whose elastic properties are described by the WLC model. Fig. 2.6 shows a force extension curve obtained by stretching of a single Ig8 titin fragment (a recombinant titin fragment consisting of an 8-Ig segment in the I-band of titin, see Ref. [18]). Several peaks are evident. The force vs extension curve ($F(x)$ vs x) leading up to each peak

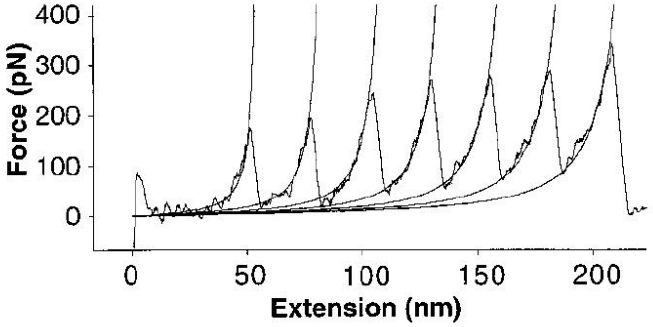

Figure 2.6: Sawtooth pattern of the unfolding of a single Ig8 titin fragment (from Ref. [18]).

is well described by the WLC equation (see Ref. [11]):

$$\beta L_p F(x) = \frac{1}{4(1-x/L_c)^2} - \frac{1}{4} + \frac{x}{L_c}, \tag{2.1}$$

with a persistence length $L_p = 0.4$ nm and contour length L_c that goes from 58 nm (first peak) and then increases by $28 - 29$ nm for every peak due to each Ig domain unfolding. This value is close to the 30 nm predicted by fully extending a polypeptide chain comprising 89 amino acids (minus a folded length of 4 nm) [18]. Unfolding of the first domain reduces the force to zero, whereas unfolding of consecutive domains reduces the force to a lesser extent. This is easily explained, since every domain lengthens the polypeptide and reduces the peak force to this predicted by the WLC model with a increased contour length.

The WLC model was firstly used to model the entropic elasticity of λ-phage DNA [11, 19]. As pointed out, DNA is unique among polymers both for its size and for its long persistence length, $L_p \simeq 50$ nm. Due to this rather peculiar feature DNA was extensively studied and many theoretical models were proposed to rationalize experimental data.

First of all double-stranded DNA (dsDNA) or B-DNA is, as already said, *very stiff*. This implies many simplifications:

- the applied force reduces the entropy of the chain;
- self-interactions are considered negligible;
- a simple elastic model is usually used.

Then, an equilibrium statistical mechanics approach is highly desiderable. During past years many models were proposed: the Edwards model [20] and the freely jointed chain (FJC) model (see Appendix A and Ref. [3]). The former describes the polymer as a chain of beads connected by springs, interacting *via* a δ-like repulsive potential. The latter depicts a chain of beads joined by rigid connections, whose orientation is free to rotate. For the FJC model an exact solution can be given (see Appendix A):

$$\frac{\langle x \rangle}{L_c} = \coth(\beta F b) - \frac{1}{\beta F b}, \tag{2.2}$$

where b is the so called Kuhn length[2].

Both these models ignore the elastic behaviour of the polymer and they are able to fit only the low force data. In particular, the main difference between Eqs. (2.1) and (2.2) is that they predict completely *different* large force behaviours:

$$1 - \frac{\langle x \rangle}{L_c} \simeq \begin{cases} 1/\sqrt{F} & \text{(WLC)} \\ 1/F & \text{(FJC)} \end{cases}. \tag{2.3}$$

In Fig. 2.7 (from Ref. [11]), a plot of experimental data together with the two fits of Eqs. (2.1) and (2.2) is reproduced. The disagreement with the FJC model (dashed line) is evident.

In Ref. [22], Odijk proposed an interesting and simple theory that adds to the hamiltonian of the bare WLC model a term which takes into account the intrinsic elasticity of the polymer. In the large force regime, this term contributes with a linear (Hooke-like) term to the force vs extension relation. The final equation is:

$$\frac{\langle x \rangle}{L_c} = 1 - \frac{1}{2\sqrt{\beta L_p F}} + \frac{F}{K_0}. \tag{2.4}$$

Here, K_0 is an elastic constant with dimension of force. As described in the caption of Fig. 2.7, $K_0 = 500 k_B T/\text{nm}$. The Odijk model predicts a *crossover* between the entropic regime described by the WLC behaviour, Eq. (2.1), and the enthalpic regime where the dsDNA follows the Hooke's law.

In Ref. [23], Smith et al. proposed a similar theory to study a conformational transition in an overstretching experiment on DNA. They, simply, added a stretching modulus to the bare FJC model, obtaining the following equation

$$\frac{\langle x \rangle}{L_c} = \left[\coth(2\beta F L_p) - \frac{1}{2\beta F L_p}\right]\left(1 + \frac{F}{K_0}\right). \tag{2.5}$$

[2]For a rigorous definition of the Kuhn length, see Appendix A.

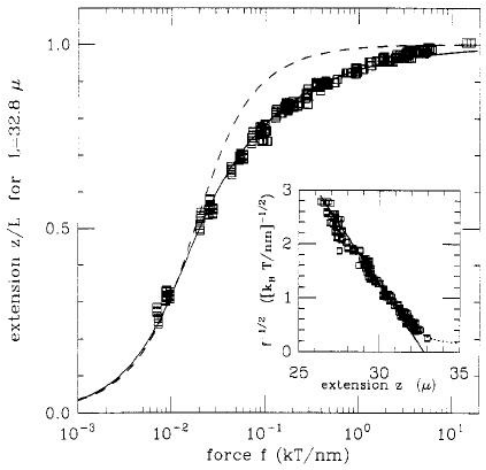

Figure 2.7: Solid line: fit of Eq. (2.1) to experimental data of Smith et al. [21] (97004 bp DNA, 10 mM Na^+). The predicted fitting parameters are $L_c = 32.8$ μm and $L_p = 53$ nm. Dashed line: the FJC result, Eq. (2.2), for $b = 2L_p = 100$ nm (see Appendix B) approximates the data well only in the low force regime. Inset: $F^{-1/2}$ vs x for the highest force; the WLC result (solid line) is in this plot a straight line extrapolating to $L_c = 32.8$ μm from which the experimental points begin to diverge above $x \simeq 31$ μm; including intrinsic elasticity (see Eq. 2.4) with $K_0 = 500 k_B T/$nm, dotted curve, improves the fit (from Ref. [11]).

The authors observed that under a longitudinal stress of ~ 65 pN, dsDNA molecules in aqueous buffer undergo a highly cooperative transition into a stable form with 5.8 Å rise per base pair, that is, 70% longer than B-form dsDNA. When the stress was relaxed below 65 pN, the molecules rapidly and reversibly contracted to their normal contour lengths. This transition was affected by changes in the ionic strength of the medium and the water activity or by cross-linking of the two strands of dsDNA. Individual molecules of single-stranded DNA (ssDNA) were also stretched giving a persistence length of 7.5 Å and a stretch modulus of 800 pN. The overstretched form may play a significant role in the energetics of DNA recombination.

In the following, we are going to describe three experiments [24, 25] on the stretching behaviour of DNA molecules under various solvent conditions. For the sake of convenience, we shall call them EXP1, EXP2 and EXP3, respectively.

1. **EXP1**:

   The $F - x$ curve of a single λ DNA molecule under various ionic conditions is plotted in Fig. 2.8. In the presence of monovalent cations the curve displays a WLC behaviour, with a persistence length $L_p = 95$ nm and a contour length $L_c = 16.5$ μm. When strong condensing agents (such as 25 μM CoHex or 100 μM spermidine) are added to the solution, the high force regime is characterized by a lower stiffness. The low force behaviour shows a new regime: a force plateau appears near three-fourths maximal extension ($x = 13 - 14$ μm) and stretched λ DNA molecules abruptly depart from WLC behaviour. Moreover, this behaviour is reproducible during both stretch and release cycle.

2. **EXP2**:

   In Ref. [25], the authors obtained a similar result, recording the stretching behaviour of a single DNA molecule under different solvent conditions. Fig. 2.9 shows the force-extension curve before and after the solution exchange. The above force change was observed at (A $\rightarrow$ B). When the DNA molecule was stretched after the solution exchange a force plateau at $1.6 \sim 2$ pN was observed at (B $\rightarrow$ C). It is considered that the force plateau indicates a coil-globule bimodal state due to an intramolecular collapse. After the molecule was stretched at D, the molecule was relaxed. In this relaxed process, the force plateau could not be observed (D $\rightarrow$ C $\rightarrow$ A). Then, the stretched and relaxed processes were repeated; however, the force plateau could not be observed (A $\rightleftharpoons$ C $\rightleftharpoons$ D). In this case, the $f - x$ curve is well fit in Eq. (2.1) with $L_p = 27$ nm and $L_c = 5.0$ μm. After the intramolecular collapse, the hysteresis on the $f - x$ curve was observed in the stretched and relaxed processes.

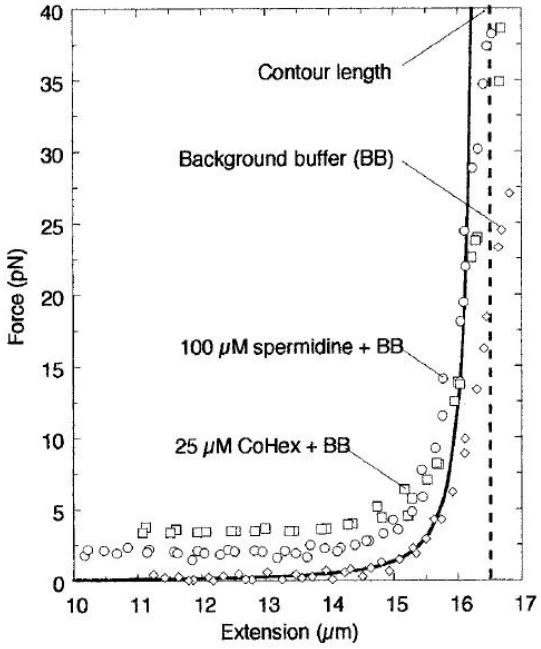

Figure 2.8: Response of single λ DNA molecules to an applied force with condensing concentrations of the trivalent cations CoHex and spermidine. The molecule in the low monovalent salt background buffer ($\Diamond$) displayed low and high force entropic elasticity indicative of a WLC with $L_p = 95$ nm and $L_c = 16.5$ μm (*solid curve*). Upon addition of either 25 μM CoHex ($\Box$) or 100 μM spermidine ($\circ$) to this low monovalent salt buffer, λ DNA molecules displayed high force elasticity indicative of a WLC with increased chain flexibility ($L_p < 50$ nm). Near three-fourths extension ($x = 13 - 14$ μm), an abrupt loss of WLC behaviour occurred, replaced by a force plateau ($1 - 4$ pN in magnitude) which was reproducible during both stretch and release cycles. The *vertical broken line* represents the B form contour length of λ DNA (from Ref. [24]).

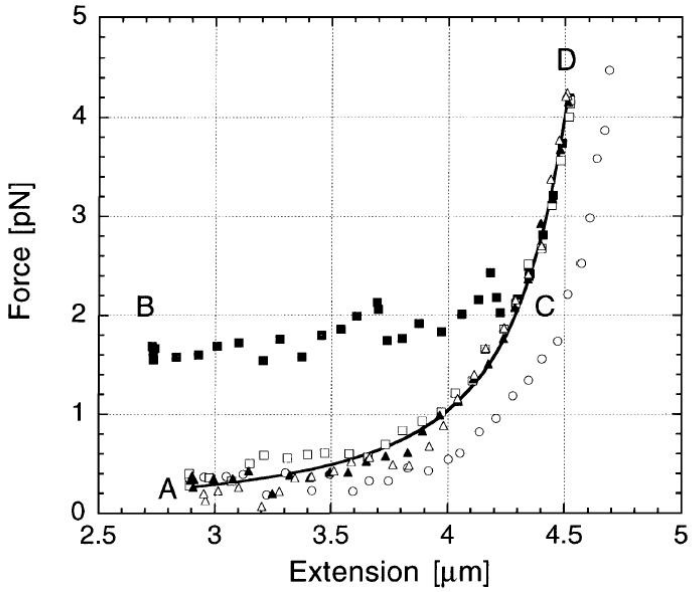

Figure 2.9: The $f - x$ curve before and after the exchange of the solution in the sample cell from buffer solution to 2 mM spermidine. Before the exchange (open circle) the DNA molecule was stretched at A. After the exchange the force increased at B, and then the DNA molecule was stretched (solid square) to D following the force plateau (B $\rightarrow$ C). When the molecule was relaxed (open square) the force plateau could not be observed (D $\rightarrow$ C $\rightarrow$ A). After reaching A, though the stretched (solid triangle) and relaxed (open triangle) processes were repeated, the force plateau could not be observed (A $\rightleftharpoons$ C $\rightleftharpoons$ D). The solid line describes the WLC in Eq. (2.1) with $L_p = 27$ nm and $L_c = 5.0$ μm (from Ref. [25]).

3. **EXP3**:

   Another experiment recorded the force-extension relation for plasmid-length DNA molecules at relatively high spermidine concentrations ($> 200\ \mu$M), where most of the DNA molecules are condensed and only a small fraction are not condensed. In Fig. 2.10(A), the $F-x$ curve for *uncondensed* molecules is plotted. The data follow a WLC behaviour, with $L_p = 38.25$ nm and $L_c = 1324$ nm. In Fig. 2.10(B) and (C), the $F - x$ curve for condensed molecules show two different behaviours: a stick-release pattern and a plateau, respectively. The first behaviour is similar to the experiment reproduced in Fig. 2.6: the DNA begins with a given stiffness and apparent contour length, and then slips into a different stiffness and contour length. The $F - x$ curves preceding the four peaks in Fig. 2.10 represent polymers of decreasing stiffness (see the caption, for more details). The completely stretched polymer has a stiffness identical to an uncondensed DNA tether ($L_p \simeq 40$ nm). Again, this phenomenon can be due to the release of successive turns of DNA in a coiled structure. A condensed plasmid forms several *independent* condensed globules. The plateau reproduced in Fig. 2.10(C) is reminiscent of the overstretching behaviour of DNA discussed above [23] and may be due to an interaction between two or more condensed DNA tethers.

EXP1 and EXP2 seem to be in apparent conflict with the results of EXP3. A possible explanation on this *puzzling* question will be given in Sec. 3.2.

2.3 Conclusions

In this Chapter we have introduced some recent techniques probing the stretching behaviour of polymers. After a brief description of the most popular devices we have focused on some recent intriguing results.

- We have shown that, under condensing conditions, some polymers such as titin [18] (Fig. 2.6) and plasmid-length DNA [24] (Fig. 2.10) unfolds following a sawtooth pattern. This reveals a cooperative mechanism through which different polymer domains successively unfold. Every unfolding domain pathway is well described by the WLC model.

- This result seems to be in contrast with other experimental results obtained studying the stretching behaviour under condensing conditions of λ DNA. In

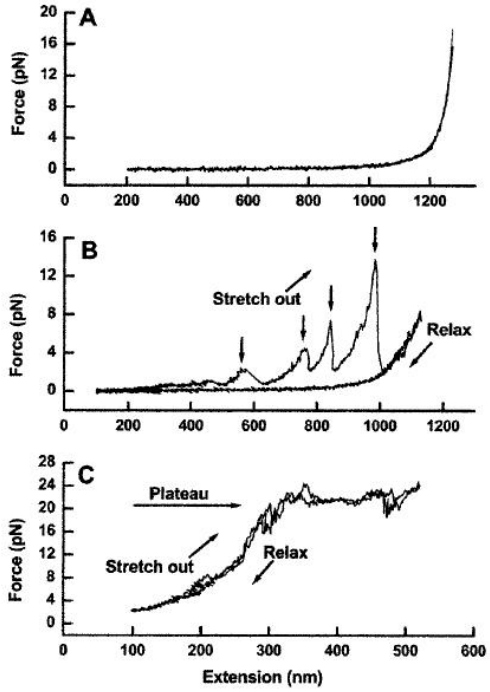

Figure 2.10: Stretching plasmid-length DNA tethers at condensing conditions where the spermidine > 200 μM. (A) Uncondensed molecules displayed force-extension curves characteristics of a worm-like chain. Data at $F < 5$ pN was well fit by Eq. (2.1), yielding $L_p = 38.25$ nm and $L_c = 1324$ nm (*solid line*). Force-extension curves for condensed DNA molecules showed two distinct behaviours. (B) Most of the curves showed a stick-release pattern. Here the DNA molecule begins with a given stiffness and apparent contour length, and slips into a different stiffness and contour length, with a variable degree of slip (100-150 nm). The $F - x$ curves preceding the four force peaks represent polymers of decreasing stiffness ($L_p = 24, 19, 18$, and 11 nm from left to right), with the completely stretched polymer possessing a stiffness identical to an uncondensed DNA tether ($L_p = 40$ nm). During the relaxing phase, the DNA shows no stick-release behaviour, but the $F - x$ curve displays hysteresis. (C) A few DNA tethers show a force plateau behaviour during both stretch and release. The $F - x$ curve displays a plateau (~ 20 pN) where little or no additional force is required for increased extension (from Ref. [24]).

fact, these curves show a clear force *plateau* (Fig. 2.8), as the one observed also in Fig. 2.9 during a stretching experiment of a collapsed single DNA molecule.

In Chap. 3, we shall show that this question can be answered in the framework of a very simple model.

Chapter 3

Stretching of a polymer below the θ point

That Crawford Tillinghast should ever have studied science and philosophy was a mistake. These things should be left to the frigid and impersonal investigator for they offer two equally tragic alternatives to the man of feeling and action; despair, if he fail in his quest, and terrors unutterable and unimaginable if he succeed.

Howard Phillips Lovecraft, *From Beyond*

As already stressed, new experimental tools (see Chap. 2) make it possible to monitor the behaviour under tension of various biopolymers and then to elucidate the mechanism of some force-driven phase transitions occurring at the single molecule level, such as the unfolding of the giant titin protein [18, 26], the stretching of single collapsed DNA molecules [24, 27], the unzipping of DNA [6]. Theoretically, on the other hand, quite a few statistical mechanics models have been subsequently proposed to explain the experimental results and to identify the physical mechanisms behind these phase transitions [28, 29, 30, 31, 32, 33, 34, 35, 36, 37].

In particular, the nature of the collapsed phase that a polymer attains in poor solvent conditions (see Appendix D and Ref. [10]) is still under debate (see e.g. [38, 39] and references therein). Until very recently, most of the existing studies on this subject dealt with refined version of the mean field studies originally proposed in Ref. [28]. A common characteristic of such studies is that, for a self-attracting polymer, they predict a first order phase transition in any dimension at a critical force $f_c(T)$. At temperatures below the θ-transition, where the self-attraction prevails, and for an applied force less than f_c the polymer is in a compact phase. For forces greater than

f_c the self-attraction is unable to maintain the polymer in its compact conformation and the polymer chain is stretched along the force direction. However in $d = 2$ extensive Monte-Carlo simulations [32], performed on a self-avoiding walk (SAW) model, suggested that the transition is second order. An exactly solvable model, on a lattice of fractal dimension 2, has been analyzed in Ref. [33] and a second order transition was found at a critical force $f_c(T)$.

In the following we shall propose some simple models which will clarify some aspects on this important issue.

The Chapter is organized as follows:

- In Sec. 3.1 we shall introduce an exactly solvable model for a stretched self-interacting directed self-avoiding walk (DSAW) on a $2d$ lattice; a complete characterization of the unfolding transition is given. In particular, the phase diagram in the (T, f)-plane is found exactly and the phase transition is found to be *second* order.

- In Sec. 3.2 (see also Ref. [40]) we shall make the previous model more realistic, studying an on-lattice (off-lattice) model of self-interacting self-avoiding walk (SAW) in $d = 2$ ($d = 3$).

    1. Studying the ground state conformations of our models, we shall give a simpler explanation about some recent experimental results (see Sec. 2.3).
    2. In $d = 2$, we also characterize the thermodynamic behaviour of the SAW and the corresponding phase diagram is found numerically.
    3. A rationale was given for the change in order of the transition as the spatial dimension, d, goes past 2, by means of a renormalization group based argument. Within that framework, it was found that, near criticality, the projection of the end-to-end distance along the force direction per monomer goes like $(f - f_c)^{1/\Delta - 1}$ ($f > f_c$), near the phase transition, where Δ is a *new* critical exponent. Numerical uncertainties are too big to critically test this prediction in the SAW model of Refs. [32, 40], whereas $\Delta = 2/3$ for the DSAW model (i.e. the transition is second order [32]).
    4. Another feature of interest of the $2d$ SAW model is that the transition line $f_c(T)$ shows a re-entrance at low temperature, i.e. $f_c(T)$ increases at low T and after reaching a maximum it decreases becoming zero at T_θ, the temperature of the θ-transition. The re-entrant behaviour is due to the fact that, in the low T limit, since the entropy does not play any role, the

energy dominates the free energy and the open chain is the most favorable configuration. Let us notice that this behaviour is similar to the one found in theoretical models of pulling of double stranded DNA [37, 41, 42].

3.1 Directed polymers: an exactly solvable case

As already anticipated, in this Section we study the thermodynamics of an exactly solvable model of a $2d$ self-interacting partially directed self-avoiding walk (DSAW), i.e. steps with negative projection along the $x-$axis, $(1,0)$, are forbidden. This model proved to be helpful in the past in order to find the phase diagram in the (temperature, fugacity) plane for a simplified θ transition [43, 44, 45, 46, 47]. We take advantage of previous contributions and generalize the model to the presence of a pulling force along the direction $(1,0)$ (see also Ref. [48]). With a sophisticated enumeration technique [46] we show the correlation critical exponent, ν, takes on a non trivial value on the critical line, numerically very close to $\nu_\theta = 2/3$, the exponent at the θ transition. It is not clear whether this is an accidental degeneracy or if it can apply also in the undirected case, too. For example in the $3d$ Sierpinski gasket an exact renormalization leads to a non trivial f-dependence of ν [33].

This Section is structured as follows. In Subsec. 3.1.1, we introduce the model and the basic quantities of interest. In Subsec. 3.1.2, we outline how the transfer matrix can be applied to our model, find explicitly the phase diagram (critical line) and give a rough estimate of the exponent Δ. A scaling argument is proposed to suggest that at criticality $\nu = \Delta$. In Subsec. 3.1.3, we review the enumeration technique proposed in Ref. [46], which we use in Subsec. 3.1.4 in order to estimate the value of ν on the critical line. In Subsec. 3.1.5, we critically analyze our scaling ansatz and the hypothesis that $\nu = \Delta$. Finally, in Subsec. 3.1.6 we draw our conclusions. In Appendix E, we derive the *exact* critical exponents in the continuum approximation, through a technique developed in Ref. [47] and generalized for $f \neq 0$.

3.1.1 The model

The model is a DSAW on a two-dimensional square lattice (see Fig. 3.1), with (non-consecutive) nearest-neighbor interactions. A force $\mathbf{f}$, directed along the same axis of the walk, is pulling on one end of the DSAW, the other one being fixed at the origin. Given a particular configuration $\mathcal{C}$ the energy is

$$E_{\mathcal{C}} = -\epsilon m - f R_x, \tag{3.1}$$

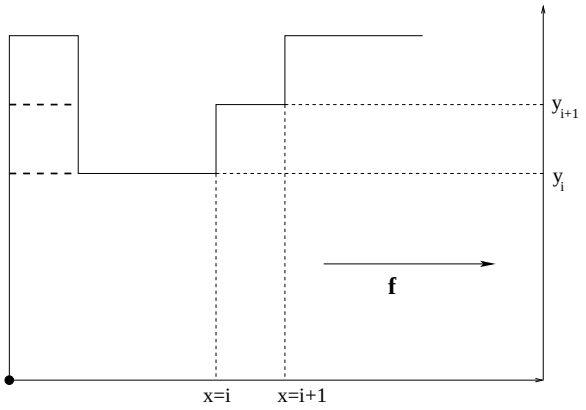

Figure 3.1: An example of DSAW configuration. The quantities y_i and the force direction are also displayed. Thick dashed lines indicate contacts.

where m is the number of interacting pairs and ϵ the energy per pairs, f the modulus of the applied force and R_x the longitudinal extension of the walk. Then, the canonical partition function can be written

$$\mathcal{Q}_L = \mathcal{Q}_L(\beta\epsilon, \beta f) = \sum_{\mathcal{C}} e^{-\beta E_{\mathcal{C}}}, \tag{3.2}$$

where L is the number of the steps of the walk and $\beta^{-1} = T$, is the temperature in units of the Boltzmann constant. From now on will set $\epsilon = 1$ without loss of generality. From the canonical partition function we construct the grancanonical partition function (generating function),

$$\mathcal{G}(T, f, z) = \sum_{L=1}^{\infty} \mathcal{Q}_L z^L, \tag{3.3}$$

z being the step fugacity. The (real) singularity closest to the origin, $z_c(T, f)$, of the generating function Eq. (3.3) is related to the free energy per monomer as follows

$$\ln z_c(T, f) = -\lim_{L\to\infty} \frac{\ln \mathcal{Q}_L}{L} \tag{3.4}$$

From the singularities of the generating function when $f = 0$, a complete phase diagram can be extracted (see Refs. [44, 45, 47]). In particular, a singularity is found in the free energy at $T = T_\theta$, called the θ temperature.

3.1.2 Transfer matrix calculations and phase diagram

Starting from the definition of the generating function, Eq. (3.3), when $f = 0$, we observe that it can be conveniently rewritten [43, 44] as

$$\mathcal{G}(T, f, z) = \sum_{L_x} \mathcal{G}_{L_x}(T, z) \exp(\beta f L_x), \tag{3.5}$$

where $\mathcal{G}_{L_x} = \sum_L \mathcal{Q}_{L,L_x} z^L$, $\mathcal{Q}_{L,L_x}$ being the partition function restricted to walks of total length L of which L_x steps are along the x direction.

This is useful because now $\mathcal{G}_{L_x}$ can be written in terms of a transfer matrix, T, of dimensionality L_y^2, where L_y is the size of our system along the y-direction [43, 44][1]. Such a transfer matrix T is defined via its actions on the vectors $\{v_i\}_{i=1,\ldots,L_y^2}$, with $v_i = (y_i, y_{i+1})$, y_i being the height of the site in the $i-$th row which precedes the right-bound horizontal link in that column (see Fig. 3.1), as follows:

$$T(v_i, v_{i+1}) = \exp[\beta (\min\{|r_i|, |r_{i+1}|\})\Theta(-r_i \cdot r_{i+1})] \exp[(|r_i| + 1) \ln z]. \tag{3.6}$$

where $r_i = y_{i+1} - y_i$ and $\Theta(x)$ is the Heaviside step function. It can be shown that $\mathcal{G}(T, f = 0, z)$ develops a singularity when λ, the largest eigenvalue of T, goes through 1 [49]. This means that for large L_x

$$\mathcal{G}_{L_x} \propto (\lambda(T, z))^{L_x}. \tag{3.7}$$

Consequently the force-dependent singularity, $z_c(T, f)$ occurs when

$$\lambda(T, z) \exp(\beta f) = 1. \tag{3.8}$$

Eq. (3.8) has a rather deep consequence. If the critical fugacity and hence the free energy has to display a singularity at a non-zero value of the force, i.e. in order for the force induced unfolding transition to exist as a thermodynamic transition and not only as a crossover, it is necessary that $\lambda(T, z)$, the largest eigenvalue of the transfer matrix when there is no force, has itself a singularity as z approaches $z_c(T, f = 0) \equiv {z_c}^2$. Otherwise, from Eq. (3.8) it is clear that there can be no such singularity. If there is a transition, then we get the following equation for the critical force:

$$f_c(T) = -T \lim_{z \to z_c^-} \ln \lambda(T, z). \tag{3.9}$$

[1] A brief introduction to the transfer matrix formalism applied to the SAW problem is given in Appendix G.

[2] Here we are *conjecturing* that the smallest singularity comes only from z_c, which from now on indicates the singularity at $f = 0$ and $T < T_\theta$.

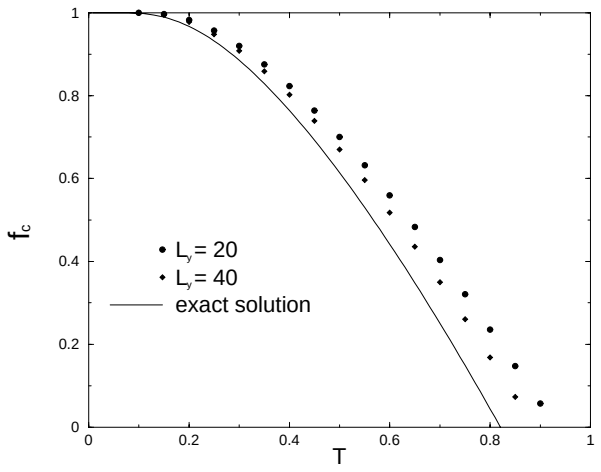

Figure 3.2: Exact critical line as in Eq. (3.11) together with points corresponding to estimates with the transfer matrix calculation, with strip size $L_y = 20, 40$.

In Eq. (3.9) the value of λ to be put in the right hand side of the equation is the one pertaining to the infinite system. $\lambda(T, z)$ for z slightly less than z_c is plotted in Fig. 3.3 with a lateral size L_y up to 40. It is rather clear that a singularity has to be expected at $z = z_c$ in the infinite size limit. It was indeed shown [44, 45] that for $T < T_\theta$ ($T_\theta = 0.8205\ldots$ in this model) there is a singularity of the grand partition function for $z = z_c = \exp(-\beta)$ and for this value of the fugacity the biggest eigenvalue is strictly smaller than 1, being [44]:

$$\lambda(\beta, z = z_c = \exp(-\beta)) \equiv \lambda(\beta) = \frac{z_c\left(1 + \sqrt{z_c}\right)}{1 - \sqrt{z_c}}. \tag{3.10}$$

The θ transition temperature is obtained when $\lambda(\beta, z = z_c = \exp(-\beta)) = 1$. Consequently, the critical line, $f_c(T)$, is obtained by putting $\lambda(\beta) = \exp\left(-\beta f_c(T)\right)$, i.e.:

$$f_c(T) = T \ln\left[\frac{1 - \exp\left(-\beta/2\right)}{\exp\left(-\beta\right)\left(1 + \exp\left(-\beta/2\right)\right)}\right], \tag{3.11}$$

and is plotted in Fig. 3.2, where also the results obtained with the transfer matrix with system size up to $L_y = 40$ are displayed. In view of Eqs. (3.8) and (3.9), we can define a new critical exponent Δ which characterizes the directed self-avoiding walk. From Eq. (3.9), if the largest eigenvalue approaches its limit value according to the law:

$$\lambda(z_c^-) - \lambda(z) \sim (z_c - z)^\Delta \tag{3.12}$$

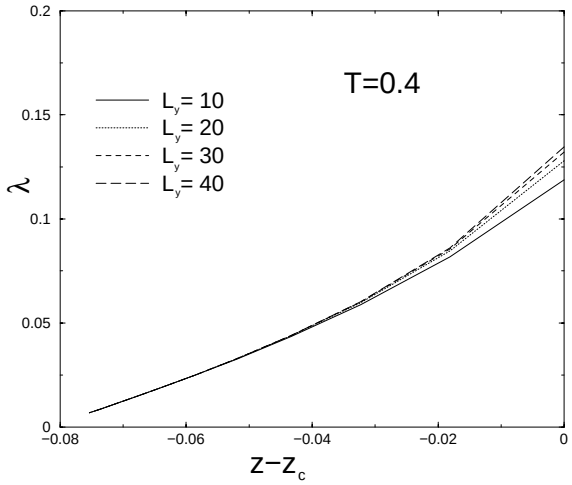

Figure 3.3: Plot of the largest eigenvalue ($T = 0.4 < T_\theta$) versus z. It is apparent that the largest eigenvalue approaches a limit value as z approaches $z_c = \exp(-\beta)$ (< 1) from below. Thus a transition exists in the thermodynamic sense.

then one straightforwardly obtains (via Eqs. (3.8) and (3.9))

$$\lim_{L\to\infty} \frac{\langle R_x(L)\rangle}{L} \sim (f - f_c(T))^{1/\Delta - 1} \tag{3.13}$$

where $\langle R_x(L)\rangle$ is the average projection of the end-to-end distance of the DSAW along the axis $(1, 0)$. From Fig. 3.3 we estimated $1/2 < \Delta < 1$, with $\Delta \simeq 0.7$ though a precise determination is difficult. If $\Delta < 1$ we call the transition second order. It is widely accepted that for $d > 2$ the transition is first order and so $\Delta = 1$. In the Sec. 3.2 a renormalization group based argument in $d = 2$, on the other hand, will give for the (undirected) SAW $\Delta = 1/2$. This argument would apply also to the present case. Given that the transition is second order in our model, it is also sensible to look for the value of the critical exponent ν (defined as $R_g \sim L^\nu$, for large number of steps L, where R_g is the gyration radius of the $L-$site polymer. In Section 3.1.5, using a scaling argument, we shall demonstrate that $\nu = \Delta$.

In the next Subsection, we shall study the complete canonical partition function, Eq. (3.2), using a powerful method of exact enumeration introduced in [46], that allows us to reach large values of L.

3.1.3 The method of enumeration

As already said, the configurations of the model are directed walks on a two-dimensional square lattice with nearest-neighbor interactions. For convenience, we demand that these walks end with a horizontal segment. Since the walks are directed in the x-direction we can describe these configurations through the distance r_i between two horizontal steps, measured in the positive y direction. Thus, we associate to each configuration an N-tuple $(r_1, r_2, ..., r_N)$ corresponding to a configuration of total length $L = \sum_{i=1}^{N} |r_i| + N$.

The energy due to the nearest-neighbor interactions for each of these configurations is (see Eq. (3.6))

$$U(r_1, r_2, ..., r_N) = -\sum_{i=1}^{N-1} \min(|r_i|, |r_{i+1}|)\Theta(-r_i \cdot r_{i+1}). \tag{3.14}$$

In the following, we assign weights x for steps in the horizontal direction and y for steps in the vertical direction. Then, the canonical partition function is

$$\mathcal{Q}_L(x, y, \omega) = \sum_{N=1}^{L} (xe^{\beta f})^N \sum_{|r_1|+|r_2|+...+|r_N|=L-N} y^{L-N} \omega^{U(r_1,r_2,...,r_N)},$$

where $\omega = \exp(\beta)$.

Now, it is convenient to consider the partition functions $\mathcal{Z}_L^{(r)} = \mathcal{Z}_L^{(r)}(x, y, \omega)$ for walks of total length $L + 1$ which start with a vertical segment of height r. Then, we have

$$\mathcal{Q}_{L+1}(x, y, \omega) = \sum_{r=-L}^{L} \mathcal{Z}_L^{(r)}, \tag{3.15}$$

(note that $\mathcal{Z}_L^{(0)} = x\mathcal{Q}_L(x, y, \omega)$) which satisfies the following recursion relation

$$\mathcal{Z}_L^{(r)} = xy^{|r|} \left\{ \delta_{|r|,L} + e^{\beta f} \sum_{s=-L+|r|+1}^{L-|r|-1} \omega^{U(r,s)} \mathcal{Z}_{L-|r|-1}^{(s)} \right\}, \tag{3.16}$$

obtained concatenating these walks. In Eq. (3.16), $r = -L, ..., L$, with $L = 0, 1, 2, ...$ Using the symmetry $\mathcal{Z}_L^{(r)} = \mathcal{Z}_L^{(-r)}$, Eq. (3.16) can be written only for non negative r as

$$\mathcal{Z}_L^{(r)} = xy^r \left\{ \delta_{r,L} + e^{\beta f} \sum_{s=0}^{L-r-1} \mathcal{Z}_{L-r-1}^{(s)} + e^{\beta f} \sum_{s=1}^{L-r-1} \omega^{\min(r,s)} \mathcal{Z}_{L-r-1}^{(s)} \right\}. \tag{3.17}$$

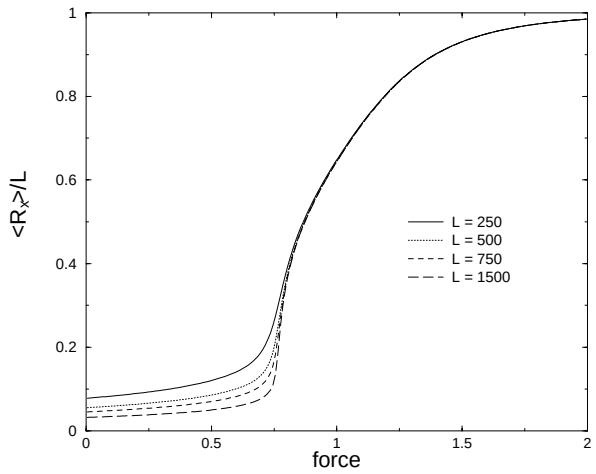

Figure 3.4: Plot of $\langle R_x(L)\rangle/L$ vs. f for various length, L, of the walk.

Setting $x = y = 1$ in (3.17), we obtain the iteration scheme and the free energy $\mathcal{F}_L(\omega) = -\frac{1}{\beta L}\ln \mathcal{Z}_L^{(0)}$. The average longitudinal length of the walk $\langle R_x(L)\rangle$ is simply

$$\langle R_x(L)\rangle = \frac{\partial}{\partial(\beta f)}\ln \mathcal{Z}_L^{(0)}. \tag{3.18}$$

Then, we shall proceed as follows:

1. we calculate the free energy using the iteration scheme proposed in Eq. (3.17);
2. using Eq. (3.18), we determine how the quantity $\langle R_x(L)\rangle/L$ varies against the applied force f.

3.1.4 Results

The plot of $\langle R_x(L)\rangle/L$ vs. f for various values of L is represented on Fig. 3.4 at $T = 0.4$ which is below the θ transition occurring at $T_\theta \simeq 0.8205...$. From Eq. (3.11) we have $f_c(T = 0.4) \simeq 0.764...$

From a careful examination of Fig. 3.4, we deduce that the quantity $\langle R_x(L)\rangle/L$ decreases as $L^{\nu-1}$, where the *critical exponent* ν might depend on the temperature T. In particular the data are consistent with $\nu < 1$ if $f \leq f_c(T)$ and $\nu = 1$ if $f > f_c(T)$. In order to find more precise values for the critical exponent, we shall proceed along the same lines of Ref. [46].

An estimation of the critical exponent through the use of the Padé approximants (see, e.g., A. J. Guttman in [50]) is given in Table 3.1.

f	ν	L
$< f_c$	$0.501(7)$	≤ 1900
$= f_c$	$0.68(8)$	≤ 1900
$> f_c$	1.00000	≤ 1300

Table 3.1: Estimates for the critical exponents from a Padé approximants analysis. Note that in the $f > f_c$ case the error is completely negligible.

Our estimate of the critical exponent, at the critical force, is close to $\frac{2}{3}$, the ν value at the θ point at $f = 0$ [45, 47]. As shown in Appendix E, this is the *exact* value.

To get a deeper insight, let us define an $L-$dependent critical exponent $\nu(L)$ through the formula

$$\nu(L) = \frac{\ln\langle R_x(L+1)\rangle - \ln\langle R_x(L)\rangle}{\ln(L+1) - \ln L} \tag{3.19}$$

Plotting $\nu(L)$ versus an estimated correction-to-scaling term a careful extrapolation to $L \to \infty$ can be performed, determining the critical exponent ν for all the values of the force. Let us consider three different regimes:

1. $f < f_c$.

   As an example let us consider $f = 0.4$. We have found that successive estimates for the exponent $\nu - 1$ with increasing L follow a straight line when plotted against a correction-to-scaling term of $1/L^{0.5}$ (see also the case of Ref. [46] at $f = 0$). The plot is shown in Fig. 3.5. The extrapolated value for $L \to \infty$ gives $\nu - 1 \simeq -0.4998$, then $\nu \simeq \frac{1}{2}$, the exponent typical of a compact phase.

2. $f > f_c$.

   As before, we have plotted the exponent $\nu - 1$ against a well-defined correction-to-scaling term. Now, this term is order of $1/L$. Fig. 3.6 shows the $f = 1.0$ case as typical example. Now, the extrapolated value gives $\nu - 1 \simeq 3.0 \times 10^{-6}$, then $\nu = 1$ within the numerical precision.

3. $f = f_c$.

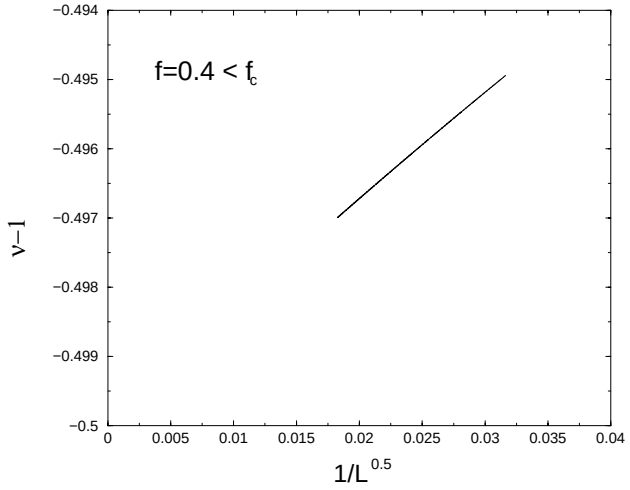

Figure 3.5: Plot of $\nu - 1$ vs. $1/L^{0.5}$, for $f < f_c$ and L up to 3000.

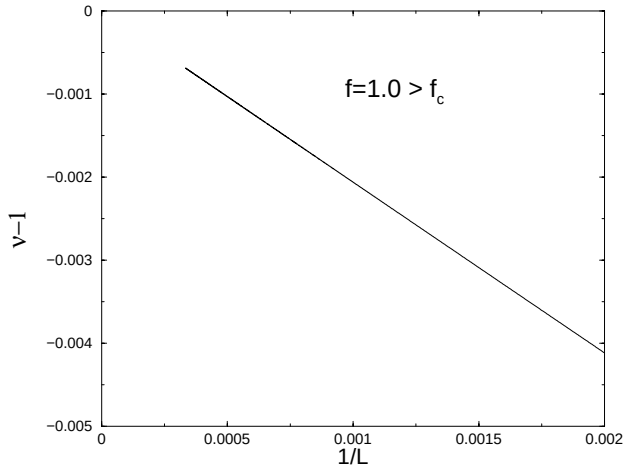

Figure 3.6: Plot of $\nu - 1$ vs. $1/L$, for $f > f_c$ and L up to 3000.

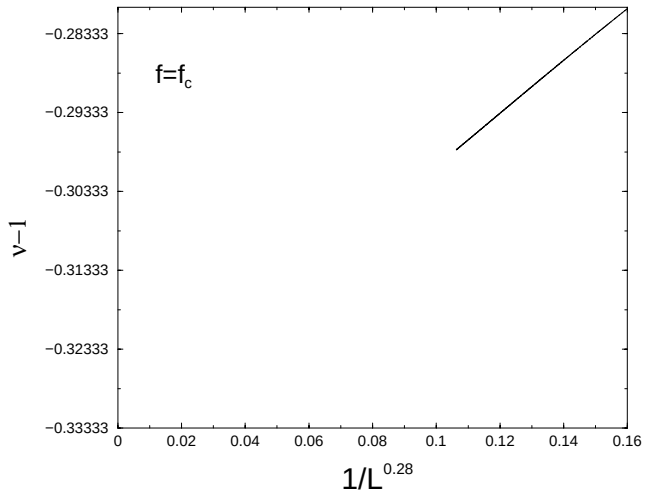

Figure 3.7: Plot of $\nu - 1$ vs. $1/L^{0.28}$, for $f = f_c$ and L up to 3000.

Now, the correction-to-scaling term is of $1/L^{0.28}$ (see Fig. 3.7) and $\nu - 1 \simeq -0.3336$, which implies $\nu \simeq \frac{2}{3}$.

Thus we find that the value of ν for $f = f_c(T)$ is equal (in the limit of numerical precision) to the value $\frac{2}{3}$, which corresponds to that for $f = 0$ at $T = T_\theta$ [45, 47]. This is a non trivial result. In particular, we have to expect that along all the critical line $f = f_c(T)$, ν takes the value $\frac{2}{3}$ (see also the Appendix E). Moreover, as pointed out in [47], the correction-to-scaling term when $f = 0$ and $T = T_\theta$ is of $1/L^{1/3}$. In our case, we found that this correction increases to $1/L^{0.28}$, for $T = 0.4$. Within the numerical errors, this implies that the correction to scaling term depends on force as well as on temperature[3].

Finally, in Table 3.2 we have summarized the above results.

In the next Subsection, we shall introduce a scaling theory that rationalizes what we have found on the critical behaviour of the average horizontal end-to-end displacement $\langle R_x(L) \rangle$.

3.1.5 Scaling theory

Our previous results suggest the following scaling ansatz (see also Ref. [32]):

$$\langle R_x(L) \rangle = L^\nu \Phi(\Delta f L^\psi) \tag{3.20}$$

[3]Let us remark that with other correction-to-scaling terms the data *do not* fall on a straight line.

f	ν
$< f_c$	$1/2$
$= f_c$	$2/3$
$> f_c$	1

Table 3.2: Estimates for the critical exponents from an extrapolation to $L \to \infty$, obtained plotting the L-dependent critical exponent $\nu(L)$, Eq. (3.19), versus an estimated correction-to-scaling term.

where $\Delta f \equiv f - f_c(T)$. The scaling function $\Phi(x)$ must have the following behaviour:

$$\Phi(x) \sim \begin{cases} x^{(1-\nu)/\psi} & \text{if} \quad x \to +\infty \\ \Phi_0 & \text{if} \quad x \to 0 \\ |x|^{(1/2-\nu)/\psi} & \text{if} \quad x \to -\infty \end{cases} , \tag{3.21}$$

with Φ_0 a *not*-zero constant value. Then, the quantity $\langle R_x(L) \rangle$ obeys to the equations:

$$\langle R_x(L) \rangle \sim \begin{cases} L \Delta f^{(1-\nu)/\psi} & \text{if} \quad \Delta f > 0, \quad \frac{1-\nu}{\psi} > 0 \\ L^{\nu} & \text{if} \quad \Delta f = 0 \\ L^{1/2} |\Delta f|^{(1/2-\nu)/\psi} & \text{if} \quad \Delta f < 0, \quad \frac{1/2-\nu}{\psi} < 0 \end{cases} , \tag{3.22}$$

in agreement with the results found in the previous Subsection.

Now, let us observe that the free energy contribution to the singular part is

$$\begin{aligned} \Delta F &= \langle R_x(L) \rangle f - \langle R_x(L) \rangle f_c = \langle R_x(L) \rangle \Delta f \\ &= \Delta f L^{\nu} \Phi(\Delta f L^{\psi}) \end{aligned} \tag{3.23}$$

where we have used Eq. (3.20) and f is the applied force. Since ΔF is a contribution to the *total* free energy (*not* a free energy density), we expect it depends only on the "dimensionless" combination of the scaling fields Δf and L with the appropriate

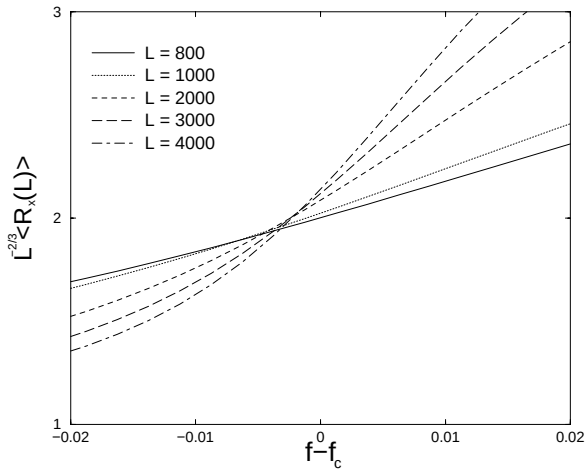

Figure 3.8: Plot of $\langle R_x(L)\rangle$ scaled by $L^{2/3}$ versus $f - f_c$. Finite size scaling corrections to the critical force are evident.

exponents. This implies that $\nu = \psi$. Comparing Eqs. (3.13) and (3.22), we deduce that $\Delta = \nu = 2/3$.

Let us again remark that it is not clear if the relation $\nu = 2/3$ is an accidental degeneracy due to the model. In fact, in Ref. [33], the authors found that for a $3d$ Sierpinski gasket $\nu = \nu(f)$. Anyway, we think that the relation $\nu = \psi$ has a more general validity and does not depend on the simple model described here.

Now, Eq. (3.20) can be written as $\langle R_x(L)\rangle = L^{2/3}\Phi(\Delta f L^{2/3})$.

To test this prediction, we have plotted in Fig. 3.8 the function $L^{-2/3}\langle R_x(L)\rangle$ versus $f - f_c$, where f_c is again determined from the exact formula, Eq. (3.11). It is evident that, apart from obvious finite size scaling corrections, our ansatz is justified. Then, we have derived the scaling function $\Phi(x)$. The final result is shown in Fig. 3.9.

3.1.6 Conclusions

In spite of the relative simplicity of the model studied above, the critical indices of the unfolding transition, which is second order, are not trivial.

- The transition is characterized by two exponents, the usual correlation length critical exponent ν, and one which we called Δ. In particular, the exponent ν at $f = f_c$ (see Eq. (3.22)) is different both from $1/2$, the collapsed polymer value, and from 1, the extended polymer value (see again Eq. (3.22)). The Δ expo-

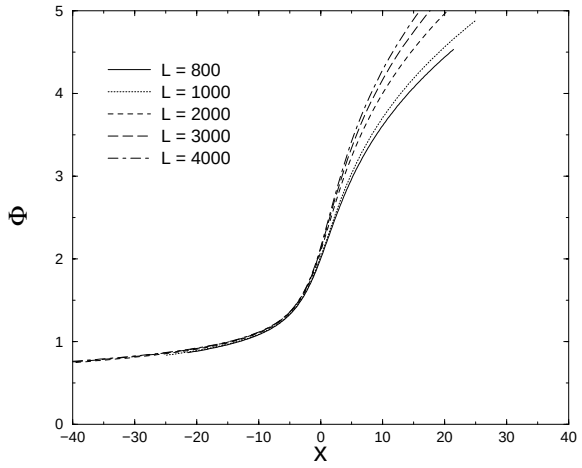

Figure 3.9: Successive estimates for the scaling function $\Phi(x)$ are shown for increasing lengths of the walk.

nent characterizes the singular behaviour of the chain elongation per monomer along the force direction as the critical force is approached from above (see Eq. (3.13)).

- Through a powerful enumeration technique taken from the literature [46], coupled with a finite size scaling to extrapolate our results to infinitely long chains, we find that ν is very close to $2/3$. A scaling analysis also suggests that $\nu = \Delta$ at least within our numerical precision.

In the Sec. 3.2, we are going to extend these results to the more important case of a self-interacting self-avoiding walk (SAW). Then, we shall also introduce some simple off-lattice models of polymers.

3.2 More sophisticated models

In this Section, the unfolding of a polymer below the θ point when pulled by an external force is studied introducing a $2d$ model on the lattice (self-interacting SAW) and a $3d$ off lattice model. As shown, we have found the following intriguing results:

- at $T = 0$ and for finite length chains, it is found that the globule unfolds via multiple steps, corresponding to transitions between different minima, in both cases. In $d = 3$ one of these intermediates is a regular helix. In the infinite length limit, these steps have a qualitative effect only in $d = 2$;

- the phase diagram in $d = 2$ is determined via the Transfer Matrix (TM) technique;

- we give a simple explanation about the questions arisen in Sec. 2.3, suggesting that different unfolding pathways may be due to the different contour lengths of the molecules studied.

To rationalize these results, energy-entropy and renormalization group arguments are given.

As described in Chap. 2, most cases of various force vs elongation (f vs x) curves recorded in experiments display three distinct regimes, and, in particular, a plateau for intermediate stretch [24, 25, 27]; whereas in a few examples, for shorter polymers, a stick-release peak pattern with hysteresis has been found. The first observation is in good agreement with the mean field theory proposed in Ref. [28], and the plateau strongly suggests the presence of a first order phase transition.

Our results suggest that there might be more than one possible shape for the f vs. x curves according to d, the spatial dimension and to polymer length. In particular our picture can qualitatively explain the peak pattern in Refs. [24, 25]. These models are interesting also on a purely theoretical ground. First, the numerical study recently performed in [32] has suggested that the transition may be second order in $d = 2$ and first order in $d = 3$. This has been confirmed to some extent in a hierarchical lattice model where the fractal dimension is 2 [33] and by our results sketched in Sec. 3.1.

Let us remark that the $d = 2$ case is important as it is below the upper critical dimension for θ collapse and mean field[4] predictions may well be incorrect. Then, a thorough analysis and a clear physical mechanism underlying the difference of the nature of the transition as d changes are needed. Second, the mean field analysis of Refs. [31, 51] has suggested there could be a re-entrant region [29] in the phase diagram for low temperature as the one observed for DNA unzipping [37]. However the exact results in [33] prove mean field is not valid in low dimensions.

Here we describe theoretically the unfolding transition of globules not relying on the mean field approximation. First of all, we characterize the evolution of the ground states of a finite polymer as the pulling force increases. Then, we compute the phase diagram in the temperature–force (T, f)-plane in $d = 2$ on the lattice, where we can use exact enumerations together with the Transfer Matrix method.

[4] Note that we use "mean field theory" in a broader sense, including approaches which consider the relative stability of the globule and the coil only (see also [31, 51]). Mean field theories should be all equivalent as regards universality.

3.2.1 Interacting SAWs on a $2d$ lattice

We begin by considering a self-avoiding walk (SAW) on the square lattice with *fixed* origin. The model partition function in the canonical ensemble in which T and f, the stretching force, are fixed is:

$$Z_N(f,T) = \sum_{\mathcal{C}} e^{-\beta H(\mathcal{C})} = \sum_{b,\mathbf{R}} w_{o\mathbf{R}}(N,b) e^{\beta(b\epsilon + f R_x)} \tag{3.24}$$

where N is the number of monomers (including the origin) of the SAW, $H(\mathcal{C})$ (referred to a configuration $\mathcal{C}$) is the energy of a SAW, b is the number of pairs of neighboring occupied sites not adjacent along the chain, $\beta \equiv 1/k_B T$ is the inverse temperature, $w_{o\mathbf{R}}(N,b)$ is the number of configurations of a SAW with fixed origin o and end-to-end distance $\mathbf{R}$, of length N and b contacts, R_x is the projection along the force direction (x axis) of $\mathbf{R}$. k_B and ϵ are again set to 1.

3.2.2 Phase diagram

Now, we want to characterize the thermodynamic behaviour of the SAW model. Then, we use the Transfer Matrix (TM) technique (see Appendix G and Ref. [49]).

It is convenient [49] to introduce the *generating function*

$$\mathcal{G}_{o\mathbf{R}} = \sum_{N,b} z^N e^{\beta b} w_{o\mathbf{R}}(N,b), \tag{3.25}$$

where z is the step fugacity. It is known that for $z < z_c(T) = 1/\mu(T)$, the inverse SAW connectivity, $\mathcal{G}_{o\mathbf{R}} \sim \exp[-R_x/\xi(z,T)]$, where $\xi(z,T)$ is the *correlation length* and R_x is the projection of $\mathbf{R}$ along x.

We study the stretching of an interacting SAW in a strip of finite size L along y and infinite length along x. It is possible to define [49] an L-dependent correlation length $\xi_L(z,T)$ *via* the formula $\xi_L(z,T) = -1/\log \lambda_L(z,T)$, where $\lambda_L(z,T)$ is the *largest* eigenvalue of the transfer matrix, that equals 1 at $z = z_c^L(T)$. We apply the *phenomenological renormalization*, to find successive estimates for $z_c(T) = \lim_{L\to\infty} z_c^L(T)$. The equation for the critical force $f_c(T)$ is then ideally found via (see Eq. (3.9)):

$$f_c = -T \lim_{z \to z_c(T)^-} \lim_{L\to\infty} \log \lambda_L. \tag{3.26}$$

As already stressed, the order of the limits in Eq. (3.26) and a correct choice of the boundary conditions (see below) are crucial.

In Fig. 3.10 the *phase diagram* for the stretched interacting SAW is shown. With

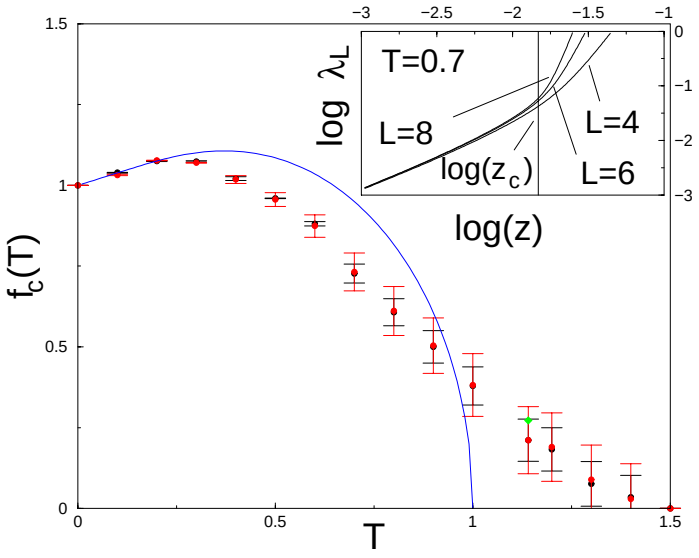

Figure 3.10: Phase diagram for the stretching of a SAW on a $2d$-lattice, obtained with the TM technique. Black dots: *even* L data. Red dots: *odd* L data. Green dot: from Ref. [32]. Error bars are also shown. Solid line: globule-coil coexistence curve, Eq. (3.27). Inset: plot of $\log \lambda$ vs. $\log z$ for $T = 0.7$.

the TM, a right choice of the *boundary conditions* is needed [49]. We have used both *periodic* (PBC) and *free boundary conditions* (FBC). PBC have been employed to get the best estimate of $z_c(T)$ through phenomenological renormalization. This value is then used with FBC, to find the correct L-dependent critical eigenvalue $\lambda_L(z_c(T), T)$. Finally, adopting the extrapolation algorithm of [52], $\lim_{L\to\infty} \lambda_L(z_c(T), T)$ is obtained which, through Eq. (3.26), allows to get the phase diagram. In principle, with FBC, there can be oscillations in data going from odd L to even L. Thus, a separated analysis of even and odd L data was done and reveals that both series of data agree within the error bars (see Fig. 3.10). One point on the transition line obtained in [32], is recovered here.

One can get an approximate description of the transition if one requires that the globule and coil phases coexist. The globule free energy is estimated in terms of hamiltonian walks [9]. On a square lattice the energy is given by minus the length of the polymer whereas the entropy is given in terms of the number of hamiltonian walks which grows exponentially with N [9]. Thus the globule free energy per monomer is $\mathcal{F}_g = -1 - T\log(4/e)$ where we have used a mean field estimate of the entropy [53]. The coil free energy $\mathcal{F}_c$ is approximated as that of an unconstrained random walk in presence of a pulling force and contacts are neglected: $\mathcal{F}_c = -\log 2[1 + \cosh(\beta f)]$. At coexistence one finds

$$f_c(T) = T\cosh^{-1}[2\exp(1/T - 1) - 1], \tag{3.27}$$

which is plotted in Fig. 3.10 (continuous curve).

We note that $f_c(0) = 1$ is the exact result and at low T the phase diagram displays a reentrant region. As $T \to T_\theta$, f approaches 0 rather smoothly, consistently with the prediction $f \sim (T_\theta - T)^{\nu_\theta/\phi_\theta = 4/3}$ [33]. As in Sec. 3.1, we notice that within the TM approach one can also infer the order of the transition, since $\langle x\rangle \sim (f - f_c)^{1/\Delta - 1}$ for $f \sim f_c$[5] (see Eq. 3.13). Our data at $T = 0.7$ are compatible with a second order transition (inset of Fig. 3.10).

Inspired by exact renormalization group (RG) on the Sierpinski lattices [33], and on approximate RG in $d-$dimensional lattices [54], we propose the following simplified real space RG which rationalizes our results.

The RG recursions relations can be written for the generating function representing polymers traversing a hypercube of linear size 1 once, A, and 2^{d-1}-times, B. The terms A and B represent parts of the chain which are in the coil and globular state

[5] We again stress that Δ is a *new* critical exponent, unrelated to those previously known for the interacting SAW.

respectively. The recursion relations can be calculated as in Ref. [55] or by enumerating the SAWs on 2×2 or $2 \times 2 \times 2$ cells as in [54]. To leading order in A at $0 \neq T \ll T_\theta$

$$A' = A^2 + \alpha(d)A^2B^2, \quad B' = \gamma(d)B^{2^d}, \tag{3.28}$$

where $\alpha(d)$ and $\gamma(d)$ are $d-$dependent constants.

There are three fixed points in the flux in Eq. (3.28): $A = 0$, $B = B^* = \gamma(d)^{-1/(2^d-1)}$ corresponds to the globular phase, $(A, B) = (1, 0)$ to the coil phase, while the last non-trivial fixed point $A = A^* = 1/[1 + \alpha(d)(B^*)^2]$, $B = B^*$ characterizes the unfolding transition.

The value of $\alpha(d)$ affects the behaviour of the RG flux near the fixed point (A^*, B^*). One can see[6] that $\alpha(d) \neq 0$ if $d = 2$ and is 0 in $d > 2$. When $\alpha(d) \neq 0$ (i.e. in $d = 2$), the RG flux is smooth near (A^*, B^*) and the critical fugacity near $f = f_c(T)$ is $z_c(f_c(T), T) - z_c(f, T) \sim (f - f_c(T))^2$ signalling a second order transition with $\Delta = 1/2$. On the other hand when $\alpha(d) = 0$ (i.e. $d > 2$), the transition is first order and two-state like. The presence of the mixed term in Eq. (3.28) is crucial and enhances the entropy of the coil phase since it contributes to A'.

Consequently, the $d = 2$ two-state approximation in Fig. 3.10 gives a transition line which is higher than the numerical result for $0 \neq T \ll T_\theta$. The entropy gain in the stretched coil, as $T \to 0$, is hampered as it costs a finite surface energy (dominant as $T \to 0$) to change locally an elongated globular region into a coil and vice-versa. This is why the solid curve in Fig. 3.10 matches our numerics as $T \to 0$.

3.2.3 Ground state analysis in $d = 2$

When T is low, one may look for the ground states among the rectangles of sides L_x and L_y that are completely covered by the SAW (in other words such that $L_xL_y = N$, where we neglect the small effects arising when this rectangle cannot be constructed with both $L_{x,y}$ integers). The energy of this rectangular hamiltonian walk with a non zero f is $-H(N \equiv L_xL_y, L_x) = N - L_x - \frac{N}{L_x} + 1 + f(L_x - 1)$. The minimum of $H(N, L_x)$ for given N with respect to L_x yields the most stable configuration for various values of f. The minimum occurs for an f-dependent value of $L_x^0 \equiv L_x^0(N, f)$, namely $L_x^0(N, f) = \sqrt{N/(1 - f)}$. For any $f < 1$ one has a compact configuration. However, when the critical value $f = 1$ (for $T = 0$) is reached all

[6] These facts can be proved exactly in a family of Sierpinski gaskets (see [33] for an example), where d is the fractal dimension. On conventional lattices, an approximate RG treatment as in [54] gives qualitatively the same behaviour.

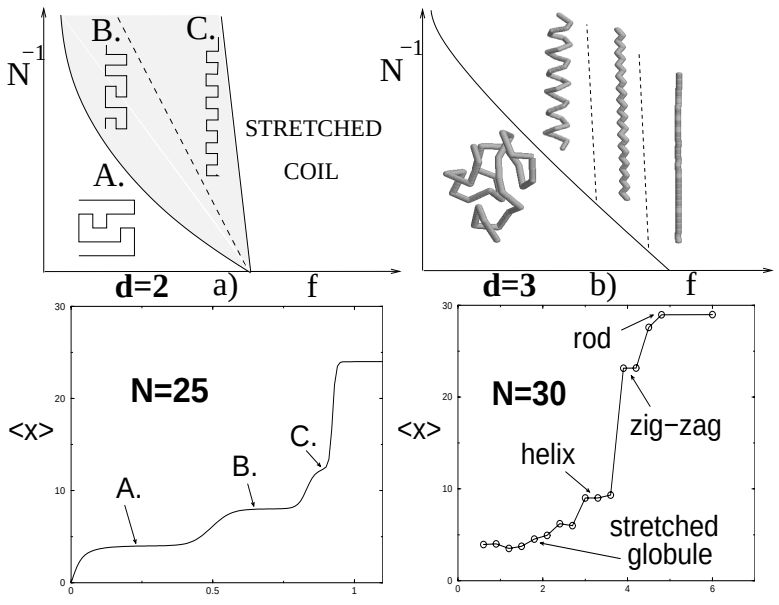

Figure 3.11: a) $d = 2$ Schematic diagram of minima for polymers of different sizes (top) and low T $\langle x \rangle$ vs. f curve for $N = 25$ (bottom) found with exact enumerations in $d = 2$. b) $d = 3$: Same as in a), except that the $\langle x \rangle$ vs. f curve (bottom) is for $N = 30$ and is found by simulated annealing.

integer values of L_x from N (stretched coil) to $L_x \sim N^{1/2}$ (compact globule) become degenerate for large N[7].

Let us notice that this does not hold in $d = 3$ where it is well known that there is a Rayleigh instability in the thermodynamic limit [27, 28, 32]. This can be seen by comparing the globule energy - which in $d = 3$ is $2N$ in the large N limit - with the energy of a parallelepiped, with elongation along **f** equal to L_x and with edges $L_y = L_z$ in the perpendicular plane. The force above which (for $T = 0$) the parallepiped is a better ground state than the three-dimensional globule is $2L_y$ ($L_y \ll N^{1/3}$), and there is no longer any degeneracy at the critical force $f_c = 2$ (at $T = 0$). A sketch is given in Fig. 3.11(a).

The minima hierarchy, shown in the shaded area in the top panel, affects the low T region of the $\langle x \rangle$ (average elongation) vs. f curves for finite length (bottom panel).

[7]Let us remark that calculations will be performed in the ensemble where the force is fixed, which is related to the experimental ensemble (fixed stretch) by means of a usual Legendre transform [56]. These two ensembles are equivalent *only* in the large N limit. A recent interesting discussion on this topic can be found in Ref. [57].

However, only one transition survives in the large N limit and represents a true phase transition (as represented in Fig. 3.11(a) by the shaded wedge ending in just one point in the $N^{-1} = 0$ axis). Similarly, when T is raised the multi-step character of the $\langle x \rangle$ vs. f curves is lost due to fluctuations which blur the ground state dominance in the partition.

In this framework, we give a simple explanation about the apparent conflict between the stretching behaviour under condensing condition of λ DNA and single DNA molecule (Figs. 2.8 and 2.9) from one side and plasmid-length DNA (Fig. 2.10) from the other. Again, we shall make use of the notation EXP1, EXP2 and EXP3 (see Sec. 2.2).

As already remarked, until very recently, many of the theoretical predictions were refined versions of the original mean field approach first proposed in Ref. [28]. The mean field approximation predicted that the force versus elongation curves should consist of a plateau followed by the steep increase which is also present in the case of a swollen polymer (i.e. DNA with no counterions). The plateau is due to configurations where stretched and globular state coexist within the same chain, as is typical in a first order transition. The instability of other configurations, such as an ellipsoid like shape for instance, with respect to these coexisting conformations can be seen as a manifestation of the Rayleigh instability [27, 32]. The mean field prediction of a force plateau successfully accounts for the curves of EXP1 and EXP2. However, these experiments seem to be in conflict with the results of EXP3.

We suggest that this behaviour may be due to the different contour lenghts of the molecules used in the experiments.

The λ phage molecule used in EXP1 was relatively long (Fig. 2.8), its contour length being ~ 16.5 μm, corresponding to roughly 48.5 kilobases or 330 persistence lengths (the base pair separation in double stranded DNA is ~ 0.34 nm and the DNA persistence length is usually agreed to be ~ 50 nm, though it has been reported to depend on the salt concentration in solution also [11]). The plasmid length DNA used in EXP1 is around 24 persistence lengths, so much shorter. Finally, the length of the DNA used in EXP2 is intermediate, and is roughly 90 persistence length (~ 4.5 μm).

Let us again consider a self avoiding polymer under the action of a stretching force along the y-direction, on the $2d$ lattice. This means that the kind of agreement we expect is qualitative. The lattice spacing corresponds to the persistence length and the walk can change its direction after it has traveled one persistence length.

The polymer in this model is fully characterized by the attraction energy between non-consecutive beads, ϵ, by the variable force, f, and by the number of persistence

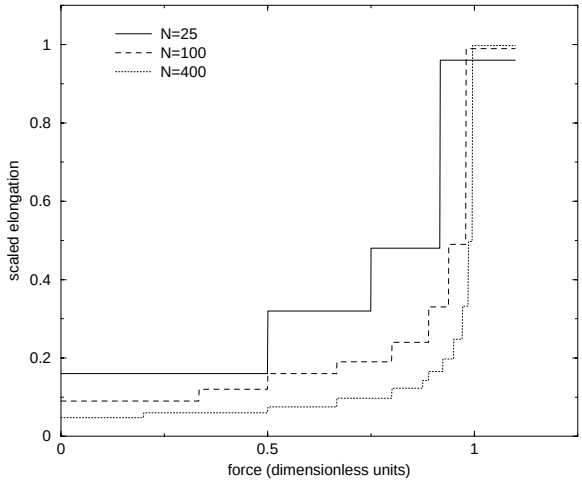

Figure 3.12: Average end-to-end scaled by N (number of persistence lengths in the chain) as a function of pulling force for a semiflexible polymer of different contour lengths in the ground state approximation ($\epsilon = 1$ in Eq. (3.29)). As the contour length increases, the transition looks more and more like an all-or none transition as will be the case for infinite length. The data have been obtained in the ground state approximation, i.e., by considering only the configurations which minimizes the energy function defined in Eq. (3.29). The minimum has been searched among all rectangles of edges of sizes m and $\mathrm{int}(N/m)$, where $\mathrm{int}(a)$ denotes the integer closest to a and smaller than or equal to a.

lengths, N. Again, we will restrict to the case of low temperature, where the entropic fluctuations are negligible and ground state dominates. Indeed, the typical energy in the unfolding experiments considered here (see, e.g., Fig. 2.8) is $\sim 10^5 k_B T$ (force $\sim$ pN and extension $\sim \mu$m) where k_B is the Boltzmann constant and T is the absolute temperature, so that T driven fluctuations are virtually absent.

In this situation, the partition function is dominated by the ground state. In our simplified model the energy of a self-avoiding polymer chain is:

$$H = -N_c\epsilon - fy, \tag{3.29}$$

where N_c is the number of self contacts of the polymer, f is the modulus of the pulling force and y is the elongation along the force direction. Since we are interested in the ground state only, we can restrict our analysis to rectangular walks elongated along the force axis which do not leave empty spaces in their interior (known also as rectangular hamiltonian walks [9]). Let us consider the case of a chain consisting of 25 persistence lengths (see Fig. 3.12): as f increases we go from a configuration

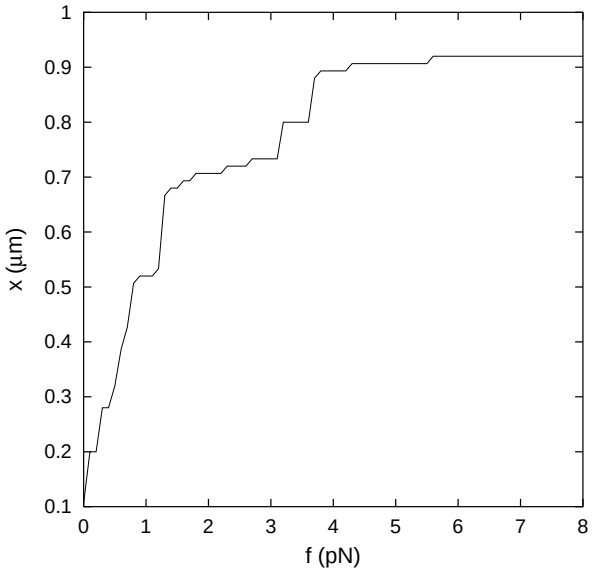

Figure 3.13: Plot of the average end-to-end distance versus pulling force in the ground state approximation ($T = 0$) for the EXP3 data (see Fig. 2.10).

with extension 4 along the y axis to one with elongation 8 and finally to the stretched coil. Thus here the unfolding occurs in steps, and each step is stable in a window of force values. In Fig. 3.12 we plot the average (scaled) elongation versus force for different lengths of the chain (different values of N): as the chain gets longer each step is stable only for a very small interval of forces, apart from the globule and the coil states, and indeed for infinitely long chains there would be an abrupt transition between these two states only.

What one learns from this simple exact calculation is that the steps are less and less pronounced as the chain gets longer, and that for short chains there is a number of intermediate states which is likely to be responsible of the observed peak pattern. We then come to a quantitative analysis of the experimental data. This is shown in Figs. 3.13 and 3.14.

From the available force versus elongation characteristic curves, which are not easily obtainable in theoretical calculations, we can extract via a numerical integration the free energy as a function of the end to end elongation.

If $\mathcal{F}(x)$ is the free energy of a polymer with end-to-end elongation (along a chosen axis) equal to x and $f(x)$ denotes the average force needed to keep an end-to-end

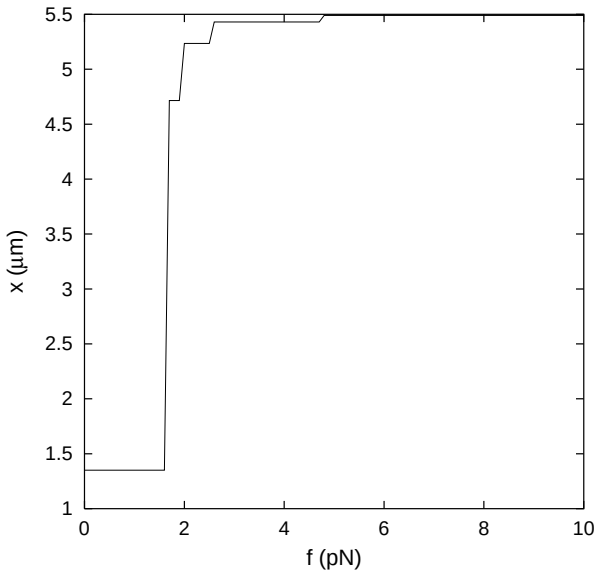

Figure 3.14: Plot of the average end-to-end distance versus pulling force in the ground state approximation ($T = 0$) for the EXP2 data (see Fig. 2.9).

distance of x, the two quantities are related by (we choose $\mathcal{F}(0) = 0$):

$$\mathcal{F}(x) = \int_0^x f(x')dx'. \tag{3.30}$$

From this, by neglecting thermal fluctuations, we can find the average elongation versus force characteristic curves. This is equivalent to find how the minimum of the function $\mathcal{F}(x) - fx$ moves as the parameter f is varied. We used data coming from EXP2 and EXP3. In the curve extracted from EXP3 data, multi-step behaviour is very pronounced (Fig. 3.13), while it gets less clear in the curve obtained from the EXP2 data (Fig. 3.14) and finally disappears for EXP1 data (Fig. 2.8)[8].

As noted, the experimental ensemble is not the same of the one in which we did the calculations. Indeed, it is known [56] that the two ensembles are not equivalent. Our analysis shows in particular that the fixed stretch ensemble uniquely determines the fixed force curve, while the converse is not true, since non-monotonicity can not appear in our theoretical calculations. However, in general an ascending peak pattern

[8]Let us remark that the agreement with our theory is only qualitative as $\mathcal{F}(x)$ obtained from the experiments might not correspond to the equilibrium free energy. It might indeed have dynamical effects in it. Moreover, when dealing with double-stranded DNA, one should also consider the stiffness of the molecule. Nevertheless the agreement with our picture is quite remarkable.

– where by ascending we mean that the peak values of the force increase as the elongation increases – always gives rise to a multistep elongation versus force curve, so that the ground state changes with force. This is the case observed in the experiments for short and medium size chains. Conversely, as the steps in the fixed force ensemble resemble *first order* transition though at finite size, one can apply the usual theory of phase transition. Thus there is a *latent heat* connected with these *transitions*, and it can be shown that the fixed stretch characteristic curve will show peaks.

3.2.4 An off-lattice model in $d = 3$

The model we used is the freely jointed chain (FJC) (see Appendix A and [20]) in the continuum (off-lattice). The FJC is subject to a compacting pairwise attractive potential between non-consecutive beads and to a stretching force $\mathbf{f}$ at the extrema. The pairwise potential is chosen to be an asymmetric square well with a hard core radius, $2R_{hc}$, which acts between non-consecutive beads along the chain, and an attraction range $R_1 > 2R_{hc}$, i.e. the distance up to which the particles interact. We have checked that the results reported in the following do not appreciably depend on the two-body potential details. The parameters we have used to generate the configurations shown in Fig. 3.11(b) (top panel) are $R_{hc} = 0.6$, $R_1 = 1.6$ where the unit length is the distance between successive beads along the chain.

The ground states of short chains (up to $N = 30$) have been determined by performing simulated annealing [58] employing Monte Carlo dynamical simulations (see Appendix F and Refs. [59, 60, 61]). The FJC is evolved dynamically by means of three sets of moves: the pivot, reptation and crankshaft moves [59]. We lower T during the simulation according to a standard annealing schedule. We found evidence also in this $d = 3$ case that the unfolding of a finite length homopolymer proceeds in a multistep fashion. The collapsed globule first orients itself along the pulling force as soon as there is a nonzero f. At larger f the globule is slightly elongated (much less than in the $d = 2$ case) and after this a helix forms followed by a zig-zag curve and finally by a stretched coil.

This succession of minima, shown in Fig. 3.11(b) is intriguing for a two-fold reason: firstly because it suggests that helices, one of the well known building block of proteins, come out rather naturally as one of a few stable minima of a homopolymer in a poor solvent subject to a finite stretching force; secondly because the unfolding transition of a finite polymer in this model appears to be markedly different from a globule-to-coil (two-state) transition. The mean field picture of an all or none transition is recovered for infinite length. The situation is depicted in Fig. 3.11(b). Since

in $d = 3$ the transition is first order, the mean field treatment is correct in the thermodynamic limit.

The fact that helices become better ground states than compact globules could be easily verifiable in experiments done in the fixed force ensemble. These can now be confidently performed, with not more substantial difficulties than the more conventional ones, performed in the fixed stretch ensemble.

Helices appear as ground states for a potential consisting of a force term and a hydrophobic contact potential because they are both elongated and offer a good shielding from the outside solvent to the monomers lying in its interior. Note also that helices arise as optimal states of tubes of non-zero thickness subject to compaction [62].

3.2.5 Conclusions

Briefly, here we have discussed the unfolding transition of a homopolymer under the action of an external pulling force in $d = 2$ on the lattice and in $d = 3$ off lattice. We have found many intriguing results:

- a ground state analysis shows that for finite length polymers, the unfolding is not abrupt, rather it occurs via a multi step sequence of states. These are more elongated than the globule and make more contacts than a coil. In $d = 3$ helices arise naturally as ground states at intermediate forces. For infinite polymers, on the other hand, the situation is different: in $d = 3$ the intermediate ground states disappear due to the Rayleigh instability, and the transition is effectively two-state, whereas in $d = 2$ they survive in the thermodynamic limit. Data taken from some recent experiments [24, 25] confirm this picture;

- indeed, from the Transfer Matrix results, it is apparent that the mean field hypothesis is incorrect in $d = 2$ even at low T: the transition is second order as also found in Ref. [32] and confirmed in Sec. 3.1, although the prediction of the re-entrant region agrees with the TM results. A renormalization group based argument is in agreement with this picture.

Chapter 4

A new interpolation formula

A mind truly opened to what science has to teach must see that it is a little thing. It may be that save in this little planet, this speck of cosmic dust, invisible long before the nearest star could be attained – it may be, I say, that nowhere else does this thing called pain occur. But the laws we feel our way towards – Why, even on this earth, even among living things, what pain is there?

Herbert George Wells, *The Island of Doctor Moreau*

In this Chapter, we focus our attention mainly on the pulling of a polymer under good solvent conditions [10], in which case we give an analytical prediction for the force versus extension curve. We also discuss other cases by means of numerical simulations and direct connections to experiments. Usually, the models adopted describe the polymer as an elastic (ideal) chain, where self-avoidance is not taken into account. Typically, freely jointed (FJC) or worm like chain (WLC) are studied [63].

The former describes a chain of beads connected by links of constant distance (see Appendix A), whereas the latter, which has received considerably great attention in the recent past [64, 65, 66, 67, 68], introduces an intrinsic *stiffness* between two consecutive bonds (see Appendix B) and, in particular, is shown to correctly describe a wide range of experimental results on double-stranded (ds) DNA, single plasmid and lambda phage DNA [11, 24, 69]. In this case, the large force behaviour $1 - z/L_c \sim 1/\sqrt{F}$ is found, where z is the elongation along the direction of the force, L_c the contour length of the polymer and F is the applied force [11, 68]. Let us note that in these cases the *continuous* version of the WLC model is always used, where the *persistence* length [11] L_p is very large, compared to the base separation (roughly one persistence length is 150 base pairs).

Here, we focus on the *discrete* version of the WLC model, that satisfactorily describes the pulling behaviour of a polymer in good solvent. We broadly identify three regimes in the force vs extension curves obtained in our analytical and numerical calculations. The low force (or low stretch) regime is highly affected by the details of the interactions between the beads (which in nature are, e.g., caused by the different concentration of ions in solution). This regime is discussed only marginally here, as, though it is potentially very interesting, experimental data in this range of forces are quite rare and not precise enough to allow a comparison with theoretical predictions. There is then a second regime, of intermediate stretches or forces, in which the force versus extension characteristic curves obey approximately the laws predicted a few years ago in Ref. [11] by means of a continuum theory of the WLC. Finally, for very large forces (beyond a polymer dependent crossover value), we get a universal, model-independent, freely-jointed-chain like behaviour. The Chapter is organized as follows:

- in Section 4.1, we show how the discrete WLC model can be related to the well known continuous version;
- in Section 4.2, we compare our theory with some recent experiments;
- then, in Section 4.3, we introduce some extension vs force curves obtained from Monte-Carlo calculations for models of stiff polymers with a chosen potential between *non* nearest neighbour beads. We shall consider two different cases: a pure repulsive potential and a more realistic Lennard-Jones potential and we show that in the latter case our formula agrees with the numerical data only in the case of high temperatures or, for lower temperatures in the high force regime. Below the θ point a force plateau appears, as predicted by some recent theoretical works [28, 40, 70, 71] and confirmed by experiments [24].
- Finally, Sections 4.4 and 4.5 are left for discussion and conclusions, respectively.

4.1 The model

As discussed in Appendix B, our model describes a chain of beads, where the distance between the nearest neighbours is kept fixed (we can put it equal to b) and a suitable *stiffness* K is introduced. Then, the corresponding Boltzmann weight reads [72, 73,

74]:

$$e^{-\beta\mathcal{H}} = \prod_{i=1}^{N} \delta(|\mathbf{t}_i| - b) e^{\beta K \sum_{i=1}^{N-1} \hat{\mathbf{t}}_i \hat{\mathbf{t}}_{i+1} + \beta \mathbf{F} \sum_{i=1}^{N} \mathbf{t}_i}, \tag{4.1}$$

where $\beta = 1/T$, T being the temperature in units of Boltzmann constant, $\mathbf{t}_i \equiv \mathbf{r}_i - \mathbf{r}_{i-1}$ ($\mathbf{r}_i$ being the position vector for the i-th bead, $i = 1, ..., N$ and N is the total number of bonds), $\hat{\mathbf{t}}_i = \mathbf{t}_i/b$ and $\mathbf{F} = F\hat{\mathbf{z}}$ is the applied force which defines the z-direction. The partition function for the model described by (4.1) is

$$\mathcal{Z}_N = \int \prod_{i=1}^{N} d\mathbf{t}_i e^{-\beta\mathcal{H}}. \tag{4.2}$$

The average elongation $\langle z \rangle_N$ along the stretching direction is

$$\langle z \rangle_N = T \frac{\partial}{\partial F} \log \mathcal{Z}_N . \tag{4.3}$$

Let us now consider the large force behaviour. Due to the δ-function in Eq. (4.1), the term $\beta K \hat{t}_{i,z} \hat{t}_{i+1,z}$ can be re-written with the substitution $\hat{t}_{i,z} \simeq 1 - \mathbf{t}_{i,\perp}^2/2b^2$ and, analogously, the force term in the exponential becomes $\beta \mathbf{F} \cdot \mathbf{t}_i = \beta F t_{i,z} \simeq \beta F b \left(1 - \mathbf{t}_{i,\perp}^2/2b^2\right)$, where $\mathbf{t}_{i,\perp} = (t_{i,x}, t_{i,y})$ [11]. Keeping only quadratic terms in the $\mathbf{t}_{i,\perp}$'s, we get:

$$\zeta \equiv \lim_{N\to\infty} \frac{\langle z \rangle_N}{Nb} = 1 - \frac{T}{\sqrt{(bF)^2 + 4bKF}}. \tag{4.4}$$

The continuum approximation of Eq. (4.4) (see also Appendix B) is obtained with the following substitutions [75]:

$$\beta K \to L_p/b, \tag{4.5}$$

in the formal limit $b \to 0$, where L_p is the persistence length. The final result $\zeta = 1 - 1/2\sqrt{\beta L_p F}$ does agree with the celebrated result of Marko and Siggia [11]. However, our result is more general, since it predicts a *crossover* force $F_c = \frac{4L_p}{\beta b^2}$:

$$\begin{aligned} &\text{WLC-like behaviour:} \quad 1 - \zeta \sim 1/\sqrt{F}, \quad F \ll F_c \\ &\text{FJC-like behaviour:} \quad\;\; 1 - \zeta \sim 1/F, \quad\;\; F \gg F_c \end{aligned} \tag{4.6}$$

Let us notice that the validity of the continuum approximation proposed in Ref. [11] is not simply related to the value of the dimensionless ratio b/L_p but rather to F/F_c.

A naive derivation of F_c is given in the following: from the Hamiltonian defined in Eq. (4.1), we can see that the stiffness and the force terms are of the same order at $F_c \sim K/b = L_p/\beta b^2$, where Eq. (4.5) has been used. So the meaning of F_c is the one where the bending energy competes with the external force.

From Eq. (4.4) with the substitution (4.5), we deduce that:

$$\beta b F = \frac{2L_p}{b}\left[\sqrt{1+\left(\frac{b}{2L_p}\right)^2\frac{1}{(1-\zeta)^2}}-1\right]. \tag{4.7}$$

The low force behaviour of Eq. (4.3) is

$$\zeta = \frac{\beta b F}{3}\frac{1+y(L_p/b)}{1-y(L_p/b)}, \tag{4.8}$$

where $y(x) = \coth(x) - 1/x$ [20]. Again, in the limit $b \to 0$, Eq. (4.8) agrees with the result of Marko and Siggia [11].

Following [11], we give an interpolation formula starting from Eqs. (4.7) and (4.8). We calculate the $\lim \zeta \to 0$ of Eq. (4.7) and compare to Eq. (4.8). Matching the two results gives the following approximate equation:

$$\begin{aligned}\beta b F &= \frac{2L_p}{b}\left[\sqrt{1+\left(\frac{b}{2L_p}\right)^2\frac{1}{(1-\zeta)^2}}-\sqrt{1+\left(\frac{b}{2L_p}\right)^2}\right] \\ &\quad + \left(3\frac{1-y(L_p/b)}{1+y(L_p/b)} - \frac{b/2L_p}{\sqrt{1+(b/2L_p)^2}}\right)\zeta.\end{aligned} \tag{4.9}$$

It is easy to verify that Eq. (4.9) correctly reproduces the right large and small force behaviours, Eqs. (4.7) and (4.8), and that in the *continuum* limit $b \to 0$ we obtain the well known interpolation formula [11]:

$$\beta L_p F = \frac{1}{4(1-\zeta)^2} - \frac{1}{4} + \zeta. \tag{4.10}$$

In next Section, we shall apply our formula, Eq. (4.9), to two recent experiments. The first discusses the stretching of a single plasmid DNA molecules, to which the formula (4.10) was previously applied with success [24]. Nevertheless, our formula predicts a non trivial value for the parameter b, that gives an estimate for the *intra* bead distance. Then, the second experiment [76, 77] demonstrates that Eq. (4.9) gives the right large force behaviour.

In the following, we shall define $\zeta = z/L_c$, where z is the elongation along the direction of the force and $L_c = Nb$ is the contour length of the polymer (see also Eq. (4.4)).

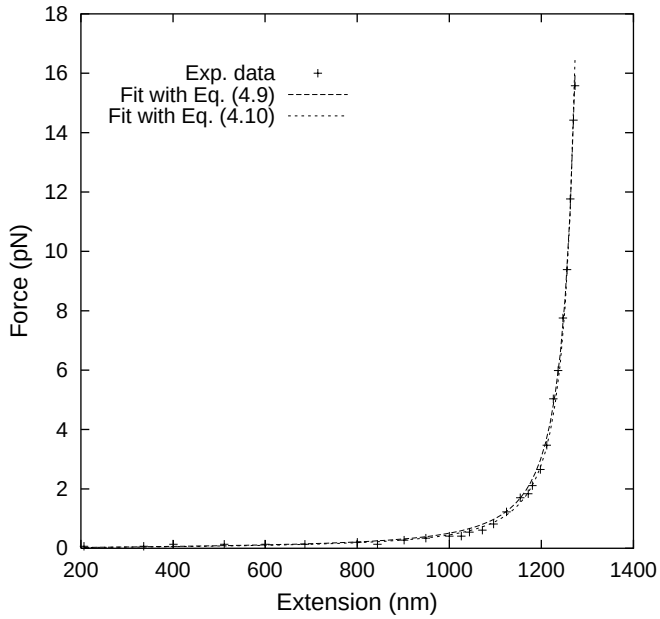

Figure 4.1: (+): experimental data taken from Ref. [24]. Long dashed line: fit with the curve, Eq. (4.9), yielding $L_c = 1324$ nm, $L_p = 38$ nm and $b = 2.5$ nm. Short dashed line: fit with the curve, Eq. (4.10), yielding $L_c = 1324$ nm and $L_p = 38$ nm, see Ref. [24].

4.2 Comparison with two recent experiments

Let us consider the experimental data reported in the plot at the top of Fig. 2.10 (from Ref. [24]). The authors considered the elastic response of a single plasmid of DNA molecules, probed using optical tweezers [6]. They found that, according to the environmental conditions, it can be very different. In particular, for condensed molecules, the stretching curves display a stick-release pattern, where the DNA molecule can be described as a succession of different WLC's of different contour and persistence lengths. We are mainly interested to the case of uncondensed molecules, whose stretching pattern is reproduced in Fig. 4.1.

As described in the caption, the contour and persistence lengths obtained with our formula, Eq. (4.9), and with Eq. (4.10) are perfectly compatible. Nevertheless Eq. (4.9) predicts a non trivial value for the intra bead effective distance $b = 2.5$ nm, that corresponds to $7 - 8$ base pairs. Let us notice that this matches the DNA hydration thickness (here, we have used ~ 0.34 nm as the distance between two consecutive base pairs [24]).

If we take $T = 300$ K, the crossover force $F_c \sim 100$ pN and $F/F_c \lesssim 0.16$ for the data of Ref. [24], thus justifying the use of the interpolation formula, Eq. (4.10). However, as pointed out in Eq. (4.6), the discrete nature of the chain does emerge, when $F \gtrsim F_c$. Notice also that for forces considerably smaller than F_c double-stranded DNA would undergo an overstretching transition [23, 78], where a more sophisticated theory is needed [63].

An interesting question is how this treatment may be applied to single-stranded DNA (ssDNA). On one hand, if we keep as physical parameters the persistence length of ssDNA ~ 1 nm, and as the equivalent of b the separation between two phosphates, i.e. 0.5 nm roughly, we would end up with a crossover force again of the order of 70 pN. Data in this regime do exist [76, 77], and suggest that the WLC grossly fails to fit the data [77, 79]. In fact (see Fig. 4, Ref. [77]), the authors pointed out that the corresponding fit with Eq. 4.10 gives good results in the large force regime, but with a calculated persistence length ($\simeq 0.21$ nm) which is clearly *not* physical. Our equation does not do much better for low and intermediate force, in which case, as shown in Ref. [77], evidently the self-interactions dominate the behaviour. Still a large force fit, even if a bit dependent on the contour length which we choose, suggests that the large force exponent in the $(\log(1-\zeta), \log(F))$ plane is -1 as predicted by our model (see Fig. 4.2). The calculated fitting parameters L_p and b (see the caption of Fig. 4.2) give $F_c \simeq 300$ pN. However, it can be seen that the fit is good already for $F \simeq 100$ pN, in order-of-magnitude agreement with the naive guess proposed above.

Let us notice that in this case $b/L_p \simeq 0.46$, an order of magnitude larger than the dsDNA value $b/L_p \simeq 0.07$. This is a clear indication of the fact that ssDNA is more flexible than dsDNA and that our formula predicts the correct high force behaviour.

In next Section we introduce some Monte-Carlo calculations and compare them to Eqs. (4.9) and (4.10).

4.3 Monte-Carlo calculations

As already said, our model is a *stiff* chain described by the Boltzmann weight, Eq. (4.1), where the *intra* bead distance b is now kept fixed to 1.

Firstly, we have considered the case when the intra bead potential is zero, $K = 40$ and $\beta = 1$. In Fig. 4.3 we have plotted the Monte-Carlo data (+) and the curves given by Eqs. (4.9) and (4.10) (long and short dashed line, respectively), for $L_p = 40$, and $\beta = 1$. As observed, the agreement is perfect only for Eq. (4.9). In fact, the discrete nature of the chain emerges around $F = F_c \sim 160$ (in the chosen units) and the WLC

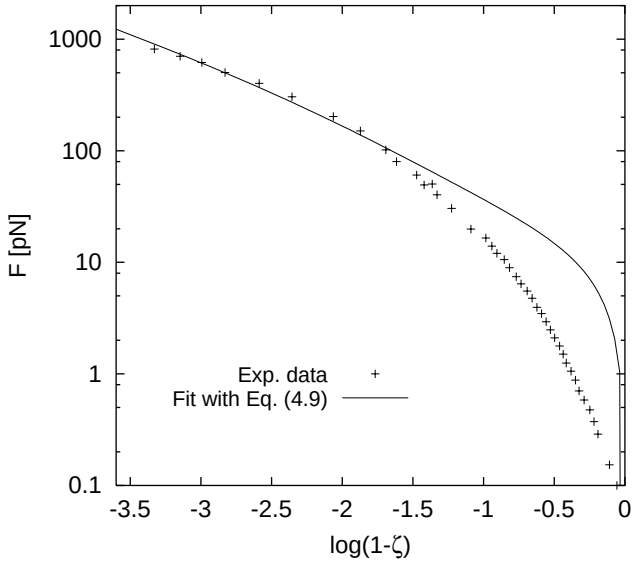

Figure 4.2: (+): experimental data taken from Ref. [77]. Continuous line: fit with the curve, Eq. (4.9), yielding $L_c = 2.31$ (in units of the contour length l^0_{ds} of the equivalent dsDNA molecule observed in 10 mM PB [77]), $L_p = 0.26$ nm and $b = 0.12$ nm.

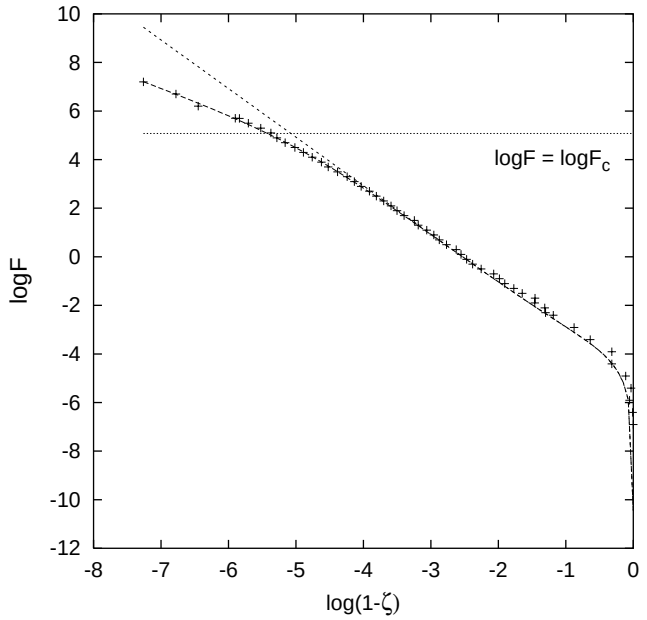

Figure 4.3: (+): Monte-Carlo data for a *stiff* chain of $N = 100$ beads and stiffness $K = 40$, for $\beta = 1$. Long dashed line: Eq. (4.9) with $L_p = 40$ and $b = 1$. Short dashed line: Eq. (4.10) with $L_p = 40$. The *crossover* force F_c, see Eq. (4.6), is also shown.

approximation is no more valid.

To render the model more realistic, let us introduce a *short* range repulsive potential $V_{rep}(r)$ between non consecutive nearest neighbour beads. We have adopted the following functional form:

$$V_{rep}(r) = \frac{1}{r^{12}} \tag{4.11}$$

where r is the distance between two beads. Then, we have to multiply the Boltzmann weight, Eq. (4.1), by

$$e^{-\frac{\beta}{2}\sum_{i\neq j=0}^{N} V_{rep}(r_{ij})} \tag{4.12}$$

where we have defined $r_{ij} = |\mathbf{r}_i - \mathbf{r}_j|$.

In Fig. 4.4 we have plotted the Monte-Carlo results (+) for $K = 30$ and $\beta = 1$, together with the two fitting lines obtained from Eqs. (4.9) and (4.10) (long and short dashed lines, respectively) where the corresponding persistence lengths are $L_p \simeq 31$ (b is kept fixed to 1) and $L_p \simeq 34.9$. Again, we can observe that our formula works better than Eq. (4.10). Moreover, this last result is in agreement with some theoretical works [69, 80, 81, 82], that predicts that the net effect of the repulsive potential is to renormalize the persistence length, making it larger than the bare one.

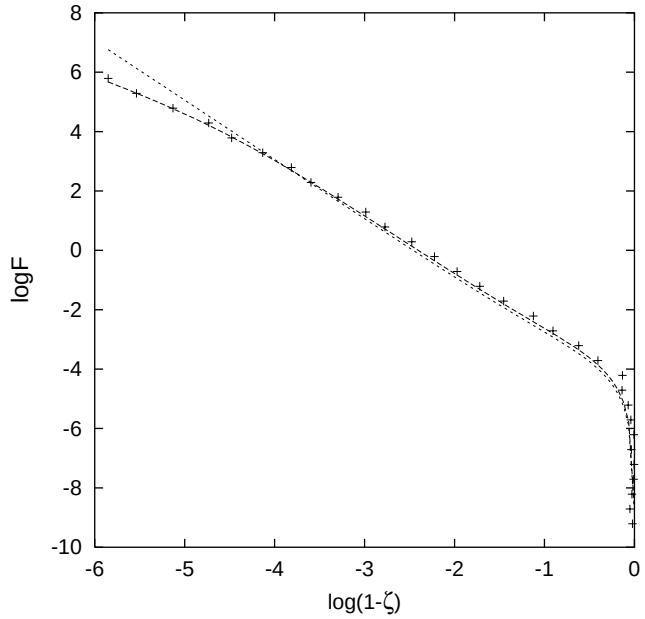

Figure 4.4: (+): Monte-Carlo data for a *stiff* chain of $N = 100$ beads, stiffness $K = 30$ and interaction potential given by Eq. (4.11), for $\beta = 1$. Long dashed line: fit obtained from Eq. (4.9) with $L_p \simeq 31$ ($b = 1$). Short dashed line: fit obtained from Eq. (4.10) with $L_p \simeq 34.9$.

In practice, for a stiff chain, self-avoidance can be treated as a perturbation and we again find a good agreement with Eq. (4.9). This suggests that the low force discrepancy observed in Fig. 4.2 between experimental results and our fit is due to other types of interactions than self-avoidance.

Now, let us introduce a more realistic potential, adding to the repulsive core an attractive part too. It is interesting to notice that the approaches of Refs. [80, 81] can not be generalized, since the attractive part introduces some instabilities and the perturbation scheme discussed there is no more valid.

We have chosen the following Lennard-Jones kind functional form $V_{LJ}(r)$:

$$V_{LJ}(r) = V_0 \left(\frac{1}{r^{12}} - \frac{\alpha}{r^6} \right) . \tag{4.13}$$

The parameters V_0 and α are chosen in such a way that the minimum of the energy is located at $r = r_{min} = 1.5$ and $V_{LJ}(r = r_{min}) = -1$. We expect that Eq. (4.10) does not work well in this case. Our goal is to test our formula, Eq. (4.9).

Firstly, we show the effects of increasing stiffness on the force vs extension curves. To fix the ideas, we begin to consider a sufficiently high temperature, i.e. *above* the θ point [10, 20], whose location, however, is not exactly known. In Ref. [83], the authors were able to numerically determine the θ temperature T_θ for a model of homopolymer with a square well potential, whose depth is fixed to -1. They found that $T_\theta \simeq 3$. Our T_θ should be somewhat smaller due to the stiffness.

Initially, we fix $\beta = 0.3$ ($T = 3.333...$), with $K = 10$. The numerical results and the corresponding fitting line are plotted in Fig. 4.5. The corresponding fitting parameters are described in the caption. In this case we allowed b to be a free parameter and we have determined it through a best fit of the data even though in the simulated model $b = 1$. The fit with our formula is surprisingly good, in contrast with the result obtained with Eq. (4.10). Moreover, the predicted value for b is of the correct order. This means that the effect of the stiffness compensates the attraction due to the potential and the behaviour is similar to a FJC. Let us stress on the fact that if we fix $b = 1$, the corresponding fits are considerably less precise.

We have also simulated the case with $K = 80$. In Fig. 4.6 we have plotted the numerical data together with the two fitting lines (the fitting parameters are reported in the caption). The agreement with our formula is again perfect, in contrast with Eq. (4.10).

For both situations plotted in Figs. 4.5 and 4.6, we note that the main effect due to the potential is a considerable reduction in the persistence length due to the attractive part, which evidently renormalize also the intra bead distance.

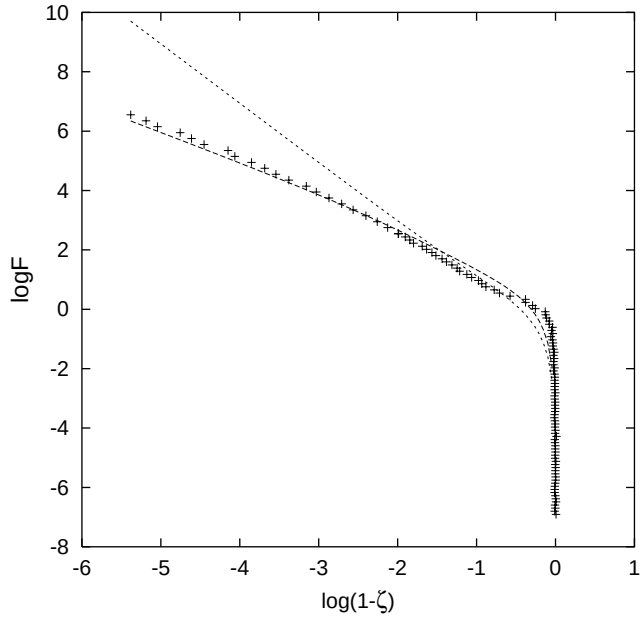

Figure 4.5: (+): Monte-Carlo data for a *stiff* chain of $N = 100$ beads, stiffness $K = 10$ and interaction potential given by Eq. (4.13), for $\beta = 0.3$. Long dashed line: fit obtained from Eq. (4.9) with $L_p \simeq 2.12$, $b \simeq 1.26$. Short dashed line: fit obtained from Eq. (4.10) with $L_p \simeq 2.41$.

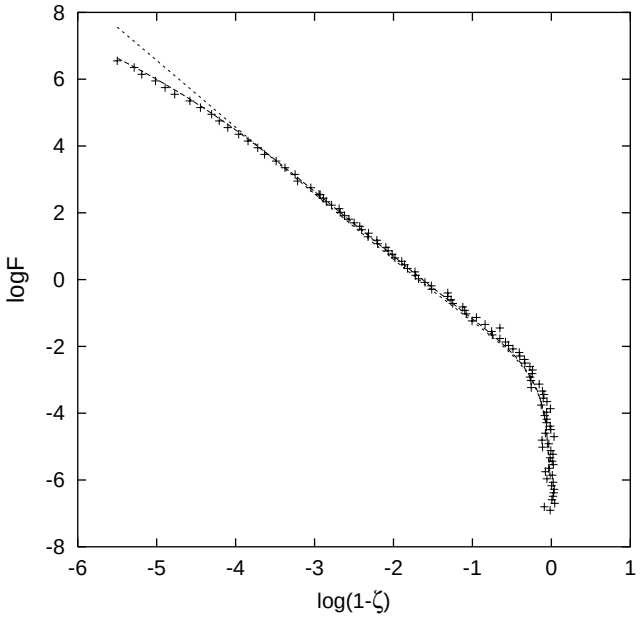

Figure 4.6: (+): Monte-Carlo data for a *stiff* chain of $N = 100$ beads, stiffness $K = 80$ and interaction potential given by Eq. (4.13), for $\beta = 0.3$. Long dashed line: fit obtained from Eq. (4.9) with $L_p \simeq 23.33$ and $b = 0.86$. Short dashed line: fit obtained from Eq. (4.10) with $L_p \simeq 25.95$.

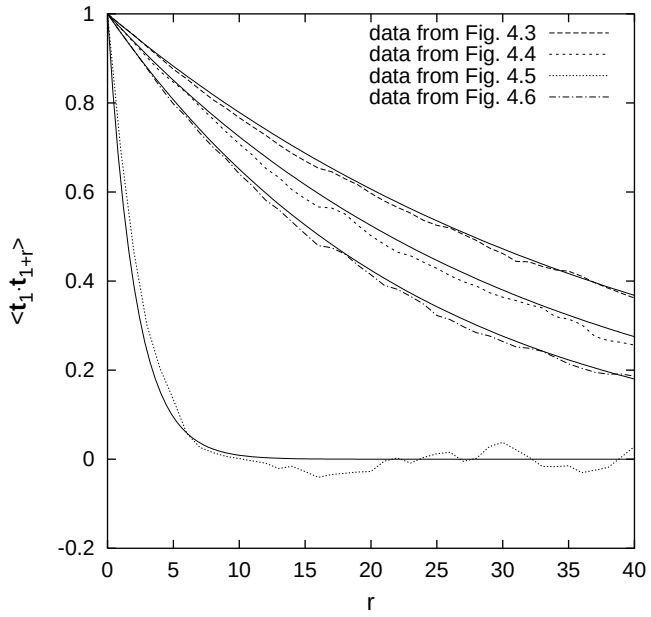

Figure 4.7: Plot of the correlation functions $\langle \mathbf{t}_1 \cdot \mathbf{t}_{1+r} \rangle$ vs r, calculated from the data of Figs. 4.3 to 4.6 and the corresponding theoretical predictions (continuous lines), given by Eq. (4.15).

As a check, let us notice that the correlation function $\langle \mathbf{t}_i \cdot \mathbf{t}_{i+r} \rangle$ for the WLC is [20]:

$$\langle \mathbf{t}_i \cdot \mathbf{t}_{i+r} \rangle = y(\beta K)^r, \tag{4.14}$$

where the function $y(x)$ has been defined above. In the continuum limit

$$\langle \mathbf{t}_i \cdot \mathbf{t}_{i+r} \rangle = \exp(-r/L_p). \tag{4.15}$$

This result is exact for all r but holds in a more general context, like the case with interaction, in the large r limit. In Fig. 4.7 we have plotted the correlation functions $\langle \mathbf{t}_1 \cdot \mathbf{t}_{1+r} \rangle$ vs r for the data of Figs. 4.3 to 4.6 and compared them to the theoretical ones as given by Eq. (4.15). The corresponding persistence lengths are those found with our formula. The agreement is perfect.

Let us now consider the case of $\beta = 0.5$ ($T = 2$). In Fig. 4.8 we have plotted the case for $K = 10$. As it can be seen a *first order* phase transition emerges [40, 84]. In this case our formula is able to describe only the part of the plot at relatively large forces.

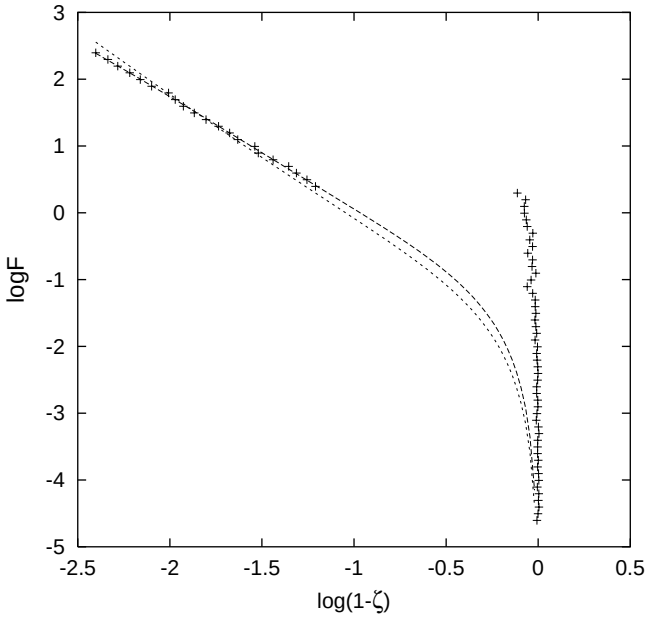

Figure 4.8: (+): Monte-Carlo data for a *stiff* chain of $N = 100$ beads, stiffness $K = 10$ and interaction potential given by Eq. (4.13), for $\beta = 0.5$. Long dashed line: fit obtained from Eq. (4.9) with $L_p \simeq 4.42$ and $b = 1.03$. Short dashed line: fit obtained from Eq. (4.10) with $L_p \simeq 4.85$. Let us remark that we have tried to fit only the range of data at large forces.

A complete characterization of the force vs extension behaviour in this case needs a more complete theory (see also Ref. [85] for some recent Monte-Carlo results about stiff polymers).

4.4 Discussion

Though our main results refer to a situation in which attractive interactions are not very important, it is useful to further comment on how our results change in the presence of such a situation in a real experiment. Such attractions change the picture depicted so far as, if they are strong enough, they can cause a phase transition in the molecule (see Chap. 3).

An effective self-attraction, like the one considered here by means of a $6-12$ Lennard-Jones potential, arises due to hydrophobic interactions in polypeptides and due to a suitably large concentration of polyvalent counterions in the case of double-stranded DNA. If this is the case, the polymer is in poor solvent conditions or equivalently below the θ point (in the nomenclature of the models discussed above). In these cases at zero stretch the force attains (in a thermodynamically long chain) a non-zero value followed by a force plateau for long molecules [40]. This indicates the presence of a first order transition. From Molecular Dynamics simulations reported in [86], it can be seen that in this situation (i.e. in poor solvent conditions) the two ensembles, fixed force and fixed stretch, are not equivalent for short chains[1] and indeed in the experiments the stretching curves of small DNA's or of DNA's in presence of a high concentration of polyvalent counterions in reality show peaks. As seen in Chap. 3, a thorough explanation of this effect includes polyelectrolyte modeling, finite size corrections as well as dynamical effects. More details can be found in Refs. [40, 70].

A different scenario holds for ssDNA and for RNA (this scenario would also be retraced if a self-attractive polymer such as dsDNA in presence of condensing agents is restricted conformationally to stay in a quasi-two-dimensional film). In these cases the single molecule phase transition is second order and thus at low stretch the characteristic force curves are non-zero and then rise smoothly. Furthermore, the attraction in ssDNA and RNA is brought forth by the base pairing interactions between bases far apart in the chain. If sequence disorder is neglected, the low force regime can be written as follows (see Eq. (3.13)):

$$\zeta \sim (f - f_c)^{1/\Delta - 1} \tag{4.16}$$

[1] This topic has been discussed in several papers. See, e.g., [56, 57, 87, 88, 89].

where f_c is the critical force. The exponent Δ is between 0.5 (the value of native branched polymer-like configurations arising from base stacking [90]) and 1 (for a polymer in a good solvent). While present day experiments show that as the extension goes to 0 the force is non-zero [91], the data are not clean enough to allow discriminating between the exponents above. To be noted that within a simplified theory [91], it was possible to find a law implying $\Delta = 1/2$.

4.5 Conclusions

Here, we have revised the well known WLC model that correctly describes the behaviour under pulling of a *stiff* polymer.

- We have pointed out that its discrete version has a different large force behaviour respect to the continuous version by Marko and Siggia [11], Eq. (4.6). We predict a *crossover* force between these two different regimes. It should be noticed that a recent paper by Livadaru et al. [92] reports a similar result. However, here we have given a simpler formula, Eq. (4.9), which can be tested on real polymers as well as on numerical simulations, where self-interactions are present.

- So, firstly, we have used it to fit some experimental data on dsDNA, Fig. 4.1, and ssDNA, Fig. 4.2. In the former case, where Eq. (4.10) was already applied with success, we find that Eq. (4.9) predicts a not trivial intra bead distance, which is much smaller than the predicted persistence length. This implies that the crossover force is much greater than the achievable experimental forces and justifies the approach by Marko and Siggia. In the latter case, we observe a clear crossover between the two regimes. In fact, now the intra bead distance is of the same order of magnitude of the persistence length and the crossover force can be easily achieved. Thus our Eq. (4.9) is more appropriate than Eq. (4.10) in this case.

- Then, we have performed some Monte-Carlo simulations to verify the validity of our formula. We have analyzed different kinds of intra bead potentials. For a short range *repulsive* potential we have correctly found that our formula is in good agreement with the numerical data, predicting a renormalized stiffness [80, 81]. For a more realistic Lennard-Jones potential the situation is more complicated. For temperatures above the θ point, Eq. (4.9) gives a good fit. The main result is that, now, both the persistence length and the intra bead distance

b are renormalized by the potential. For temperatures below the θ point, our formula agrees with the numerical data only at large forces.

- Finally, we have discussed how an attractive potential can modify the pulling behaviour of a polymer under poor solvent conditions.

Perspectives

– How, then, did you deduce the telegram?
– Why, of course I knew that you had not written a letter, since I sat opposite to you all morning. I see also in your open desk there that you have a sheet of stamps and a thick bundle of postcards. What could you go into the post-office for, then, but to send a wire? Eliminate all other factors, and the one which remains must be the truth.

Sir Arthur Conan Doyle, *Sign of Four*

This research work can be divided in two parts:

- In the first part, we have discussed the stretching of a polymer in *poor* solvent conditions, i.e., below the θ temperature.

  Firstly, we have described a simple $2d$ on-lattice model of directed self-avoiding walk, which is amenable to an analytical treatment. Then, we have discovered an interesting scaling relation, which seems to be rather general and not due to the simplicity of the model. In particular, we have given a strong confirmation that in $2d$ the stretching transition must be *second* order. After having complicated the model, we have discussed the Thermodynamics of the unfolding by means an applied external force, and found the corresponding phase diagram. Besides, with a Monte Carlo calculation applied to a $3d$ continuous model we have given a unifying picture of three recent experimental results (see Sec. 2.3), which in principle seem to contradict each other.

- In the second part, we have discussed the stretching pathway of a polymer in *good* solvent conditions.

  Here, we have suggested a *new* interpolation formula that generalizes the one proposed some years ago by Marko and Siggia in Ref. [11]. We have correctly taken into account the possibility of a *finite* intra bead distance, which acts as a

new parameter. Then, we have tested our equation on some Monte Carlo and experimental data. The final result is that we were able to reproduce not only the results of the old formula, but also to investigate new regimes where the Marko and Siggia's result completely fails.

Of course, our models contains a certain number of approximation and much research work must be devoted to improve and generalize our results.

In particular, it would be interesting to study the unfolding transition and Thermodynamics for an interacting model of self-avoiding polymer in $d = 3$. This was partially due [32, 93, 94] for some *on-lattice* models, although it would highly appealing to concentrate on a more realistic *off-lattice* model. We should expect a *first* order unzipping transition (for $T < T_\theta$), and, in particular, the scaling theory developed for the $2d$ model should be revised.

Then, as already said, the study of the ground states (at $T = 0$) of an interacting flexible polymer has explained the multistep behaviour of some real polymers. In principle, the introduction of a suitable *stiffness* in our model could complicate this picture and modify the ground states described above. In particular, we can suspect that the *globule* conformation at zero force is no more achievable, due to the large amount of stiffness energy. But other more or less compact configurations could be found.

We think these future investigations could be helpful not only from a theoretical point of view, but they could be also an intriguing starting point for further experimental observations.

Appendix A

The *freely jointed chain* (FJC) model

We have already stressed that during the last years much research work was devoted to the development and study of many models of polymers. One of the most widely used is the random-walk model by Edwards [20], that adequately describes the global properties of several polymeric systems. Another simple model is the so called *freely jointed chain* (FJC) model that describes a polymer whose bonds have a fixed length (we put it equal to 1) and whose bond angle are unconstrained. Then the energy of a FJC chain is the same for all the configuration.

The corresponding Boltzmann weight in the presence of an external force field reads:

$$e^{-\beta\mathcal{H}} = \frac{1}{(4\pi)^N}\prod_{i=1}^{N}\delta(|\mathbf{t}_i|-1)e^{\beta\mathbf{F}\cdot\mathbf{t}_i}, \tag{A.1}$$

where $\mathbf{t}_i = \mathbf{r}_i - \mathbf{r}_{i-1}$ ($\mathbf{r}_i$ being the chain vector of the i's monomer), $\mathbf{F} = F\hat{\mathbf{z}}$ is the applied force and $N+1$ is the total number of monomers along the discrete chain. The partition function is:

$$\mathcal{Z}_N(F) = \frac{1}{(4\pi)^N}\int\prod_{i=1}^{N}d\mathbf{t}_i\delta(|\mathbf{t}_i|-1)e^{\beta\mathbf{F}\cdot\mathbf{t}_i} = \left(\frac{\sinh(\beta F)}{\beta F}\right)^N, \tag{A.2}$$

from the simple factorization of Eq. (A.1). Then, the normalized extension $\zeta \equiv \langle z\rangle_N/N$, where z is the extension along the direction of the applied force, is

$$\zeta = \frac{\partial}{\partial\beta F}\log\left(\frac{\sinh(\beta F)}{\beta F}\right) = \coth(\beta F) - \frac{1}{\beta F}. \tag{A.3}$$

The large force behaviour predict that $1-\zeta \sim 1/F$.

Fixing $F=0$, let us now calculate the average end-to-end distance $R_N \equiv \sqrt{\langle\mathbf{R}_N^2\rangle}$ where $\mathbf{R}_N \equiv \mathbf{r}_N - \mathbf{r}_0$.

It is evident that

$$\langle \mathbf{R}_N^2 \rangle = \sum_{i,j=1}^{N} \langle \mathbf{t}_i \cdot \mathbf{t}_j \rangle = N + \frac{1}{2} \sum_{i<j=2}^{N} \langle \mathbf{t}_i \cdot \mathbf{t}_j \rangle = N, \tag{A.4}$$

since $\langle \mathbf{t}_i \cdot \mathbf{t}_j \rangle = 0$ if $i \neq j$. Then, $R_N = N^{1/2}$, which is the well-known end-to-end displacement of a *random walk* [20].

If the bonds have a length equal to b (instead of 1), we simply have $R_N = bN^{1/2}$. Though the FJC is a very simple model, the result $R_N \propto N^{1/2}$ holds for more general result (see Appendix B and Ref. [20]).

Now let us *define* the Kuhn length [20], $L_K \equiv R_N^2/R_{max}$, where R_{max} is the maximum length of the end-to-end vector[1]. For a FJC with $b \neq 1$, $L_K = b$.

[1]The physical meaning of the Kuhn length was given in Sec. 1.3.

Appendix B

The *worm like chain* (WLC) model

This Appendix is a systematic introduction to the so called worm like chain (WLC) model, which has already been examined in Chap. 4.

This model does take into account the internal *stiffness* that many polymeric molecules have and it was introduced much time ago by Kratky and Porod [95]. Its relevant physical parameter is the *persistence* length L_p, which gives an estimate of the length scale over which the tangent vector along the contour of the chain backbone are correlated. Then, we are interested in those cases when L_p is of the same order of magnitude of the total contour length of the chain L_c. A well known example is the double stranded DNA (dsDNA) filament, whose persistence length is about ~ 53 nm [11].

As known, to estimate the persistence length a force must be applied to the polymeric chain and then the end-to-end distance is measured [96]. So, from the extension vs. force plot is possible to obtain L_p, which then acts as a free parameter. The WLC model with stretching [95, 11] is described by the following hamiltonian:

$$\beta\mathcal{H}_{WLC} = \frac{L_p}{2}\int_0^L \left(\frac{d\mathbf{t}}{ds}\right)^2 ds - \mathbf{f}\cdot\int_0^L \mathbf{t}(s)ds. \tag{B.1}$$

In Eq. (B.1), $\beta = 1/k_BT$, $\mathbf{f} = \beta\mathbf{F}$, where $\mathbf{F}$ is the applied force and $\mathbf{t}(s) = \partial_s\mathbf{r}$, where $\mathbf{r}(s)$ is the position of a monomer along the chain, labeled by the internal coordinate, s. $\mathbf{t}(s)$ satisfies the constraint

$$\mathbf{t}^2(s) = 1. \tag{B.2}$$

This means that the bonds between nearest monomers in the polymeric chain are *fixed* (see, for example, Thirumalai and Ha in [16]). As a matter of convenience, we

introduce the following discrete version of the WLC model (see Eq. 4.1):

$$\beta\mathcal{H}_{discr} = -K\sum_{i=1}^{N-1}\mathbf{t}_i\cdot\mathbf{t}_{i+1} - \mathbf{h}\cdot\sum_{i=1}^{N}\mathbf{t}_i \text{ with } \left\{\begin{array}{rcl} K & \equiv & \beta J \\ \mathbf{h} & \equiv & \beta\mathbf{H}\end{array}\right. , \tag{B.3}$$

with the condition

$$\mathbf{t}_i^2 = 1,\ \forall i = 1, ..., N, \tag{B.4}$$

where, as described in Appendix A, $\mathbf{t}_i = \mathbf{r}_i - \mathbf{r}_{i-1}$ ($\mathbf{r}_i$ being the chain vector of the i's monomer) and $N+1$ is the total number of monomers along the discrete chain. The definition for the partition function and the average extension are given in Eqs. (4.2) and (4.3)[1]. To recover the *continuum* version, Eq. (B.1), from Eq. (B.3) we require that [75]:

$$\begin{array}{rcl} L_p & = & \lim_{b\to 0} Kb \\ \mathbf{f} & = & \lim_{b\to 0} \mathbf{h}/b \end{array} , \tag{B.5}$$

where b is the monomer-monomer distance along the chain. In Eq. (B.3) we have used *periodic boundary conditions*, i.e, $\mathbf{t}_{N+1} \equiv \mathbf{t}_1$. This is not a serious assumption: at the end we shall perform the thermodynamic limit $N \to \infty$, which is independent of the chosen boundary conditions.

Let us stress the fact that Eq. (B.3) with the condition (B.4) is the hamiltonian for an Ising chain [97], where we indicate with d the dimension of the spin vector $\mathbf{t}_i$ ($O(d)$-model). It is a well known result that the model (B.3) is exactly solvable only for $d = 1$ (see, for example, Stanley in [98]). The $d = \infty$ case is exactly solvable, too and it corresponds to the so called *spherical* model [99]: the demonstration was firstly given by Stanley [100].

B.1 Exact results

Here, we briefly review some well known results:

1. $F \to 0$.

   This means (Eqs. (B.3) and (B.5)) that $h \to 0$. Then, the partition function

[1] As in Appendix A, in the following we shall make use of the *normalized* extension $\zeta \equiv \langle z\rangle_N/N$.

$\mathcal{Z}_N^d(K,h)$ is

$$\begin{aligned}\mathcal{Z}_N^d(K,h) &\simeq \mathcal{Z}_N^d(K,0)\left(1+\frac{1}{2}\sum_{l,m=1}^{N}\langle(\mathbf{h}\cdot\mathbf{t}_l)(\mathbf{h}\cdot\mathbf{t}_m)\rangle\right)\\ &= \mathcal{Z}_N^d(K,0)\left(1+\frac{h^2}{2d}\sum_{l,m=1}^{N}\langle\mathbf{t}_l\cdot\mathbf{t}_m\rangle\right).\end{aligned} \tag{B.6}$$

where $\langle\cdot\rangle$ indicates the average value with the hamiltonian (B.3) and $h=0$. Using well known results [101], it is easy to verify that ζ in the thermodynamical limit ($N\to\infty$) is

$$\zeta = \frac{h}{d}\times\frac{1+y_d(K)}{1-y_d(K)}, \tag{B.7}$$

where $y_d(K)=I_{d/2}(K)/I_{d/2-1}(K)$ and $I_q(K)$ is the first kind modified *Bessel* function of order q and argument K [102]. In the continuum limit, Eq. (B.7) becomes, simply,

$$\zeta = \frac{2}{d}\frac{2}{d-1}\beta L_p F. \tag{B.8}$$

2. $F\to\infty$.

   In complete analogy as before, this means that $h\to\infty$. Then, writing the vector $\mathbf{t}=(\mathbf{t}^\perp,t^\parallel)$, that is along the components perpendicular and parallel to the applied field, respectively, we can write

$$t^\parallel = \sqrt{1-(\mathbf{t}^\perp)^2}\simeq 1-\frac{(\mathbf{t}^\perp)^2}{2}. \tag{B.9}$$

   So, the hamiltonian (B.3) becomes

$$\beta\mathcal{H}_{discr}\simeq\sum_{i,j=1}^{N}\left[\left(K+\frac{h}{2}\right)\delta_{ij}-\frac{K}{2}(\delta_{i,j-1}+\delta_{i,j+1})\right]\mathbf{t}_i^\perp\cdot\mathbf{t}_j^\perp\equiv\sum_{i,j=1}^{N}\mathcal{M}_{ij}\mathbf{t}_i^\perp\cdot\mathbf{t}_j^\perp. \tag{B.10}$$

   Let us compute the average value $\langle(\mathbf{t}_i^\perp)^2\rangle$:

$$\langle(\mathbf{t}_i^\perp)^2\rangle = \frac{d-1}{2}\frac{1}{K\left[(1+h/(2K))^2-1\right]^{1/2}}. \tag{B.11}$$

   Now, the average value $\langle\cdot\rangle$ is made with the hamiltonian (B.10)[2]. In the continuum limit Eq. (B.11) becomes $\langle(\mathbf{t}^\perp(s))^2\rangle=\frac{d-1}{2\sqrt{\beta L_p F}}$, where we have substituted the discrete index i with the continuum index s. Then $\zeta=\langle t^\parallel(s)\rangle$ is,

[2]Let us notice that Eq. (B.11) corresponds to Eq. 4.4 with $d=3$.

simply,

$$\zeta = 1 - \frac{d-1}{2}\frac{1}{\sqrt{4\beta L_p F}}. \tag{B.12}$$

Fixing $F = 0$, let us now calculate the average end-to-end distance $R_N \equiv \sqrt{\langle \mathbf{R}_N^2 \rangle}$ (see Appendix A) and consider the particular case $d = 3$.

It is easy to show that

$$R_N^2 = \frac{1 + y_3(K)}{1 - y_3(K)} b^2 N. \tag{B.13}$$

where we have fixed the bond length equal to $b \neq 1$ and $y_3(K) = \coth(K) - 1/K$. Then, $R_N \propto N^{1/2}$ holds and the Kuhn length (see Appendix A) L_K obeys the equation

$$L_K = \frac{1 + y_3(K)}{1 - y_3(K)} b. \tag{B.14}$$

In the continuum limit, Eq. (B.5), $L_K = 2L_p$, which is a well known result [4].

Appendix C

Including $1/d$ corrections in wormlike chains

C.1 Introduction

Here, we perform a $1/d$-expansion on the WLC model described in Appendix B, where d is the number of the spatial components of the spatial vectors. The corresponding continuum limit extend the calculations reported in Ref. [103]. The calculation shows that the $1/d$ terms give an improved behaviour in the limit of low forces and the *correct* one in the limit of large forces.

We shall proceed along the following lines:

1. expanding around the $d = \infty$ limit, we calculate the free energy for the system up to the $1/d$ term;

2. we calculate the *equation of state* (see [99]) in the form of $\zeta = \zeta(h, \beta)$, where ζ is the normalized extension of the chain;

3. then, we calculate the continuum limit, with the help of the Eqs. (B.5);

4. at the end of the calculation we shall fix $d = 3$, which is the case of physical interest.

In Sec. C.2, we shall proceed along the same lines of Refs. [81, 103], while the general formalism about one-dimensional $O(d)$ and more complicated models can be found in [104].

In next Section, we shall analyze the exact behaviour of the model in the limiting cases $F \to 0$ and $F \to \infty$. Then, at the end we shall compare our approximate formula with these results.

C.2 Outline of the calculations

Focusing our attention on the hamiltonian $\beta\mathcal{H}_{discr}$ (Eq. (B.3)), with the constraint given by Eq. (B.4), the partition function reads as:

$$\mathcal{Z}_N^{(d)}(\beta) = \int \prod_{i=1}^{N} d\Omega(\mathbf{t}_i) e^{-\beta\mathcal{H}_{discr}}, \tag{C.1}$$

where

$$d\Omega(\mathbf{t}_i) = \frac{\Gamma(d/2)}{\pi^{d/2}}\delta(\mathbf{t}_i^2 - 1)d^d t_i = \frac{\Gamma(d/2)}{\pi^{d/2}} \times \frac{1}{2\pi i}\int_{c_i - i\infty}^{c_i + i\infty} e^{-\alpha_i(\mathbf{t}_i^2 - 1)} d\alpha_i \times d^d t_i. \tag{C.2}$$

In Eq. (C.2), c_i is chosen large enough in order the integral representation of the δ-function makes sense.

Finally, inserting Eq. (C.2) in (C.1), we easily obtain:

$$\mathcal{Z}_N^{(d)}(\beta) = \left(\frac{\Gamma(d/2)}{\pi^{d/2}}\right)^N \int_{c_i - i\infty}^{c_i + i\infty} \prod_{i=1}^{N} d\alpha_i \int_{-\infty}^{+\infty} \prod_{i=1}^{N} d^d t_i \exp\left\{\sum_{i=1}^{N} \alpha_i - \mathbf{t}_i \mathcal{M}_{ij} \mathbf{t}_j + \mathbf{h} \cdot \sum_{i=1}^{N} \mathbf{t}_i\right\}, \tag{C.3}$$

with the matrix $\mathcal{M}$ defined as

$$\mathcal{M}_{ij} = \alpha_i \delta_{ij} - \frac{K}{2}(\delta_{i,j-1} + \delta_{i,j+1}),\ \delta_{ij} = \begin{cases} 1 & \text{if} \quad i = j \\ 0 & \text{if} \quad i \neq j \end{cases} \tag{C.4}$$

Now, with the above prescription on the c_i's, we can invert the integration in (C.3), with the result

$$\begin{aligned} \mathcal{Z}_N^{(d)}(\beta) \quad &\propto \quad \int_{c_i - i\infty}^{c_i + i\infty} \prod_{i=1}^{N} d\tilde{\alpha}_i \exp\left[-d\left(-\sum_{i=1}^{N}\tilde{\alpha}_i + \frac{1}{2}\operatorname{Tr}\log\tilde{\mathcal{M}} - \frac{1}{2}\tilde{h}^2 \sum_{i,j}\tilde{\mathcal{M}}_{ij}^{-1}\right)\right] \\ &\equiv \quad \int_{c_i - i\infty}^{c_i + i\infty} \prod_{i=1}^{N} d\tilde{\alpha}_i \exp\left[-d\mathcal{F}(\{\tilde{\alpha}\}, \tilde{h})\right], \end{aligned} \tag{C.5}$$

where we have neglected unimportant multiplicative constants, "Tr" is the Trace operator and $\{\tilde{\alpha}\}$ indicates the whole set of the variables $\tilde{\alpha}_i$. In Eq. (C.5) we have made

the following statements:

$$\begin{aligned} \tilde{\alpha}_i &= \alpha_i/d \\ \tilde{\mathbf{h}} &= \mathbf{h}/d \\ \tilde{\mathcal{M}} &= \mathcal{M}/d. \end{aligned} \tag{C.6}$$

and analogous definitions for the corresponding quantities $\tilde{J}$ and $\tilde{\mathbf{H}}$ (see Eq. (B.3)) hold.

In the large d limit, it is possible to calculate the integral in Eq. (C.5) using the *saddle point* approximation [100, 104]. The equation for the saddle point is simply given by

$$\frac{\partial}{\partial \tilde{\alpha}_i}\mathcal{F}(\{\tilde{\alpha}\},\tilde{h}) = 0,\ \forall i = 1,...,N. \tag{C.7}$$

It is a well known result [100] that Eq. (C.7) leads to the uniform solution $\tilde{\alpha}_i = \tilde{\alpha}_0$. So, the equation for the saddle point becomes

$$\tilde{K}\left[1 - \left(\frac{\tilde{h}}{2\tilde{K}}\right)^2 \frac{1}{z_0^2}\right] = \frac{1}{2\sqrt{(z_0+1)^2-1}},\ \text{with } z_0 \equiv \frac{\tilde{\alpha}_0 - \tilde{K}}{\tilde{K}}. \tag{C.8}$$

In the continuum limit (Eq. (B.5)) and using the definitions (C.6), Eq. (C.8) reads as

$$2L_p\left[1 - \left(\frac{\beta F}{2L_p}\right)^2 \frac{1}{\hat{z}_0^2}\right] = \frac{d}{\sqrt{2\hat{z}_0}},\ \text{with } \hat{z}_0 = \lim_{b\to 0}\frac{z_0}{b^2}. \tag{C.9}$$

Eq. (C.8) gives the saddle point for the spherical model ($d = \infty$) (see, for example, [99]); instead Eq. (C.9) gives the saddle point in the large d limit, but for $d < \infty$. This agrees with the results of the Refs. [81, 103]. But, let us notice that the $1/d$ expansion must be performed in the variables normalized to d (see Eqs. (C.6)) and that only at the end of the calculations, we can substitute the "normalized" variables with those that appear in the definition of the hamiltonian, Eq. (B.1), in the continuum limit.

Now, to include the $1/d$ terms, we had to expand in a Taylor series the function $\mathcal{F}(\{\tilde{\alpha}\},\tilde{h})$, defined in Eq. (C.5), around the saddle point $\tilde{\alpha}_i = \tilde{\alpha}_0$. Finally, we easily obtain

$$\begin{aligned} \mathcal{F}(\{\tilde{\alpha}\},\tilde{h}) &\simeq -N\tilde{K}z_0 + \frac{N}{2}\int_0^{2\pi}\frac{dp}{2\pi}\log\left[2\tilde{K}\left(z_0+1-\cos(p)\right)\right] - \frac{N}{2}\frac{\tilde{h}^2}{2\tilde{K}z_0} + \\ &\quad + \frac{1}{2}\frac{\partial^2\mathcal{F}}{\partial\xi_i\partial\xi_j}\bigg|_{\xi_i=\xi_j=z_0}(\xi_i - z_0)(\xi_j - z_0) \\ &\equiv -N\phi(z_0,\tilde{h}) + \frac{1}{2}\frac{\partial^2\mathcal{F}}{\partial\xi_i\partial\xi_j}\bigg|_{\xi_i=\xi_j=z_0}(\xi_i - z_0)(\xi_j - z_0) \end{aligned} \tag{C.10}$$

where $\xi_i \equiv \frac{\tilde{\alpha}_i - \tilde{K}}{\tilde{K}}$ and

$$\left.\frac{\partial^2 \mathcal{F}}{\partial \xi_i \partial \xi_j}\right|_{\xi_i=\xi_j=z_0} = -2\tilde{K}^2 \times \left[\left(\tilde{\mathcal{M}}^{-1}_{ij}\right)^2 + 2\left(\frac{\tilde{h}}{2\tilde{K}z_0}\right)^2 \tilde{\mathcal{M}}^{-1}_{ij}\right]\Bigg|_{\xi_i=\xi_j=z_0} . \quad \text{(C.11)}$$

Then we can compute the free energy $F = F(\beta, \tilde{h})$ for the system, up to including the $1/d$ terms. The final results is

$$\frac{-\beta F(\beta,\tilde{h})}{dN} = \phi(z_0,\tilde{h}) - \frac{1}{2d}\int_0^{2\pi}\frac{dq}{2\pi}\log\left|\hat{\mathcal{F}}_{\xi_i\xi_j}(q)\right| . \quad \text{(C.12)}$$

In Eq. (C.12), the function $\left|\hat{\mathcal{F}}_{\xi_i\xi_j}(q)\right|$ is the modulus of the *Fourier* transform of the function defined in the Eq. (C.11)[1]:

$$\begin{aligned}\hat{\mathcal{F}}_{\xi_i\xi_j}(q) &= -\frac{1}{2}\left[\int_0^{2\pi}\frac{dp}{2\pi}\left(\frac{1}{z_0+1-\cos(q-p)}\times\frac{1}{z_0+1-\cos(p)}\right)+\right.\\ &\left.+\frac{1}{\tilde{K}}\left(\frac{\tilde{h}}{z_0}\right)^2\frac{1}{z_0+1-\cos(q)}\right]\\ &= -\frac{1}{2}\left[\frac{2(z_0+1)}{\sqrt{z_0^2+2z_0}}\frac{1}{2(z_0^2+2z_0)+1-\cos(q)}+\frac{1}{\tilde{K}}\left(\frac{\tilde{h}}{z_0}\right)^2\frac{1}{z_0+1-\cos(q)}\right] .\end{aligned} \quad \text{(C.13)}$$

ζ is defined *via* the relation

$$\zeta = \frac{d}{d\tilde{h}}\left(\frac{-\beta F(\beta,\tilde{h})}{dN}\right) \equiv \frac{\partial}{\partial z_0}\left(\frac{-\beta F(\beta,\tilde{h})}{dN}\right)\frac{\partial z_0}{\partial \tilde{h}} + \frac{\partial}{\partial \tilde{h}}\left(\frac{-\beta F(\beta,\tilde{h})}{dN}\right) . \quad \text{(C.14)}$$

Then, at the end of the calculation we obtain the following relation:

$$\zeta = \frac{\tilde{h}}{2\tilde{K}z_0}\left[1 - \frac{1}{2d}\int_0^{2\pi}\frac{dq}{2\pi}\frac{1}{\left|\hat{\mathcal{F}}_{\xi_i\xi_j}(q)\right|}\left(\frac{1}{z_0\phi''(z_0)}\frac{\partial\left|\hat{\mathcal{F}}_{\xi_i\xi_j}(q)\right|}{\partial z_0} + \frac{4}{z_0}\times\frac{1}{z_0+1-\cos(q)}\right)\right] , \quad \text{(C.15)}$$

where we have used the equation

$$\frac{\partial z_0}{\partial \tilde{h}} = \frac{1}{2\phi''(z_0)}\frac{\tilde{h}}{\tilde{K}z_0^2}, \text{ with } \phi''(z_0) = \frac{\tilde{h}^2}{2\tilde{K}z_0^3} + \frac{1}{2}\frac{z_0+1}{\left[(z_0+1)^2-1\right]^{3/2}} \quad \text{(C.16)}$$

[1] Again, let us remark that we have made use of periodic boundary conditions.

To obtain Eq. (C.16), we have taken into account the fact that $\phi'(z_0(\tilde{h}),\tilde{h})) \equiv 0$, by definition. Now, let us notice that in the limit $d = \infty$, Eq. (C.15) becomes, simply, $\zeta = \frac{\tilde{h}}{2\tilde{K}z_0}$, that in conjunction with Eq. (C.8) gives the equation of state for the *spherical* model in one dimension [99].

Now, starting from the Eq. (C.16) and using the definitions (B.3), (B.5), (C.6), and that for $\hat{z}_0$ (see Eq. (C.9)), it is possible to obtain the final expression for ζ in the continuum limit. The calculations are quite boring, so we report the final results and give a detailed description of them. This will be done in next Section.

C.3 Final results

The final expression for ζ is:

$$\zeta = \frac{\beta F}{2L_p\hat{z}_0}\left[1 - \frac{1}{2d}\mu(F, L_p, \beta, \hat{z}_0)\right] \tag{C.17}$$

where, as already said, $\hat{z}_0$ satisfies Eq. (C.9). μ has the following functional form:

$$\mu = \mu_1 + \mu_2 - \mu_3 \tag{C.18}$$

with

$$\begin{aligned}
\mu_1 &= \frac{4\hat{z}_0\sqrt{2\hat{z}_0}}{\left[\left(\hat{z}_0\sqrt{2\hat{z}_0} + 4(\beta F)^2/(dL_p)\right)\left(\hat{z}_0\sqrt{2\hat{z}_0} + (\beta F)^2/(dL_p)\right)\right]^{1/2}}, \\
\mu_2 &= \frac{12\hat{z}_0^3\sqrt{2\hat{z}_0}}{\left(2\hat{z}_0^2 + (\beta F)^2/(dL_p)\sqrt{2\hat{z}_0}\right)\left[\left(\hat{z}_0\sqrt{2\hat{z}_0} + 4(\beta F)^2/(dL_p)\right)\left(\hat{z}_0\sqrt{2\hat{z}_0} + (\beta F)^2/(dL_p)\right)\right]^{1/2}}, \\
\mu_3 &= \frac{4\hat{z}_0^2\sqrt{2\hat{z}_0}}{\hat{z}_0^2 + 2(\beta F)^2/(dL_p)\sqrt{2\hat{z}_0}}\left(\frac{3\hat{z}_0\gamma}{2\hat{z}_0^2 + (\beta F)^2/(dL_p)\sqrt{2\hat{z}_0}} + \frac{3}{\sqrt{2\hat{z}_0}}\right), \\
&\text{and } \gamma = \frac{3(\beta F)^2/(dL_p)\sqrt{2\hat{z}_0}}{2\left[\left(\hat{z}_0\sqrt{2\hat{z}_0} + 4(\beta F)^2/(dL_p)\right)\left(\hat{z}_0\sqrt{2\hat{z}_0} + (\beta F)^2/(dL_p)\right)\right]^{1/2}}.
\end{aligned} \tag{C.19}$$

Then, let us calculate the leading behaviour in the two important limits: $F \to 0$ and $F \to \infty$. The final results are:

$$m = \begin{cases} 1 - \frac{d-1}{2}\frac{1}{\sqrt{4\beta L_p F}} & \text{if} \quad F \to \infty \\ \left(\frac{2}{d}\right)^2 \beta\left(\frac{d+1}{d}L_p\right)F & \text{if} \quad F \to 0 \end{cases}. \tag{C.20}$$

It is interesting to compare Eq. (C.20) with the exact results of Sec. B.1.

While the results for $F \to 0$ agree at first order in d, as one could expect, the corresponding ones for $F \to \infty$ give, *surprisingly*, the same behaviour. This is a beautiful result, showing that if we perform the expansion including $1/d^2$ terms we do not gain nothing in the large force limiting case.

Appendix D

Excluded volume effects

In this Appendix, we shall briefly discuss the important problem of the excluded volume effects in real polymers. For more details, we shall refer to some excellent reviews and books, present in literature (see, e.g., Refs. [3, 10, 12, 20, 105])

D.1 Formulating the problem

The models introduced in Appendices A and B describe an *ideal* polymer. This means that we have systematically neglected all the interactions between different monomers along the chain. For many practical purposes this may be a good approximation. In fact monomer-monomer attraction energy along the chain has a typical scale of 5 eV (covalent bond), that is much higher than other interactions (say, between the polymer and the solvent or between different monomers far apart along the chain, whose scale is ~ 0.1 eV).

At room temperatures ($K_B T \sim 0.025$ eV) covalent bonds can not be broken. But this energy scale can compete with the other interactions described above: consequently, the properties of real polymers may be richer than those predicted by the simple models described in Appendices A and B.

As already said, the excluded volume effects arise due to *long range* interactions, i.e., to interactions involving pairs of monomers which are remote in the chain sequence, though, of course, near to one another in space when involved in mutual interaction. This interaction can be roughly described by a potential $V(r)$ (where r is the distance between two monomers), whose shape is plotted in Fig. D.1.

Let us notice that:

- if r is small, $V(r)$ is positive and very large. This is because two monomers

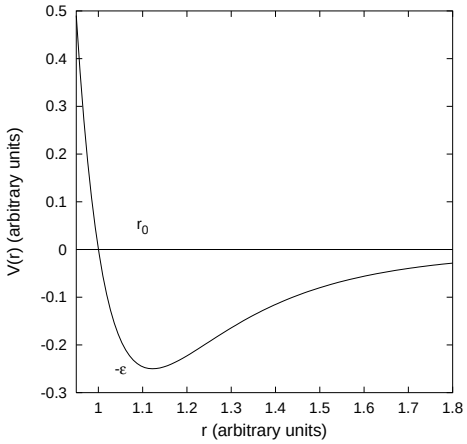

Figure D.1: A typical dependence of the interaction energy $V(r)$ between two monomers on the distance r between them. The units on the x and y axes are arbitrary. The minimum $-\epsilon$ is located at $r = r_0$.

can not penetrate into each other (excluded volume effect);

- as r becomes larger, monomers usually start to attract each other.

The crossover distance between these two regimes is located at r_0, which should have the same magnitude as the size of a monomer unit, that is, $r_0 \sim 10$ Å.

In practice, to bring two monomers together, as close as r, some work has to be done. This work is stored in $V(r)$. It is done against the solvent molecules, as they need to be squeezed out of the way. Hence, $V(r)$ represents the effective interaction of monomers through the solvent. It should depend, therefore, on the contents and state of the solvent, as well as on the temperature.

D.2 Good and bad solvents

If $K_B T$ is large compared to the absolute value of the minimum of the potential ϵ, only repulsion at short distance dominates. It makes the coil swell. In this case the polymer behaves as a self avoiding walk (SAW), rather than a random walk. The end-to-end displacement R_N is no more given by $R_N \sim N^{1/2}$ (see Appendix A). In this case, $R_N \sim N^\nu$, where ν is the SAW critical exponent. It is known that a good approximation for the exponent ν is given by the Flory formula [3, 10]

$$\nu = \frac{3}{d+2}, \tag{D.1}$$

where d is the number of spatial dimensions. If $K_B T \gg \epsilon$, we say that the polymer is in a *good* solvent.

If $K_B T \ll \epsilon$, attraction becomes important. Now the polymer is in a special compact state, called a *globule*. Its behaviour resembles the one of a hamiltonian walk [9, 105] and its end-to-end distance $R_N \sim N^{1/d}$. We say that the polymer is in a *bad* (or *poor*) solvent.

Finally, a special condition may be realized, when at a given temperature $T = T_\theta$ attraction and repulsion exactly compensates. In this case (θ condition) the polymer behaves as ideal[1].

[1]Let us remark that, rigorously, this is true for $d \geq 3$, when we can neglect *three*-body interactions. For $d < 3$ the polymer at the θ temperature does not behave as a random walk [9, 10, 105].

Appendix E

Exact evaluation of the critical exponents

In this Appendix we will show that, generalizing the *continuous* DSAW model introduced in Ref. [47] for $f \neq 0$, the exact critical line $f_c(T)$ can be calculated. More importantly, we have obtained an exact derivation of the critical exponents at $f > f_c$ and $f = f_c$ and we will show that they do not depend on T for $T \leq T_\theta$. The Appendix is organized as follows:

- in Sec. E.1 we introduce some general concepts about tricritical scaling;
- in Sec. E.2 we review the analytical methods developed in Ref. [47] and apply them to extract the critical exponents.

E.1 A brief outline on the tricritical scaling

We here introduce some concepts about the theory of the tricritical scaling, which is believed to describe the θ transition of a dilute solution of polymers. As already said, the model we have in mind is the self-interacting DSAW (see Chap. 3). However, our approach is rather general and far beyond the DSAW model[1].

The partition function for a self-interacting DSAW with L sites is given by:

$$\mathcal{Z}_L(\omega) = \sum_{\mathcal{C}} c_L(m)\omega^m, \tag{E.1}$$

where $c_L(m)$ is the *total* number of walks of L steps with m contacts and $\omega = e^{\beta\epsilon}$, being $-\epsilon$ the nearest-neighbour energy contact and the sum is over all configurations

[1] More details may be found in Refs. [106, 107, 108].

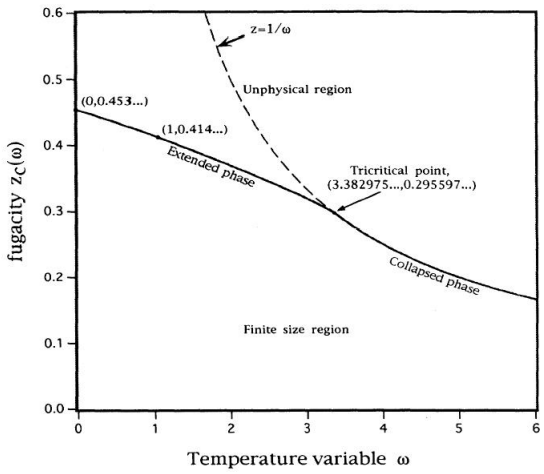

Figure E.1: Singularity diagram for a DSAW with self-interactions (from Ref. [46]).

of the L-step walk. The generating function is defined as

$$\mathcal{G}(\omega, z) = \sum_{L=1}^{\infty} \mathcal{Z}_L(\omega) z^L, \tag{E.2}$$

where z is the *fugacity*. The total free energy is given by

$$F_L(\omega) = -\frac{1}{\beta} \log \mathcal{Z}_L(\omega). \tag{E.3}$$

In the large L limit we have the free energy per step

$$f_\infty(\omega) = \lim_{L\to\infty} \frac{1}{L} F_L(\omega), \tag{E.4}$$

which in turn implies

$$F_L(\omega) \simeq L f_\infty(\omega) + o(L). \tag{E.5}$$

Inserting Eq. (E.5) in Eq. (E.2), we deduce that the generating function has a singularity for $z = z_\infty(\omega) = e^{\beta f_\infty(\omega)}$. A plot of $z_\infty(\omega)$ in the (ω, z)-plane is named a singularity diagram. For a DSAW, it is shown in Fig. E.1 [44, 46].

Different parts of the singularity diagram correspond to distinct features of the model. For the DSAW model, in the thermodynamic limit, the model undergoes a phase transition at some temperature T_θ and the free energy $f_\infty(\omega)$ (and so $z_\infty(\omega)$) is singular at $\omega_\theta = e^{\beta_\theta \epsilon}$, where $\beta_\theta = 1/k_B T_\theta$. The line $z_\infty(\omega)$ for $\omega < \omega_\theta$ corresponds to the high temperature phase, whilst for $\omega > \omega_\theta$ corresponds to the low temperature

collapsed phase. It is possible to show that the average length of the walk is finite in the region $0 \leq z < z_\infty(\omega)$. Let us notice that the region *above* $z_\infty(\omega)$ has not physical meaning.

A suitable transformation of coordinates in the (ω, z)-plane

$$(\omega, z) \to (\omega, q = \omega z)$$

makes it easier to characterize the tricritical scaling [106]: of course the critical line is now $q_\infty(\omega)$. Then, we continue by defining the ingredients that go into forming our picture.

At high temperature (small ω) the generating function, Eq. (E.2), diverges in the limit $q \to q_\infty(\omega)$ as

$$\mathcal{G}(\omega, q) \sim (q_\infty(\omega) - q)^{-\gamma_+}, \tag{E.6}$$

whereas at the tricritical (or θ) point

$$\mathcal{G}(\omega_\theta, q) \sim (q_\infty(\omega_\theta) - q)^{-\gamma_\theta}. \tag{E.7}$$

Instead, at low temperature ($\omega > \omega_\theta$), $\mathcal{G}(\omega, q)$ converges in the limit $q \to q_\infty(\omega)$, with an essential singularity.

Now, let us assume that a tricritical scaling holds and consider the following thermal scaling field $t = \omega_\theta - \omega$ and fugacity field $p = q_\infty(\omega_\theta) - q$. In this framework, the θ point is simply $(t, p) = (0, 0)$. For $t > 0$, the shape of the critical line $p^+ \sim t^\psi$, where ψ is the *shift* exponent. The singular part $\mathcal{G}^s$ of the generating function reads:

$$\mathcal{G}^s(t, p) \sim |t|^{-\gamma_u} g^\pm(p|t|^{-1/\phi}), \tag{E.8}$$

where the $\pm$ superscripts refer to temperatures above and below the θ point,

$$g^-(x) \sim \begin{cases} |x|^{-\gamma_u \phi} & \text{if } x \to \infty \\ 1 & \text{if } x \to 0 \end{cases}, \tag{E.9}$$

$\gamma_u = \gamma_\theta/\phi$ and ϕ is the tricritical *crossover* exponent. For $t > 0$, $\mathcal{G}$ is singular along the critical line $p^+(t)$. Then, we have

$$g^+(x) \sim (x - \dot{x}^+)^{-\gamma_+} \text{ if } x \to \dot{x}^+, \tag{E.10}$$

where $\dot{x}^+$ is the singularity. This ensures that $\psi = 1/\phi$. From the generating function it is possible to calculate $\langle L_{x,y} \rangle$, the average lengths along the x and y directions. In the same fashion, it is possible to define the critical exponents $\nu_+^{x,y}$, $\nu_\theta^{x,y}$ and $\nu_u^{x,y}$. The following scaling relations hold: $\phi = \nu_\theta^x \nu_u^x$ and $\phi = \nu_\theta^y / \nu_u^y$.

E.2 Detailed calculations

We briefly outline the main results of Ref. [47]. The authors proposed a continuous model of DSAW, where the r_i's in the nearest-neighbor energy term, Eq. (3.14), are not restricted to integer values. As shown, this model is the continuous limit of the discrete DSAW and has the same critical exponents.

We assign an energy $U(r_1, ..., r_N)$ to each configuration of length L and number of vertical segments N, where each vertical segment, $i = 1, ..., N$, has length r_i measured in the positive y direction, giving $L = \sum_{i=1}^{N} |r_i|$. This energy is given by

$$U(r_1, ..., r_N) = -\epsilon \sum_{i=1}^{N-1} u(r_i, r_{i+1}) \tag{E.11}$$

where

$$u(r_i, r_{i+1}) = \min(|r_i|, |r_{i+1}|)\mathcal{H}(-r_i \cdot r_{i+1}) \tag{E.12}$$

and $\mathcal{H}(r)$ is the Heaviside step function:

$$\mathcal{H}(r) = \begin{cases} 0, & r < 0 \\ 1/2, & r = 0 \\ 1, & r > 0 \end{cases} . \tag{E.13}$$

The function $u(r_i, r_{i+1})$ measures the overlap of successive segments. The thermodynamics can be deduced from the canonical partition function

$$\mathcal{Z}_L(\omega) = \sum_{N=1}^{\infty} \int_{-\infty}^{\infty} dr_1 ... \int_{-\infty}^{\infty} dr_N \delta \left(\sum_{i=1}^{N} |r_i| - L \right) \omega^{\sum_{i=1}^{N-1} u(r_i, r_{i+1})}, \tag{E.14}$$

where, as stated, $\omega = e^{\beta\epsilon}$ ($\omega \geq 1$). For mathematical convenience we introduce the generalized partition function:

$$\mathcal{G}(y; \omega) = \int_0^{\infty} y^L \mathcal{Z}_L(\omega) dL, \tag{E.15}$$

where y is a fixed monomer fugacity. Using Eq. (E.14), Eq. (E.15) can be written as

$$\mathcal{G}(y; \omega) = \sum_{N=1}^{\infty} Z_N(y; \omega) \tag{E.16}$$

where

$$Z_N(y; \omega) = \int_{-\infty}^{\infty} dr_1 ... \int_{-\infty}^{\infty} dr_N e^{-\beta E[r_i]} \tag{E.17}$$

and

$$-\beta E[r_i] = -\tau \sum_{i=1}^{N} |r_i| + \beta\epsilon \sum_{i=1}^{N-1} u(r_i, r_{i+1}) \tag{E.18}$$

where $\tau > 0$ and $y = e^{-\tau} < 1$. Our goal is to find the generalized partition function $\mathcal{G}(y;\omega)$.

Then, we extend our aim introducing a counting variable $x \leq 1$ for the number of horizontal steps, defining the function

$$\mathcal{G}(x, y;\omega) = \sum_{N=1}^{\infty} x^N Z_N(y;\omega) \tag{E.19}$$

and the function

$$\Sigma_N(z) = \int_{-\infty}^{\infty} dt \exp[-\tau|t| + \beta\epsilon \min(|t|, |z|)\mathcal{H}(-tz)]\Sigma_{N-1}(t) \tag{E.20}$$

with $\Sigma_0(z) = 1$; hence $Z_N(y;\omega) = \Sigma_N(0)$. We are interested in finding $\mathcal{G}(x, y;\omega)$ via the generating function

$$\Gamma(z) = \sum_{N=1}^{\infty} x^N \Sigma_N(z) \tag{E.21}$$

and hence $\mathcal{G}(x, y;\omega) = \Gamma(0)$. Next step, is to find an integral equation which $\Gamma(z)$ satisfies. Defining $\Phi(z) \equiv e^{-Kz}\Gamma(z)$, where $K = \beta\epsilon/2$, we obtain after some algebra the following differential equation

$$\frac{d^2\Phi}{dz^2} = K^2\Phi(z) - 2Kxe^{-Hz}[\Phi(z) + e^{-Kz}] \tag{E.22}$$

where $H = \tau - \beta\epsilon$. Eq. (E.22) can be put in the more familiar form

$$u^2\frac{d^2F}{du^2} + u\frac{dF}{du} + (u^2 - \lambda^2)F(u) = -\frac{u^{2+\lambda}}{a^\lambda} \tag{E.23}$$

where $\lambda = 2K/H$. Eq. (E.23) is an inhomogeneous form of Bessel's differential equation.

Solving Eq. (E.23) the following *exact* form for the x-generalized partition function is derived [47]:

$$\mathcal{G}(x, y;\omega) = -1 + \sigma^{-1}\frac{J_\lambda(\sigma\lambda)}{J_\lambda^{'}(\sigma\lambda)}, \tag{E.24}$$

where $\sigma = (4x/\beta\epsilon)^{1/2}$ and $\lambda = \frac{\beta\epsilon}{\tau - \beta\epsilon}$. J_λ and $J_\lambda^{'}$ are, respectively, the Bessel function of order λ and its derivative. The generalized partition function, Eq. (E.15), is given

by Eq. (E.24), with $x = 1$. The critical fugacity is given by the solution of the equation $J'_\lambda(\sigma\lambda) = 0$[2] and the critical point is given by $\sigma = 1$ or $\beta_\theta\epsilon = 4$ [102]. In fact, for $\sigma > 1$, $J'_\lambda(\sigma\lambda) = 0$ has a solution at some *finite* λ. Instead, for $\sigma < 1$, only the solution $\lambda = \infty$ ($y = \omega^{-1}$) exists. Then, $\sigma > 1$ (< 1) describes the high (low) temperature phase.

From known properties of the Bessel's functions $\mathcal{G}(y;\omega)$ can be written

$$\mathcal{G}(y;\omega) \simeq -\left(\frac{\zeta}{1-\sigma^2}\right)^{1/2} \frac{\mathrm{Ai}(\lambda^{2/3}\zeta)}{\mathrm{Ai}'(\lambda^{2/3}\zeta)}\lambda^{1/3} \tag{E.25}$$

where $\mathrm{Ai}(x)$ and $\mathrm{Ai}'(x)$ are, respectively, the Airy function and its first derivative [102] and

$$\frac{2}{3}|\pm\zeta|^{3/2} = \begin{cases} \log\frac{1+\sqrt{1-\sigma^2}}{\sigma} - \sqrt{1-\sigma^2} & \text{if } \sigma < 1 \\ \sqrt{\sigma^2-1} - \cos^{-1}\left(\frac{1}{\sigma}\right) & \text{if } \sigma > 1 \end{cases} . \tag{E.26}$$

Around the θ point ($\beta_\theta\epsilon = 4, y = y_\theta = e^{-\beta_\theta\epsilon}$), we have

$$|\zeta| \sim |1-\sigma^2| \sim |T - T_\theta| \equiv |t| \text{ and } \lambda \sim (y_\theta - y) \equiv \Delta y^{-1}. \tag{E.27}$$

Eq. (E.25) can be recast in the following form:

$$\mathcal{G}(\Delta z;t) \simeq \frac{\mathrm{Ai}(-\Delta z^{-2/3}t)}{\mathrm{Ai}'(-\Delta z^{-2/3}t)}\Delta z^{-1/3}. \tag{E.28}$$

From Eqs. (E.8) and (E.28) the critical exponents can be deduced: $\gamma_t = 1/3$ and $\phi = 2/3$. For $t > 0$ there is a simple pole, so $\gamma_+ = 1$ (for $t < 0$ there are no poles). In the limit $\Delta z \to 0$, $\mathcal{G} \sim t^{-1/2}$ and $\gamma_u = 1/2$. Then, the scaling relation $\gamma_u = \gamma_\theta/\phi$ is verified.

From Eq. (E.24), it is possible to define an average horizontal length as

$$\langle N\rangle = \left.\frac{\partial \log \mathcal{G}(x,z;\omega)}{\partial \log x}\right|_{x=1} . \tag{E.29}$$

When $f = 0$, the *exact* critical exponents are $\nu^x_+ = 1$ for $T > T_\theta$ ($\sigma > 1$), $\nu^x_\theta = 2/3$ for $T = T_\theta$ ($\sigma = 1$) and $\nu^x_u = 1$. Again, the scaling relation $\phi = \nu^x_\theta\nu^x_u$ is verified[3].

To generalize for $f \neq 0$, we have replaced x with $xe^{\beta f}$ (as in Sec. 3.1) and, then, put $x = 1$. Formally, Eqs. (E.24) and (E.29) still remain valid, with $\sigma = (4e^{\beta f}/\beta\epsilon)^{1/2}$. The critical line, determined by the equation $\sigma = 1$, gives $f_c = f_c(T) = \frac{1}{\beta}\log(\frac{\beta\epsilon}{4})$ and is plotted in Fig. E.2. It can be easily understood, once it is realized that Eq.

[2] We are supposing $\lambda \geq 0$, i.e. $y \leq \omega^{-1}$.

[3] Here, the notation is slightly different from that proposed in Sec. 3.1 and consistent with that used in this Appendix.

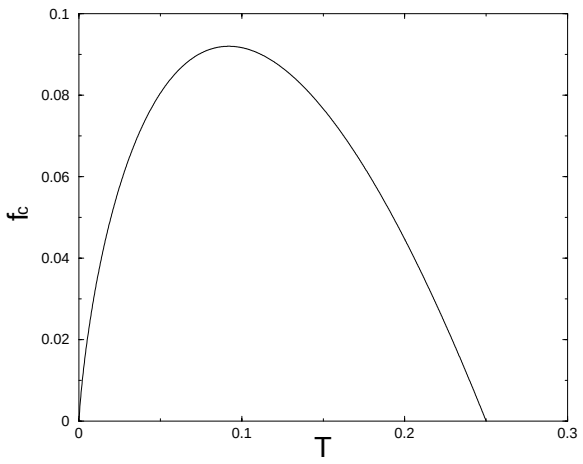

Figure E.2: Exact critical line in the continuum approximation.

(3.11) for $\epsilon \neq 1$ reads

$$f_c(T) = T \ln \left[\frac{1 - \exp\left(-\beta\epsilon/2\right)}{\exp\left(-\beta\epsilon\right)\left(1 + \exp\left(-\beta\epsilon/2\right)\right)} \right]. \tag{E.30}$$

It is easy to verify that the continuum limit is formally achieved when $\epsilon \to 0$.

The exact critical exponents are $\nu_+^x = 1$ for $f > f_c$ ($\sigma > 1$) and $\nu_{f_c}^x = 2/3$ for $f = f_c$ ($\sigma = 1$), which agree with the results of the discrete model (Sec. 3.1.4).

Notice that the shape of the transition line at low T is an unphysical feature of the continuum approximation, as discussed in [41, 37].

Appendix F

A brief introduction to Monte Carlo techniques

In this Appendix we briefly introduce some Monte Carlo techniques we have adopted in this Thesis (see Chapp. 3 and 4). Here, we will focus on dynamic methods [60] and describe in details the moves we have chosen to perform.

The idea of *dynamic* Monte Carlo is to invent a stochastic process with state space S having π as its unique equilibrium distribution. In this Thesis, the state space contains all the configurations of (off-lattice) self-avoiding walks with a well defined potential between non nearest neighbour monomers and $\pi = e^{-\beta\mathcal{H}}$ is the Boltzmann weight, where $\mathcal{H}$ is the energy of a particular configuration of the walk.

In practice, we assume that our stochastic process is a *Markov* process. We then suppose that *ergodicity* hold (each state can be reached from each other state) and π is a *stationary* distribution. Next step consists in specifying the set of elementary moves, i.e. the transitions from one configuration to another and the probabilities for the allowed elementary moves. As stated above, we suppose that the probabilities are given by the Boltzmann weight. Moreover, we suppose that the detailed balance condition is satisfied[1] and we shall adopt the Metropolis rejection criterion [61].

F.1 Classification of Moves

Here, we focus on moves that conserve the total number of monomers of the walk [60]. We have used a *local* move (crankshaft), a *bilocal* move (reptation) and a *non local* move (pivot).

[1] This condition automatically implies the stationarity condition [61].

F.1.1 Local moves

A *local* move is one that alters only a few consecutive sites of the walk, leaving the other sites unchanged. In this Thesis we have used the so called *crankshaft* move.

We have selected randomly two beads i, j ($i < j$) such that $j - i \leq n_c + 2$, with $n_c \ll N - 1$ (most frequently we have used $n_c = 6$ or $n_c = 3$). Then rotate beads $i + 1, \ldots, j$ of an angle $\Delta\phi_c$ around the axis $\mathbf{r}_j - \mathbf{r}_i$. The angle $\Delta\phi_c$ is chosen randomly with a uniform distribution in the interval $[-\Delta\phi_m/2, \Delta\phi_m/2]$, where $\Delta\phi_m$ is a suitable chosen angle. So it may well correspond to a *physical* move of the polymer in a real dynamics.

F.1.2 Bilocal moves

A *bilocal* move is one that alters two disjoint small groups of consecutives sites of the walk; these two groups may in general be very far from each other. One trivial way of making an N-conserving bilocal move is to make two independent (nonoverlapping) N-conserving local moves, i.e. those in which one subwalk loses sites and the other subwalk gains them.

The *reptation* move used here is also known as the *slithering-snake* move. It consists in deleting n_r ($n_r = 1, \ldots, N_r$, with N_r most frequently chosen as 5) beads from one end of the chain and appending them to the other end, after a rotation around a random axis of an angle $\Delta\phi_r$, chosen uniformly from 0 to π. Then, it alters two disjoint small groups of consecutive beads of the chain. Reptation is used as a physical dynamical move in models in which the polymer migrates in a fixed environment or is subject to some displacing field and is subject to no constraints.

F.1.3 Non local moves

The *pivot* move adopted in this Thesis is an example of non local move.

We have selected randomly one bead i ($0 < i < N - 1$) as the pivot point, and then rotated the part of the chain subsequent to the pivot point while keeping fixed the rest of the chain, using the pivot point as the origin. The rotation is around a random axis chosen with uniform probability among all the versors on the unit sphere and the pivot rotation angle is uniformly chosen between $-\Delta\phi'_m$ and $\Delta\phi'_m$ (which in general is different from $\Delta\phi_m$).

Pivot moves are *global* ones, since they involve a rearrangement of a macroscopic portion of the chain. A pivot move is unlikely as a physical dynamical move.

Appendix G

Transfer Matrix and Phenomenological Renormalization

In this Appendix, we briefly explain the Transfer Matrix (TM) technique used in Sec. 3.2, followed by a discussion on phenomenological renormalization (PR).

Let us suppose that one wants to study the critical properties of a two-dimensional model with coupling constant x. Using the TM one can calculate the correlation length $\xi_n(x)$ of a strip of width n. The PR, which is based on finite-size scaling arguments [109], consists in writing a renormalization equation

$$(1/n)\xi_n(x) = (1/m)\xi_m(x') \tag{G.1}$$

which expresses the changes of the interaction x associated with the change of scale of ratio n/m. The critical point and the exponent ν of the two-dimensional problem can be calculated from the following equations:

$$(1/n)\xi_n(x_c) = (1/m)\xi_m(x_c) \tag{G.2}$$

$$\frac{1}{\nu} = \frac{\log\left[d\xi_n/dx|_{x_c}(d\xi_m/dx|_{x_c})^{-1}\right]}{\log(n/m)} - 1. \tag{G.3}$$

As far as n and m are finite, the method is an approximation which can be improved by choosing n as large as possible and $m = n - 1$ [109].

In order to use the PR method for the SAW, one has to define the correlation length as a function of a parameter x in the same way as for spin models. This can be done using the famous $q \to 0$ limit of the classical q-component Heisenberg model [110]

$$\lim_{q\to 0}\langle \mathbf{S}_0\mathbf{S}_R\rangle = \sum_{p=0}^{\infty} x^p \mathcal{N}_{0R}(p) = \mathcal{G}_{0R}(x). \tag{G.4}$$

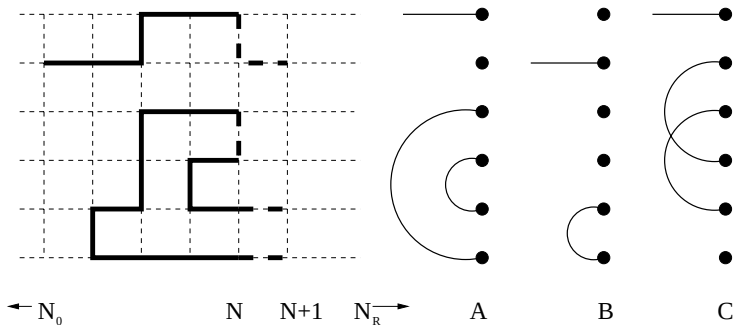

Figure G.1: The configurations A and B represent the part of the polymer on the strip at the left of columns N and $N+1$ respectively. The dashed links are the monomers one has to add to configuration A at column N to give rise to configuration B at column $N+1$. The number of these monomers is here five. So the matrix element between these configurations A and B is x^5. Configuration C is an example of a forbidden configuration.

Eq. (G.4) relates the correlation function $\langle \mathbf{S}_0 \mathbf{S}_R \rangle$ of Heisenberg spins located on sites 0 and R to the number of self-avoiding walks $\mathcal{N}_{0R}(p)$ of length p going from site 0 to site R, x is the nearest-neighbour interaction in the Heisenberg model. When the distance R between the two sites becomes large, the correlation function decreases exponentially in the high-temperature phase. In the $q \to 0$ limit this defines the correlation length $\xi(x)$ for the polymer problem as a function of x which is a chemical potential of monomers

$$\mathcal{G}_{0R}(x) \sim \exp(-R/\xi(x)). \tag{G.5}$$

It is now possible to explain how $\xi(x)$ can be calculated for a strip of any width. Suppose that sites 0 and R belong to two columns N_0 and N_R on the strip. If one cuts the strip at column N between N_0 and N_R, the part of the polymer at the left of column N is made of several branches: one site of column N is connected to site 0 of column N_0 whereas some of the other sites of column N are connected by pairs (Fig. G.1). The writing of the TM needs two steps.

First, one needs the list of all the possible configurations $\mathcal{C}$ at column N. One configuration is defined by the site of column N connected to site 0 and by the pairs of sites connected by the part of the strip at the left of column N. Configurations A and B of Fig. G.1 are examples of such configurations. One can notice that the different branches which reach column N will be connected together by the right part of the strip to form a single polymer. So, some configurations are eliminated (like configuration C of Fig. G.1) where there are crossings between the different branches

of the configuration.

For each allowed configuration $\mathcal{C}$, one can define the function $H_N(\mathcal{C})$ by

$$H_N(\mathcal{C}) = \sum_{p=0}^{\infty} x^p \mathcal{N}_N(p, \mathcal{C}) \tag{G.6}$$

where $\mathcal{N}_N(p, \mathcal{C})$ is the number of ways one can put p monomers at the left of column N in order to realize configuration $\mathcal{C}$ at column N. The transfer matrix T is defined by the set of linear relations which allow the calculation of the $H_{N+1}(\mathcal{C})$ as functions of the $H_N(\mathcal{C})$:

$$H_{N+1}(\mathcal{C}) = \sum_{\mathcal{C}'} T(\mathcal{C}, \mathcal{C}') H_N(\mathcal{C}'). \tag{G.7}$$

Obviously $T(\mathcal{C}, \mathcal{C}') = x^{t(\mathcal{C}, \mathcal{C}')}$ where $t(\mathcal{C}, \mathcal{C}')$ is the number of monomers one has to add to configurations $\mathcal{C}'$ at column N to give rise to configuration $\mathcal{C}$ at column $N+1$. If there is no way to connect two configurations $\mathcal{C}$ and $\mathcal{C}'$, the matrix element $T(\mathcal{C}, \mathcal{C}')$ is zero.

So the size of the TM is the number of configurations $\mathcal{C}$ and its elements are either zeros or integral powers of x[1]. Clearly, when the two columns N_0 and N_R are very far from one another, one has

$$\mathcal{G}_{0R}(x) \sim [\lambda(x)]^R \tag{G.8}$$

where $\lambda(x)$ is the largest eigenvalue of the matrix T. So the correlation length $\xi(x)$ can be calculated by

$$\xi(x) = -\frac{1}{\log(\lambda(x))}. \tag{G.9}$$

Finally, let us remark that in Sec. 3.2 we focused our attention on a self-interacting SAW. This means that the corresponding TM is slightly more complicated than the simple model discussed in this Appendix. There, the configurations are built considering *two* columns, since the energy parameter $\omega = e^{\beta\epsilon}$ is present. Nevertheless, the generalization is rather straightforward [111, 112].

[1]From a practical point of view, the size of the matrix can be reduced using the symmetries of the strip.

Bibliography

[1] A. Fersht. *Structure and mechanism in protein science: a guide to enzyme catalysis and protein folding*. Freeman W. H., New York, 1999.

[2] J. D. Watson and F. H. C. Crick. *Nature*, **171**:737, 1953.

[3] P. J. Flory. *Statistical Mechanics of Chain Molecules*. Interscience Publishers, New York, 1969.

[4] A. Yu. Grosberg and A. R. Khokhlov. *Giant Molecules*. Academic Press, San Diego, 1997.

[5] C. Branden and J. Tooze. *Introduction to Protein Structure*. Garland Publishing, New York, 1999.

[6] U. Bockelmann, Ph. Thomen, B. Essavez-Roulet, V. Viasnoff, and F. Heslot. *Biophys. J.*, **82**:1537, 2002.

[7] T. E. Fisher, A. F. Oberhauser, M. Carrion-Vazquez, P. E. Marszalek, and J. M. Fernandez. *TIBS*, **24**:379, 1999.

[8] C. Bustamante, J. C. Macosko, and G. J. L. Wuite. *Nat. Rev. Mol. Cell. Bio.*, **1**:130, 2000.

[9] C. Vanderzande. *Lattice models of polymers*. Cambridge University Press, Cambridge, 1998.

[10] P.-G. De Gennes. *Scaling Concepts in Polymer Physics*. Cornell University Press, Ithaca, 1979.

[11] J. F. Marko and E. D. Siggia. *Macromolecules*, **28**:8759, 1995.

[12] P. J. Flory. *Principles of Polymer Chemistry*. Cornell University Press, Ithaca, 1953.

[13] W. H. Carothers. *Trans. Faraday Soc.*, **32**:39, 1936.

[14] W. H. Carothers. *Chem. Revs.*, **8**:353, 1931.

[15] L. Pauling. *The Nature of the Chemical Bond*. Cornell University Press, Ithaca, 1960.

[16] A. Grosberg, editor. *Theoretical and Mathematical Models in Polymer Research*. Academic Press, Boston, 1998.

[17] K. Svoboda and S. M. Block. *Annu. Rev. Biophys. Biomol. Struct.*, **68**:247, 1994.

[18] M. Rief, M. Gautel, F. Oesterhelt, J. M. Fernandez, and H. E. Gaub. *Science*, **276**:1109, 1997.

[19] C. Bustamante, J. F. Marko, E. D. Siggia, and S. Smith. *Science*, **265**:1600, 1994.

[20] M. Doi and S. F. Edwards. *The Theory of Polymer Dynamics*. Oxford University Press, Oxford, 1986.

[21] S. B. Smith, L. Finzi, and C. Bustamante. *Science*, **258**:1122, 1992.

[22] T. Odijk. *Macromolecules*, **28**:7016, 1995.

[23] S. B. Smith, Y. Cui, and C. Bustamante. *Science*, **271**:795, 1996.

[24] C. G. Baumann, V. A. Bloomfield, S. B. Smith, C. Bustamante, M. D. Wang, and S. M. Block. *Biophys. J.*, **78**:1965, 2000.

[25] Y. Murayama and M. Sano. *J. Phys. Soc. Jpn*, **70**:345, 2001.

[26] H. Granzier, M. Helmes, O. Cazorla, M. McNabb, D. Labeit, Y. M. Wu, R. Yamasaki, A. Redkar, M. S. Z. Kellermayer, S. Labeit, and K. Trombitas. *Adv. Exp. Med. Biol.*, **481**:111, 2000.

[27] B. J. Haupt, T. J. Senden, and E. M. Sevick. *Langmuir*, **18**:2174, 2002.

[28] A. Halperin and E. B. Zhulina. *Europhys. Lett.*, **15**:417, 1991.

[29] D. K. Klimov and D. Thirumalai. *Proc. Natl. Acad. Sci. USA*, **96**:6166, 1999.

[30] T. A. Vilgis, A. Johner, and J. F. Joanny. *Eur. Phys. J. E*, **2**:289, 2000.

[31] P. L. Geissler and E. I. Shakhnovich. *Phys. Rev. E*, **65**:056110, 2002.

[32] P. Grassberger and H. P. Hsu. *Phys. Rev. E*, **65**:031807, 2002.

[33] D. Marenduzzo, A. Maritan, and F. Seno. *J. Phys. A: Math Gen.*, **35**:L233, 2002.

[34] M. Cieplak, T. X. Hoang, and M. O. Robbins. *Proteins*, **49**:104, 2002.

[35] M. Cieplak, T. X. Hoang, and M. O. Robbins. *Proteins*, **49**:114, 2002.

[36] S. M. Bhattacharjee. *J. Phys. A: Math. Gen.*, **33**:L423, 2000.

[37] D. Marenduzzo, S. M. Bhattacharjee, A. Maritan, E. Orlandini, and F. Seno. *Phys. Rev. Lett.*, **88**:028102, 2002.

[38] A. J. Barrett and C. Domb. *J. Stat. Phys.*, **77**:491, 1994.

[39] A. L. Owczarek and T. Prellberg. *Phys. Rev. E*, **67**:032801, 2003.

[40] D. Marenduzzo, A. Maritan, A. Rosa, and F. Seno. *Phys. Rev. Lett.*, **90**:088301, 2003.

[41] D. Marenduzzo, A. Trovato, and A. Maritan. *Phys. Rev. E*, **64**:031901, 2001.

[42] E. Orlandini, S. M. Bhattacharjee, D. Marenduzzo, A. Maritan, and F. Seno. *J. Phys. A: Math. Gen.*, **34**:L751, 2001.

[43] D. P. Foster. *J. Phys. A: Math. Gen.*, **23**:L1135, 1990.

[44] P. M. Binder, A. L. Owczarek, A. R. Veal, and J. M. Yeomans. *J. Phys. A: Math. Gen.*, **23**:L975, 1990.

[45] R. Brak, A. J. Guttmann, and S. G. Whittington. *J. Phys. A: Math. Gen.*, **25**:2437, 1992.

[46] T. Prellberg, A. L. Owczarek, R. Brak, and A. J. Guttmann. *Phys. Rev. E*, **48**:2386, 1993.

[47] A. L. Owczarek, T. Prellberg, and R. Brak. *J. Stat. Phys.*, **72**:737, 1993.

[48] H. Zhou. *cond-mat/0112090*, 2001.

[49] B. Derrida. *J. Phys. A: Math. Gen.*, **14**:L5, 1981.

[50] C. Domb and J. L. Lebowitz, editors. *Phase Transitions and Critical Phenomena*, volume 13. Academic Press, New York, 1989.

[51] P. L. Geissler and E. I. Shakhnovich. *Macromolecules*, **35**:4429, 2002.

[52] M. Henkel and G. Schutz. *J. Phys. A: Math. Gen.*, **21**:2617, 1988.

[53] S. Lise, A. Maritan, and A. Pelizzola. *Phys. Rev. E*, **58**:R5241, 1998.

[54] A. Maritan, F. Seno, and A. L. Stella. *Physica (Amsterdam)*, **156A**:679, 1989.

[55] D. Dhar and J. Vannimenus. *J. Phys. A: Math. Gen.*, **20**:199, 1987.

[56] R. M. Neumann. *Phys. Rev. A*, **31**:3516, 1985.

[57] D. Keller, D. Swigon, and C. Bustamante. *Biophys. J*, **84**:733, 2003.

[58] S. Kirkpatrick, C. D. Gelatt, and M. P. Vecchi. *Science*, **220**:671, 1983.

[59] A. D. Sokal. *Nucl. Phys. B (Proc. Suppl.)*, **47**:172, 1996.

[60] A. D. Sokal. *hep-lat/9405016*.

[61] K. Binder, editor. *Monte Carlo and Molecular Dynamics Simulations in Polymer Science*. Oxford University Press, Oxford, 1995.

[62] A. Maritan, C. Micheletti, A. Trovato, and J. R. Banavar. *Nature (London)*, **406**:287, 2000.

[63] M. D. Wang, H. Yin, R. Landick, J. Gelles, and S. M. Block. *Biophys. J.*, **72**:1997, 2000.

[64] J. Wilhelm and E. Frey. *Phys. Rev. Lett.*, **77**:2581, 1996.

[65] J. Samuel and S. Sinha. *Phys. Rev. E*, **66**:050801, 2002.

[66] J. Samuel and S. Sinha. *Phys. Rev. Lett.*, **90**:098305, 2003.

[67] A. Dhar and D. Chaudhuri. *Phys. Rev. Lett.*, **89**:065502, 2002.

[68] A. Lamura, T. W. Burkhardt, and G. Gompper. *Phys. Rev. E*, **64**:061801, 2001.

[69] R. Podgornik, P. L. Hansen, and V. A. Parsegian. *J. Chem. Phys.*, **113**:9343, 2000.

[70] Y. Murayama, Y. Sakamaki, and M. Sano. *Phys. Rev. Lett.*, **90**:018102, 2003.

[71] N. K. Lee and T. A. Vilgis. *Eur. Phys. J. B*, **28**:451, 2002.

[72] M. Fixman and J. Kovac. *J. Chem. Phys.*, **58**:1564, 1973.

[73] S. Cocco, R. Monasson, and J. F. Marko. *Phys. Rev. E*, **66**:051914, 2002.

[74] S. Cocco, J. F. Marko, and R. Monasson. *Cr. Phys.*, **3**:569, 2002.

[75] D. Bensimon, D. Dohmi, and M. Mezard. *Europhys. Lett.*, **42**:97, 1998.

[76] M. Rief, H. Clausen-Schaumann, and H. E. Gaub. *Nat. Struct. Biol.*, **6**:346, 1999.

[77] M.-N. Dessinges, B. Maier, Y. Zhang, M. Peliti, D. Bensimon, and V. Croquette. *Phys. Rev. Lett.*, **89**:248102, 2002.

[78] C. Storm and P. C. Nelson. *Phys. Rev. E*, **67**:051906, 2003.

[79] A. Montanari and M. Mézard. *Phys. Rev. Lett.*, **86**:2178, 2001.

[80] N. Lee and D. Thirumalai. *Eur. Phys. J. B*, **12**:599, 1999.

[81] P. L. Hansen and R. Podgornik. *J. Chem. Phys.*, **114**:8637, 2001.

[82] B.-Y. Ha and D. Thirumalai. *J. Chem. Phys.*, **106**:4243, 1997.

[83] Y. Zhou, C. K. Hall, and M. Karplus. *Phys. Rev. Lett.*, **77**:2822, 1996.

[84] A. Rosa, D. Marenduzzo, A. Maritan, and F. Seno. *Phys. Rev. E*, **67**:041802, 2003.

[85] D. A. Kessler and Y. Rabin. *cond-mat/0302505*.

[86] A. Rosa, T. X. Hoang, D. Marenduzzo, and A. Maritan. *cond-mat/0307015*.

[87] D. E. Makarov, Z. Wang, J. B. Thompson, and H. G. Hansma. *J. Chem. Phys.*, **116**:7760, 2002.

[88] R. M. Neumann. *J. Chem. Phys.*, **118**:2964, 2003.

[89] D. E. Makarov, Z. Wang, and H. G. Hansma. *J. Chem. Phys.*, **118**:2966, 2003.

[90] G. Parisi and N. Sourlas. *Phys. Rev. Lett.*, **46**:871, 1981.

[91] A. V. Tkachenko. *cond-mat/0304250*.

[92] L. Livadaru, R. R. Netz, and H. J. Kreuzer. *Macromolecules*, **36**:3732, 2003.

[93] P.-Y. Lai. *Phys. Rev. E*, **58**:6222, 1998.

[94] P.-Y. Lai. *Chin. J. Phys.*, **36**:494, 1998.

[95] H. Yamakawa. *Modern Theory of Polymer Solutions*. Harper and Row, New York, 1971.

[96] C. Bouchiat, M. D. Wang, J.-F. Allemand, T. Strick, S. M. Block, and V. Croquette. *Biophys. J*, **76**:409, 1999.

[97] K. Huang. *Statistical Mechanics*. John Wiley & Sons, New York, second edition, 1987.

[98] C. Domb and M. S. Green, editors. *Phase Transitions and Critical Phenomena*, volume 3. Academic Press, New York, 1974.

[99] R. J. Baxter. *Exactly Solved Models in Statistical Mechanics*. Academic Press, London, 1982.

[100] H. E. Stanley. *Phys. Rev.*, **176**:718, 1968.

[101] H. E. Stanley. *Phys. Rev.*, **179**:570, 1969.

[102] M. Abramowitz and I. A. Stegun, editors. *Handbook of Mathematical Functions*. Dover Publications, New York, 1972.

[103] B.-Y. Ha and D. Thirumalai. *J. Chem. Phys.*, **103**:9408, 1995.

[104] A. D. Sokal and A. O. Starinets. *Nucl. Phys. B*, **601**:425, 2001.

[105] B. D. Hughes. *Random Walks and Random Environments*, volume 1. Clarendon Press, Oxford, 1995.

[106] R. Brak, A. L. Owczarek, and T. Prellberg. *J. Phys. A: Math. Gen.*, **26**:4565, 1993.

[107] R. B. Griffiths. *Phys. Rev. B*, **7**:545, 1973.

[108] C. Domb and J. L. Lebowitz, editors. *Phase Transitions and Critical Phenomena*, volume 9. Academic Press, New York, 1984.

[109] M. Nightingale. *Physica A*, **83**:561, 1976.

[110] P.-G. De Gennes. *Phys. Lett. A*, **38**:339, 1972.

[111] A. Trovato and F. Seno. *Phys. Rev. E*, **56**:131, 1997.

[112] H. Saleur. *J. Stat. Phys.*, **45**:419, 1986.

Acknowledgments

I began to write these notes with a sort of pain, simply because the risk level to forget someone is very high. The final result? One people shorter (or worse!) list of friends.

Ok! So let us begin, having in mind that this could be a serious task, more serious than writing this Thesis you have had the pleasure to read or to use as a support for the fourth leg of your favourite chair.

So firstly, I would thank my supervisor, Amos Maritan, who proposed to me this fascinating topic. His invaluable help and his suggestions were of great help to finish this work.

I would also thank all the scientific staff members of SISSA and ICTP. Each of them have contributed to create a friendly and stimulating scientific environment.

A special thanks to the staff members of the Sissa Bar. I will miss their coffee.

To my roommate Hoang and Flavio Seno from the University of Padua. Their suggestions to implement numerical calculations were more useful than dozens of books.

Let me thank in a special way Davide. His encouraging efforts and his deep observations were of great help, during these last two years.

And Cristian and Alessandro.

I had the pleasure to work with Cristian in occasion of my M.D. discussion here in Sissa and now we are again working together. I will not forget our illuminating discussions and his warmful company.

Alessandro is the best roommate a Ph.D. student may desire. His irony was of great help during the cold months here in Trieste. I would remember only one episode: at the beginning of, let us say March, he began to write a short list where he signed all the times when I was wrong and when I was right, because he claimed that I was always wrong (almost!). I was not convinced at all, but at the end of the month the number of crosses on the WRONG column was 3 order of magnitude more than the one on the RIGHT column (poor me, he was right!).

Then, I would thank Michele Cascella, who contributes to this Thesis with the

beautiful picture in Fig. 1.14. And how to forget his exciting discussions about Gina Cigna (10 $ to the lucky reader who knows her!)?

Thanks to Katrin! She gave the picture about DNA in Fig. 1.13. And Lorenzo. I can't forget all I know about ski is thanks to them (*"Fai FAU!"* is our slogan!), although they don't care their teaching method might imply the death of their pupil.

Thanks to Alessandra, who taught to me there are more shops on Earth than stars on Heaven.

And Michele Cirasuolo, who shared with me his first experience with skilift and this last hot 2003 August, here in Trieste

How to forget Andrea? He sacrificed for us many transgenic chickens he should have to study: he understood that friendship is more important than his scientific career.

A special thanks to Simone, who taught to me the secrets of free climbing (and, above all, free falling!) and Vittoria (see you next year, at Bavisela 2004!).

Besides, I would thank two people who live very far from Trieste. Marco, my best friend. Together, we began to discover Physics and the difficulties of scientific research. And Cristina. I had the pleasure to know her last year, in Trieste and to meet her again this year, in Barcelona.

Anna experienced with Katrin a marvelous travel in the South of Italy. Nevertheless, she found more interesting some pets we met along the road.

Thanks to Giacomo, Stefano, Laura and "l'Arabo", who organized an unforgettable joke at the train station in Trieste.

To Fabio and Sara who won an unexpected bath during one of these hot summer nights.

And to Michele Frigerio, Matteo, Pietro, Alejandro and all the marvelous guys who, during these long three years, have contributed to build a network of invaluable relations.

And last, but not least, I would thank my parents, my sister, my uncles and my grandmother. In spite of the fact that we live very far apart, I could always rely on their support.

Thank you!

October 9th, 2003